

**Copyright**

**by**

**Andrew Philip Stam**

**2009**

# **Fatigue Performance of Base Plate Connections Used in High Mast Lighting Towers**

by

**Andrew Philip Stam, B.S.**

**Thesis**

Presented to the Faculty of the Graduate School  
of the University of Texas at Austin  
in Partial Fulfillment  
of the Requirements  
for the Degree of

**Master of Science in Engineering**

The University of Texas at Austin  
May 2009

The Thesis committee for Andrew P. Stam

Certifies that this is the approved version of the following thesis:

**Fatigue Performance of Base Plate Connections Used in High  
Mast Lighting Towers**

**APPROVED BY  
SUPERVISING COMMITTEE:**

**Supervisor:**

\_\_\_\_\_  
Karl Frank

\_\_\_\_\_  
Lance Manuel

*I dedicate this thesis to my family.  
Without their love and encouragement, it would not be here for you to enjoy.*



## **Acknowledgements**

I would like to acknowledge the Departments of Transportation in the following states: Texas, Pennsylvania, Iowa, Wyoming, Colorado, Minnesota, North Carolina, Wisconsin, California, and South Dakota. Thank you for funding this project. Not only has your support furthered the understanding of this complex issue, but it has also introduced me to the world of research and made possible my graduate education.

Dr. Frank, thank you so much for the opportunity to take part in this research. Your guidance and wisdom have been greatly appreciated, not to mention your patience. Best wishes as you tread on through life.

Nick Richman, thanks for being the best research partner a guy could ask for. Best wishes to you also.

To Dennis Phillip, Blake Stasney, and Andrew Valentine, you guys are indispensable. Thanks for always being there when a crane was needed. And to the rest of the FSEL staff, thanks so much for all the support.

May 2009

# **Fatigue Performance of Base Plate Connections Used in High Mast Lighting Towers**

by

Andrew Philip Stam, M.S.E

The University of Texas at Austin, 2009

SUPERVISOR: Karl H. Frank

This research study examined the fatigue performance of several base plate connections used in high mast lighting towers. Recent failures of these non-redundant structures have increased the awareness of their fatigue susceptibility and the hazard posed by their potential for collapse. Failures have commonly occurred due to fracture of the pole shaft directly above the base plate connection, which indicates that wind-induced fatigue is the cause. Though design of these structures is governed by the 2001 AASHTO specifications, a recent study has found that these design provisions can be unconservative (Rios, 2007).

Several common high mast base plate connections were compared based on their fatigue performance. These comparisons were supported with the results of both full-scale experimental testing and finite element modeling in Abaqus. Additional untested connection details were investigated in analytical parametric studies.

The experimentally tested details incorporated the use of full penetration welds, external collars, and continuous stool stiffeners. Additionally, specimens from two manufacturers were considered to observe the effect of this variable. The results of the study suggest that fatigue performance can be greatly improved through the use of external collars, especially when combined with full penetration welds. The experimental results also confirmed the importance of unequal leg fillet welds for fatigue-critical details.

# Table of Contents

<b>1 Introduction</b> .....	1
1.1 Background .....	1
1.2 Typical High Mast Features .....	4
1.3 Wind-Induced Fatigue Loads .....	8
1.4 AASHTO Design Procedure .....	10
1.5 Related Research .....	11
1.5.1 Experimental Testing .....	11
1.5.2 Analytical Modeling .....	13
1.6 Project Scope .....	14
<b>2 Test Setup and Experimental Procedure</b> .....	15
2.1 Introduction .....	15
2.2 Test Setup .....	15
2.2.1 Load Box and Connection .....	19
2.2.2 Hydraulic and Control Systems .....	21
2.3 Fatigue Testing Considerations .....	21
2.4 Testing Procedure .....	24
2.4.1 Measurement and Inspection .....	24
2.4.2 Installation Procedure .....	25
2.4.3 Testing Loads and Displacements .....	25
<b>3 Test Specimen Design</b> .....	28
3.1 Introduction .....	28
3.1.1 Naming Scheme .....	30
3.2 Typical Specimen Details .....	30
3.3 Socket Details .....	33
3.4 Full Penetration Details .....	36
3.5 Stool-Stiffened Details .....	41
3.6 Summary of Tested Details .....	44

<b>4 Experimental Results</b> .....	45
4.1 Introduction.....	45
4.2 Fracture Locations .....	47
4.3 Results for Socket Details.....	49
4.4 Results for Full Penetration Details .....	51
4.5 Results for Stool-Stiffened Details .....	54
4.6 Results Summary and Discussion.....	55
4.6.1 Phase I and II Socket Details.....	58
4.6.2 Phase I and II Full Penetration Details .....	60
4.6.3 Phase I and II Stool Details .....	61
<b>5 Finite Element Modeling</b> .....	63
5.1 Introduction.....	63
5.2 Hotspot Stresses .....	64
5.2.1 DNV Extrapolation Technique.....	67
5.2.2 Structural Stress Technique.....	68
5.3 Base Model Development.....	70
5.3.1 Model Construction.....	70
5.3.2 Load and Boundary Conditions.....	73
5.3.3 Meshing .....	74
5.3.4 Submodeling.....	76
5.3.5 Model Verification .....	77
<b>6 Analytical Results</b> .....	79
6.1 Introduction.....	79
6.2 Parametric Studies .....	80
6.2.1 Wall Thickness and Shaft Diameter Study.....	81
6.2.1.1 Verification of Findings and Conclusions .....	86
6.2.2 Anchor Rod Study .....	88
6.2.3 Base Plate Inner Diameter Study.....	91
6.2.4 Collar Length Study .....	93

6.2.5 Shaft Bend Radius Study.....	95
6.3 Hotspot Results for Experimental Specimens.....	96
<b>7 Conclusions and Recommendations .....</b>	<b>100</b>
7.1 Experimental Conclusions .....	100
7.2 Analytical Conclusions .....	101
7.3 Recommendations.....	102
<b>Appendix A Recommended Installation Procedure .....</b>	<b>104</b>
<b>Appendix B Test Specimen Dimensions .....</b>	<b>110</b>
<b>Appendix C Testing Stresses and Loads .....</b>	<b>112</b>
<b>Appendix D Analytical Hotspot Stresses.....</b>	<b>113</b>
<b>References .....</b>	<b>115</b>
<b>Vita.....</b>	<b>116</b>

# 1 Introduction

This research study investigated the fatigue performance of several base plate connections used in high mast lighting towers. These connections were evaluated using the results of full-scale experimental testing and finite element modeling in Abaqus. Parametric models were also constructed to investigate additional untested connections.

The work presented herein stands as a continuation of an earlier fatigue investigation of these connections at the University of Texas at Austin. That work was documented by University of Texas student Craig Rios and is presented in his Master's thesis (Rios, 2007). In this report, the work of Rios will be referred to as "Phase I," and the current work will be considered "Phase II." The two research phases are interrelated as many of the conclusions following Phase I influenced the decisions in Phase II.

This introductory chapter will examine background information relevant to the project's motivation and will also present the project's scope.

## 1.1 Background

Recent failures of high mast towers have raised awareness about an underlying problem with these structures and the risk posed by possible collapse. Given their function, the illumination of large areas for improved visibility, installation is predominantly in locations of high human activity. In addition to their typical placement around highway interchanges, as shown in Figure 1.1, these towers are also used in and around sports venues, parking lots, and penitentiaries (Rios, 2007). As a result, failures have the potential to cause loss of human life, especially considering the hazard posed by highway towers falling across active lanes of traffic.

Recent high mast failures have been well documented in the literature (Rios, 2007) (Ocel, 2006) (Warpinski, 2006), and will not be discussed here. Unfortunately, an accurate statistic on failure volume is not possible as many collapses go unreported. Most high masts are individually owned by state DOTs, and there is no nationwide program monitoring their performance.



Figure 1.1 High Mast Towers at Highway Interchange (photo courtesy of Craig Rios)

High mast towers can fail suddenly and without warning due to an inherent lack of redundancy. In many cases, collapse is caused by a horizontal fracture in the pole shaft directly above the base plate weld. This fracture is almost always caused by vibration-induced fatigue from wind effects. Typically, the fracture will initiate on one side of the mast and slowly propagate through the shaft wall and around the perimeter. Over time, enough section loss will occur that the pole will fail by ductile yielding of the net section.

Fatigue is a phenomenon by which a cyclic load effect acts repeatedly on a structure over its lifetime, inciting gradual cracking at critical locations. These are areas of inherently high stress due to irregular geometries, and are hence called stress concentration points, or “hotspots.” Common structures that are subject to fatigue are bridges (due to truck loads) and commercial airplane frames (due to pressurization-depressurization cycles).

In high mast towers, cyclic loads are the product of two wind-induced mechanisms, both of which lead to vibration. These are natural wind gusts and vortex shedding, and they will be discussed in Section 1.3, Wind-Induced Fatigue Loads.

In steel structures, the rate of fatigue cracking is directly proportional to the stress range caused by each load cycle raised to a power of three. Therefore, the useful life of a structure subject to fatigue can be drastically improved if it is designed in such a way that critical stress ranges are kept small. This can effectively be done by minimizing stress concentrations.

Stress concentration in high mast connections occurs at the toe of the external weld connecting the high mast's shaft to its base plate. At this spot, the amplification of nominal bending stresses is a product of two geometric effects, one large in scale, the other smaller in scale.

The first is a macro-effect of base plate rotation. As the cantilevered pole is laterally loaded, the base plate does not remain planar and instead warps as shown in Figure 1.2. This bending of the base plate creates a double curvature in the pole shaft wall directly above the fillet weld, which adds local secondary bending stresses to the existing nominal bending stresses.

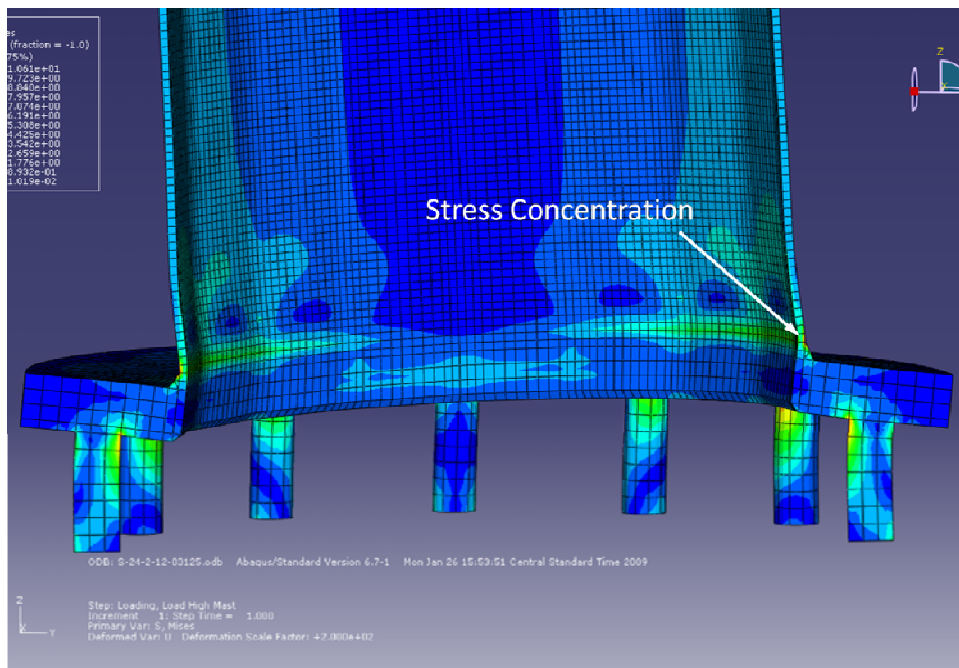


Figure 1.2 High Mast FEA Model Showing Base Plate Warping

This source of stress amplification is directly related to the base plate's level of flexibility. This interaction has been a consistent observation in the testing and modeling of these connections (see Section 1.5, Related Research), and research studies have found that its contributing effect can be



mitigated through an overall stiffening of the connection, which can be done by thickening the base plate or adding external attachments such as gusset plates and collars.

The second geometric factor that contributes to stress concentration is the presence of the weld itself, which is an effect more on a micro-scale than the base plate rotation discussed above. The weld's toe creates a sharp corner that tends to concentrate stresses, and the weld's profile plays a large role in the severity of this concentration. This factor is very much dependent on the quality of welding in a high mast connection. Smooth welds with shallow profiles and few pits or notches at their toes will have lower stress concentrations than rough welds with steep, irregular profiles or undercuts.

The weld's contribution to stress concentration can be mitigated in two ways. The first is to specify unequal leg fillet welds, where the long leg is positioned along the pole shaft, rather than equal leg fillet welds. When this is done, the weld's angle of incidence at the toe is shallower and the stress concentration is lower. The second way to reduce the weld's effect is by ensuring that welds are of high quality. This can be done by requiring proper welding technique and attentive, careful inspection.

This research project focused primarily on the first of the two stress concentration sources discussed above. This was done by experimentally testing and analytically modeling connection details of varying stiffnesses. Through this, an understanding was gained of how to best mitigate the effect of connection flexibility and its potential to cause fatigue cracking.

## 1.2 Typical High Mast Features

Typical features of high mast poles include, in descending order, the lighting apparatus, the pole shaft, the base connection, and the foundation. Common mast heights range from 50-ft to 150-ft, but can also be as high as 200-ft.

The lighting apparatus is usually composed of eight or more lights fixed to a sliding circular mount. An internal winch system allows the lighting mount to be lowered for periodic maintenance and replacement. Access to this winch system is provided by a small hatch on the side of the shaft near its base (See Figure 1.3). This access hatch presents another possible

location for fatigue cracking, but typical access hatch details have lower stress concentrations than the base connection.



Figure 1.3 Winch System Access Hatch (photo courtesy of Craig Rios)

The pole shaft is typically composed of three or more sections friction spliced over one another and is commonly tapered to reduce susceptibility to vortex shedding, a wind-induced phenomenon that will be discussed in the next section. Tapering also ensures that the spliced sections fit over one another. Typical taper slopes range from 0.1-in/ft to 0.2-in/ft, where this slope is measured as a change in diameter per increment of mast height.

The pole shaft's section is usually polygonal, with bends formed using a press brake. The masts considered for this study were all sixteen-sided ("hexadecagonal") and had variable bend radii depending on the fabricator. High mast shafts can also commonly be twelve-sided or eight-sided. Outer diameters can range from 16-in to 36-in at the mast's base. The diameters of specimens tested in this study were 24-in.

Stress concentrations have been found analytically to form at pole shaft bends (Ocel, 2006), a finding confirmed in this study. Thus the closer a polygonal section approximates a circle, the

better its potential fatigue performance. Fully circular sections, however, are very difficult to fabricate as they require unreasonably large press forces.

The high mast's base connection, the focus of this research project, has two components. The first is the connection of the polygonal pole shaft to the flat base plate. The second is the connection of the base plate to the concrete foundation.

The most common method of joining the pole shaft to the base plate is with a fillet-welded socket detail (see Figure 1.4), as this is the easiest and most straightforward connection to fabricate. The base plate is simply sized to an inserted pole shaft and the two are joined with dual fillet welds. The external weld is the primary structural weld, but the internal weld, which is placed to seal the gap between the pole shaft and base plate, also provides a small degree of structural restraint.

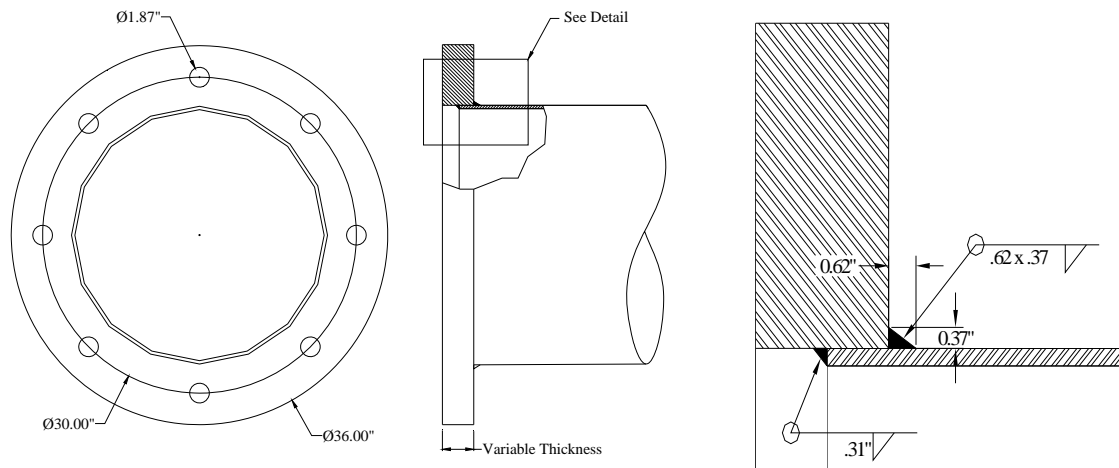


Figure 1.4 Fillet-Welded Socket Connection (Craig Rios, 2007)

Unfortunately, this detail has demonstrated very poor fatigue performance, especially where base plate thicknesses are 2-in or less (Rios, 2007). The poor performance of this detail stems from the high flexibility of its base plate. To fit the inserted shaft, a very large hole must be cut, greatly reducing the base plate's stiffness.

A better alternative is a full penetration groove-welded detail. In this connection, the pole shaft is not socketed into the base plate, but is instead butted against the plate's surface and the two are connected with a full penetration weld. See Figure 1.5 for a common full penetration detail.

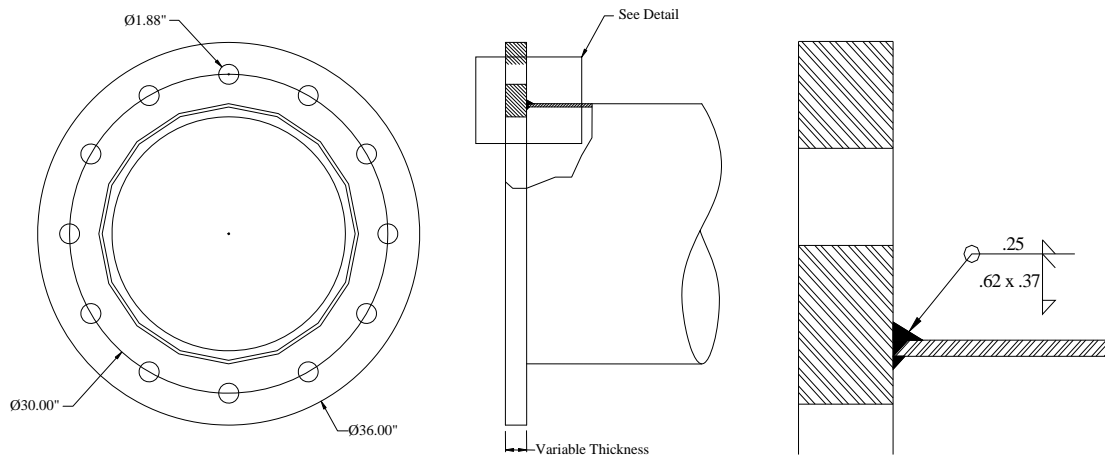


Figure 1.5 Full Penetration Groove-Welded Connection (Craig Rios, 2007)

The major improvement in this detail is the ability to reduce the size of the base plate’s inner diameter. This provides the base plate with greater stiffness and helps suppress the rotation seen in Figure 1.2.

A double-nut anchor rod connection is commonly used to join a mast’s base plate to its concrete foundation, as shown in Figure 1.6. In this connection, anchor rods are embedded into the concrete footing, usually to depths greater than 3-feet, and the mast is connected using two heavy-hex structural nuts per anchor rod. The number of rods usually depends on a DOT’s standard detail, but commonly ranges from six to sixteen.

The lower set of nuts, termed the “leveling nuts,” helps to level the base plate and ensure a vertical mast; the upper set holds the mast in place. The nuts must be tightened uniformly to provide for equal distribution of load, and to ensure that they do not loosen over the mast’s service life, they are commonly tack-welded to the base plate (see Figure 1.6). A research study at Lehigh University found that high stress concentrations can form in masts where the nuts are not tightened uniformly (Warpinski, 2006).

High masts are typically galvanized for corrosion resistance, though painted masts and masts fabricated from weathering steel are also possible. A research study focusing on traffic signal mast arms at the University of Texas found that the galvanizing process has the potential to reduce fatigue lives, possibly through the formation of micro-cracks (Koenigs, 2003).

Consequently, all high mast specimens in this study were galvanized to provide a lower bound to the fatigue behavior of un-galvanized masts.

High mast foundations are most often drilled shafts, but can also be spread footings or driven piles if appropriate for the local soil conditions (Rios, 2007). The Texas Department of Transportation specifies drilled shafts ranging from 20-ft to 60-ft in depth depending on the results of penetrometer testing (TXDOT, 1995).



Figure 1.6 High Mast Double-Nut Base Connection (photo courtesy of Craig Rios)

### 1.3 Wind-Induced Fatigue Loads

Fatigue stresses in high masts are caused by two specific aerodynamic phenomena: natural wind gusts and vortex shedding. This section will briefly examine these mechanisms and their abilities to generate cyclic loads.

The first of these mechanisms, natural wind gusting, is also the simpler of the two. Natural gusting is a simple phenomenon by which air pressures are briefly elevated on the windward side of a high mast due to natural fluctuations in the wind's velocity.

Wind gusts act as short term pulse loads and lead to damped free vibration at the mast's natural frequency. High masts have very low damping ratios, typically less than 0.5% of critical, so vibration cycles can be numerous for strong gusts. Additionally, the high flexibility of most high masts results in large stress ranges associated with these cycles.

The second mechanism leading to high mast fatigue stresses is vortex shedding. This phenomenon commonly occurs when a bluff, rounded object is positioned in a steady fluid stream. If the fluid's velocity is within a certain range, small vortices will be shed from the back of the object off alternating sides. As this occurs, the object tends to oscillate back and forth perpendicular to the direction of the fluid's flow.

Vortex shedding acts as a harmonic forcing function on the high mast, so resonance (or "lock-in") can occur if the shedding frequency is near the natural frequency of the structure. While a high mast is in a resonant state, displacements (and thus stress cycles) can grow very large, potentially large enough to cause damage. For a given mast cross-section, the shedding frequency is directly proportional to the wind speed, so there exists a critical resonant wind speed for each mast.

Tapered masts, due to their variable cross-sections, are more resistant to vortex shedding than untapered masts. For this reason, AASHTO only requires vortex shedding to be considered for mast's whose taper slopes are less than 0.14-in/ft. Natural gusting, however, must be considered for all masts, regardless of taper.

Both of these aeroelastic mechanisms are very complex, and the stress ranges resulting from their effects on high masts are variable and greatly dependent on the mast's shape, its placement relative to other structures, and local wind conditions. To simplify fatigue design, AASHTO reduces the vibratory load effect of each mechanism to an equivalent static load. These static loads account for the shape and cross-section of the mast, and, in the case for vortex shedding, the mast's critical wind speed and damping ratio.

## 1.4 AASHTO Design Procedure

Fatigue design of high mast structures is governed by Section 11 of AASHTO's *Standard Specifications for Structural Supports for Highway Signs, Luminaries, and Traffic Signals, 4<sup>th</sup> Edition* (AASHTO, 2001). Fatigue design should not to be confused with normal strength design, which is presented in Section 5.

In this specification, AASHTO makes use of the infinite-life design philosophy. Under this approach, all masts designed in accordance with the specification must be sized such that nominal stresses fall below the constant amplitude fatigue limit (CAFL) for the mast's connection detail. The CAFL represents the empirically-based minimum stress range required to incur fatigue damage and is also called the "infinite-life threshold." In theory, if fatigue stresses are kept below this level, no damage will occur.

Nominal stresses are found by applying the equivalent static loads corresponding to the wind loading mechanisms addressed previously. Stresses are calculated at the pole's base assuming the simple bending formulation of  $Mc/I$  and are kept below the CAFL by sizing the pole shaft section accordingly. AASHTO assigns groove-welded full penetration details (with backing rings) to Category E, for which the CAFL is 4.5-ksi, and fillet-welded socket details to Category E', for which the CAFL is 2.6-ksi.

It is important to note that AASHTO assigns a fatigue category based only on the weld detail and makes no accommodation for a connection's base plate thickness, number of anchor rods, or the presence of external collars or stools. Research at the University of Texas and elsewhere has shown that these variables play strong roles in determining the fatigue performance of pole-to-base plate connections (Koenigs, 2003) (Anderson, 2007) (Rios, 2007). The fatigue category assignment scheme in AASHTO is therefore oversimplified and incomplete.

## 1.5 Related Research

Prior to the Phase I experimental work done at the University of Texas, no known fatigue testing of high mast base plate-to-pole connections had been performed (Rios, 2007). However, relevant conclusions can be drawn from the testing of traffic signal mast arm connections. These smaller base plate-to-pole connections, which have been tested since the early 1980's, are very similar to high mast connections, and relationships between detailing and fatigue behavior are comparable.

Though there is limited experimental data on the fatigue response of high masts, the growing use of Finite Element Analysis (FEA) has led to several analytical studies of their connections (Ocel, 2006) (Warpinski, 2006). Though some of these studies need experimental verification, they provide a good basis for the understanding of high mast fatigue performance.

This section will briefly summarize some of the related research concerning the fatigue performance of base plate connections used in both mast arms and high masts. Experimental and analytical work will be presented.

### 1.5.1 Experimental Testing

Fatigue testing of tubular traffic structures began at Lehigh University in 1983 (Miki, 1984), and the first tests were performed on mast arm socket connections. This research focused primarily on the external weld of this connection and found that specifying an unequal leg fillet helped the detail achieve a Category E' (Miki, 1984). The relationship with base plate stiffness, however, was not considered.

The first testing of mast arm connections at the University of Texas also confirmed the unequal leg fillet welded socket detail as a Category E' (Koenigs, 2003). Additionally, this study considered the role of base plate thickness by testing 10-in diameter arms with 1.5-in and 2.0-in base plates. The thickened base plate detail showed a marked improvement with a ten-fold increase in average fatigue coefficient (Koenigs, 2003). The fatigue coefficient is a parameter that allows for direct comparison of fatigue tests performed at different stress ranges (see Section 4.1 for a more detailed definition).



Several years later, researchers at the University of Minnesota verified this base plate dependence and also considered the role played by shaft wall thickness (Ocel, 2006). Octahedral, 13-in diameter socket details of 1.25-in and 2.5-in thick base plates were tested with wall thicknesses of 0.19-in and 0.31-in. Researchers observed a fifty-fold increase in average fatigue coefficient from doubling the base plate thickness. The effect of pole wall thickness was smaller, but still evident. The specimens with thickened walls performed better, marked by a doubling of the average fatigue coefficient (Ocel, 2006).

The current program's first phase at the University of Texas represents the first known testing of base plate details large enough for high masts. For 24-in diameter masts, researchers investigated several parametric details in the base plate connection, namely, base plate thickness, number of anchor rods, and detail type (socket, full penetration, and stool-stiffened) (Rios, 2007).

Among the socket details tested, researchers found a strong dependence on base plate thickness (base plates of 1.5-in, 2.0-in, and 3.0-in were considered). They noted that doubling the thickness of the base plate had the potential to improve average fatigue coefficient by a factor of ten. Additionally, for socket details with 1.5-in and 2.0-in base plates, researchers found a benefit from increasing the number of anchor rods from eight to twelve. This improvement was marked by a two to three-fold increase in average fatigue coefficient (Rios, 2007).

The most striking result from Phase I testing of socket details, however, was how poorly they performed. All specimens, regardless of base plate thickness or anchor rod number, performed below a Category E' level (Rios, 2007). The AASHTO designation for this detail of Category E' is therefore unconservative. Additionally, the parametric variables of base plate thickness and anchor rod number were shown to have a very strong effect on fatigue life, generally improving it as they were increased. These variables are not considered in the current AASHTO category assignment scheme.

Phase I researchers did find that significant fatigue life could be gained by exchanging a socket detail for a stiffer full penetration or stool detail; however, these alternative connections still performed poorly, testing only in the Category E' region (Rios, 2007).

### 1.5.2 Analytical Modeling

Several analytical studies of traffic structure base plate-to-pole connections are available in the literature; however, to the author's knowledge, only two of these investigated connections large enough to be considered for high masts. These studies were carried out at the University of Minnesota and Lehigh University.

Both of these studies used stress concentration factor (SCF) as a quantitative measure of potential fatigue performance and as a relevant basis for comparing different details. This approach is consistent with the current project.

The University of Minnesota study examined several parametric variables in high mast socket details including base plate thickness, pole shaft diameter, pole wall thickness, and pole section shape. The most significant parametric variable was found to be base plate thickness.

Researchers found that thickening the base plate from 1-in to 3-in had the potential to reduce the stress concentration factor by 50-60% (Ocel, 2006).

Other strong variables were found to be pole shaft diameter and pole section shape. Doubling the diameter (for a constant base plate) was found to increase the SCF by roughly 50% (Ocel, 2006). The most important aspect of a pole section's shape was found to be the sharpness of its bends, which was a function of both the number of sides and the bend radii. As each is decreased, the pole shaft vertices become "sharper," and stress concentration is increased. Thus the lowest SCFs were found for round shafts (Ocel, 2006).

The parametric variable of shaft wall thickness was found to have the smallest effect on SCF. Virtually no visible relationship existed (Ocel, 2006). This variable was also investigated in the current study and a discussion of its role can be found in Section 6.2.1 of Chapter 6, Analytical Results.

The analytical study from Lehigh University investigated several of the same parametric variables as the University of Minnesota study, but for larger diameter masts (Warpinski, 2006). This study's findings concerning both base plate thickness and shaft diameter mirrored the findings from the University of Minnesota.

The Lehigh study did, however, find a slightly more significant relationship between SCF and pole shaft thickness than the University of Minnesota study. Stress concentration factors were found to increase slightly for thicker walls (Warpinski, 2006). A more detailed discussion of this matter is presented in Section 6.2.1.

## 1.6 Project Scope

The objective of this research study was to evaluate the fatigue performance of common high mast base plate connection details and build on the existing knowledge from the first phase of high mast research at the University of Texas at Austin. This appraisal was accomplished through both full-scale experimental fatigue testing and analytical modeling with FEA.

The tested connection details were chosen based on the performance of Phase I details, and in most cases, were significantly more robust. Phase II details made use of external collars, thickened shaft walls, full penetration welds, and continuous stiffening stools to further investigate the role these variables play in affecting fatigue performance. Phase II testing also investigated the variable of high mast manufacturer.

Analytical finite element models were created for all tested details to verify the experimental results. Additionally, several parametric studies were initiated to test variables that were not investigated experimentally.

The following chapters will document all experimental methods, both for physical testing and analytical modeling, and then will present all research results. The final chapter will discuss the conclusions and recommendations that can be drawn from this research study.

## 2 Test Setup and Experimental Procedure

### 2.1 Introduction

The Phase I test setup was reused for fatigue testing of high masts in Phase II. Its design was not changed for this phase with the exception of some small modifications made to improve its own fatigue strength.

This test setup facilitated the easy loading of matched-pair specimens by testing them horizontally rather than in the vertical orientation. Though the horizontal configuration restricts the fatigue stresses to tension-only, a limitation that will be discussed further, it radically decreases overall testing time by simplifying installation and allowing for simultaneous duplicate testing. This setup will be described in Section 2.2.

The testing procedure included several important tasks. The specimens were first measured to confirm sectional properties and inspect for any fabrication errors or misalignments. They were then installed into the setup using the same anchor rod and double-nut connection used in the field, and fatigue loading was executed using an MTS closed-loop control system. Details of the testing procedure will be described in Section 2.4.

### 2.2 Test Setup

This section will begin by describing the horizontal configuration used to test high mast specimens and will conclude with descriptions of several setup components.

The setup used for fatigue testing of high mast specimens tested the masts horizontally, two at a time. This setup was designed by researchers during the first phase of testing at The University of Texas at Austin (Rios, 2007). It replicated, albeit on a larger scale, the testing configuration used to test traffic signal mast arms at the University of Texas (Koenigs, 2003). A schematic of the test setup is shown in Figure 2.1.

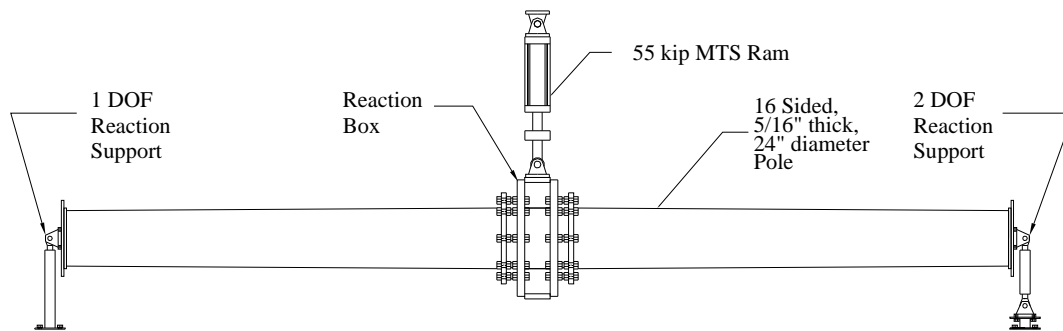


Figure 2.1 Test Setup (Rios, 2007)

Analytically, high mast poles can be considered as vertical cantilevers. Structural restraint at the base is highly complex, depending on the foundation type, surrounding soil stiffness, and connection detail, but can be considered for most cases as fully fixed. It would then follow that the masts should be tested vertically, bolted to the testing floor, and loaded horizontally at the tip. While not impossible, installation into this vertical orientation can be very difficult and time-consuming. Furthermore, this configuration permits testing of only a single mast. Given that tests can approach 5 million cycles and last up to 2 weeks, Phase I researchers recognized the appeal of simultaneously testing two masts horizontally.

The horizontal testing configuration was, in form, identical to a simply-supported beam loaded vertically at mid-span. Given the fact that a beam of length  $L$  loaded and supported in this fashion has zero rotation at the center and zero moment at the ends, it can be alternately idealized as two back-to-back cantilevers each of length  $L/2$ . Note that the requirement of zero rotation at mid-span was ensured by the symmetric testing of replicate specimens, each with identical stiffness.

End restraint of the coupled high masts was also consistent with the simply-supported beam idealization. A pin at the south end provided a single rotational degree of freedom through the use of an elevated rod-eye. The north end made use of two rod-eyes connected by a steel rod to create a roller, which offered two degrees of freedom, rotation and longitudinal translation. See Figure 2.2 for schematics of these end supports.

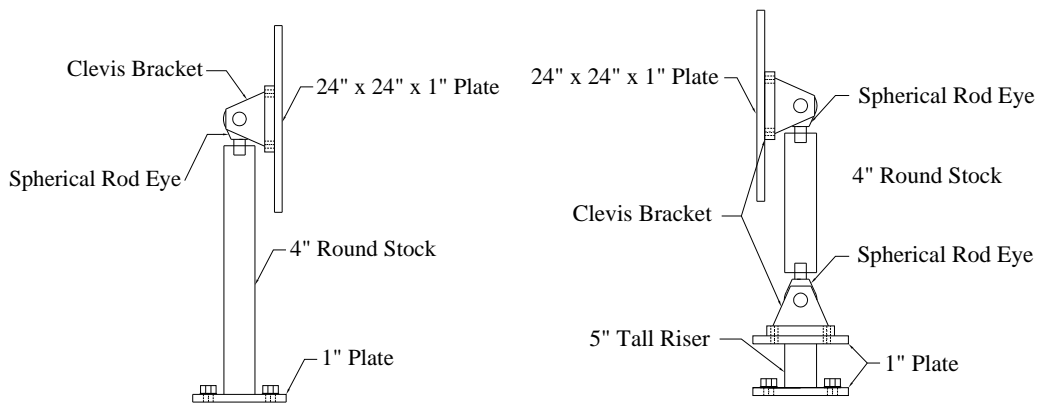


Figure 2.2 Test Setup End Supports (Rios, 2007)

Vertical loads imparted by the 55-kip ram were reacted by a portal frame designed by Phase I researchers (Rios, 2007). See Figure 2.3 for a picture of this frame. It was composed of two wide-flange columns supporting two coped wide-flange sections and two diagonal bracing elements. The diagonal bracing, not used in the portal frame for smaller-scale mast arms tested at Ferguson Lab, was installed by Phase I researchers to increase the out-of-plane stiffness of the larger frame and limit displacement from dynamic loading.

The overall test setup length was set at 32-feet. This length was chosen based on both setup flexibility and the practical limits of the Ferguson Lab strong floor. Phase I researchers were required to select a length that created a setup both flexible enough to operate within the capacity of the ram and stiff enough to keep displacement within the ram's stroke limit. Additionally, the discrete tie-down points on the Ferguson Lab strong floor are spaced at 8-feet on center, requiring the length to be in 8-foot increments.

The horizontal testing configuration did have one drawback due to an instability inherent in the setup design. The 55-kip MTS hydraulic ram used for testing had ball-and-socket type joints at both its top and bottom (See Figure 2.4). When the ram applied a compressive (downward) force into the coupled masts, the rotational and translational freedoms permitted by these joints would cause the masts to rotate about their long axis rather than forcing them into the desired positive curvature. As the masts rotated, the inclination of the ram created a lateral force, only worsening the instability. As a result, the ram was only used to apply tensile forces, and all fatigue stresses at the top fibers of the masts were tensile.



Figure 2.3 Portal Loading Frame



Figure 2.4 MTS 55 kip Hydraulic Actuator

This tension-only fatigue loading is not representative of high masts in the field, where vortex shedding oscillations can create a full stress reversal at the weld (equal valued tensile and compressive stresses). A fully tensile stress range, however, can be seen as a more severe load case and hence a lower bound estimate for fatigue life. Moreover, the relative performance among different details is still maintained under this non-ideal loading scenario, provided that all masts are tested identically.

### 2.2.1 Load Box and Connection

The two masts were connected back-to-back using a built-up steel loading box that was designed during Phase I. A schematic of this loading box is shown in Figure 2.5. The faces of the box were drilled to accommodate the anchor rod and double-nut connection commonly used in the field. This connection was included in the setup as it plays a strong role in the overall flexibility, and hence fatigue performance, of the mast-to-base plate connection.

The box was designed to be very stiff so as to minimize relative displacement among the anchor rods and accurately model the effect of a high mast foundation. A 2-inch internal plate helped provide additional stiffness to the loading box.

The box was fabricated using 3-inch steel plate and welded on site at J. J. Pickle Research Campus. It was drilled with 1-7/8" holes sized to accommodate the 1-3/4" threaded rod used to connect the box to the high mast base plate. These holes were drilled in bolt circles for both eight-bolt and twelve-bolt configurations. Two bolt circle diameters were drilled, a 30-in diameter circle for Phase I and Phase II specimens, and a 36-in diameter circle for potential future testing.

The double-nut connection was consistent with field-installed high masts where threaded rods are embedded into a concrete footing, and heavy-hex nuts are used in tandem to both level and secure the mast. See Figure 2.6 for a picture of the connection and a description of the nomenclature used to differentiate the nuts.



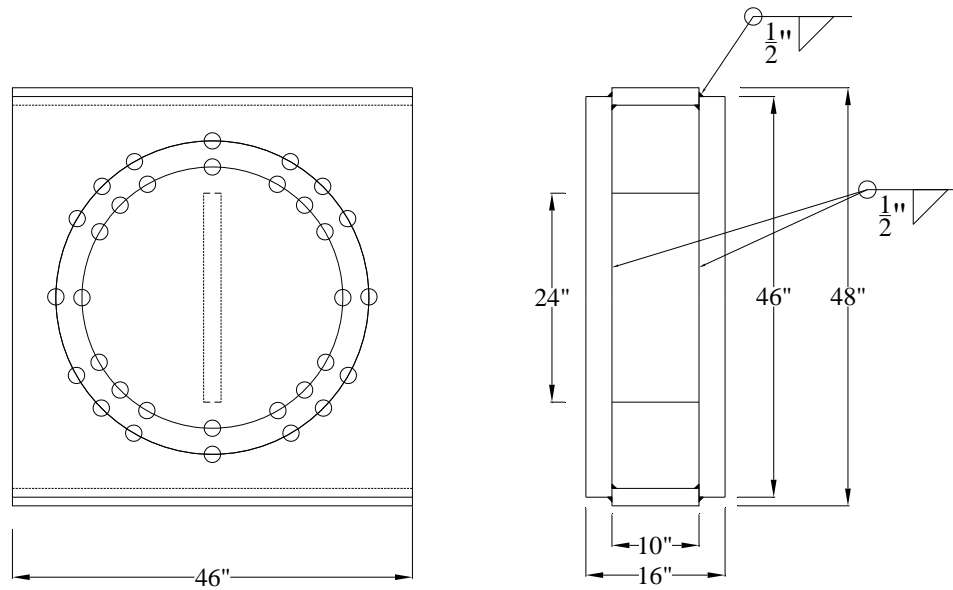


Figure 2.5 Loading Box (Rios, 2007)

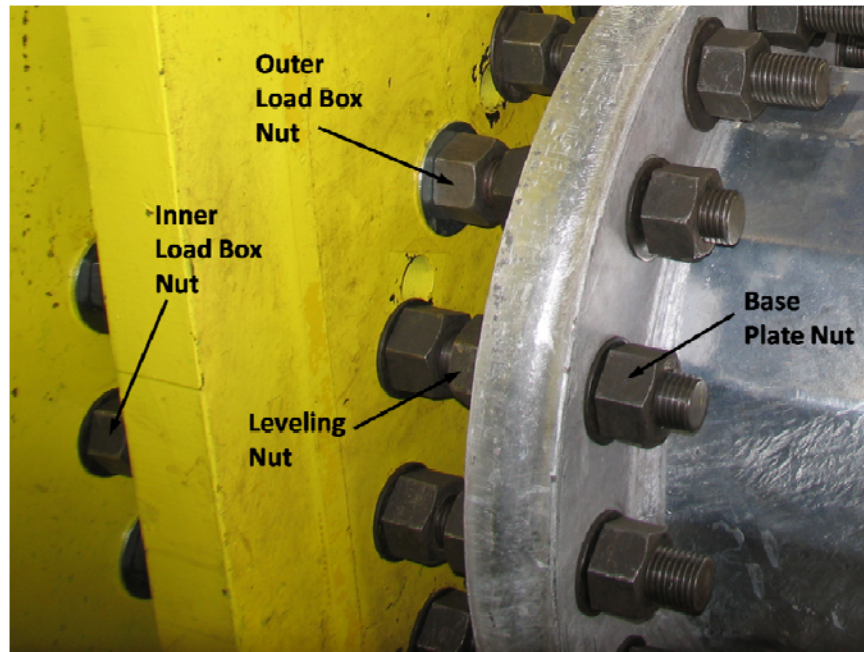


Figure 2.6 Double-Nut Connection and Nomenclature

### 2.2.2 Hydraulic and Control Systems

Tension forces were applied using a 55-kip MTS hydraulic actuator (Model 244.31), and measured with an in-line 55-kip MTS load-cell transducer (Model 661.22C-01). Hydraulic pressure for the actuator was supplied by an MTS SilentFlo Hydraulic Power Unit operating at 3000-psi with a capacity of 90-gpm. Connected in-line with this hydraulic system were two servo-valves manufactured by Moog Controls (Model 72-103). Additionally, an MTS 293 Hydraulic Manifold was used to control flow and reduce pressure fluctuations in both the pressure and return lines for the system.

A closed-loop control system was used to generate the cyclically-varying fatigue loads. This type of controller monitors the inherent disparity (the “error”) between the command and response signals for a dynamic system. It then uses this error to continually adjust the command signal through a closed feedback loop.

This updating is physically accomplished by the servo-valves, which were connected in parallel with each other and in series between the pump and actuator. The servo-valves actively regulate the pressure delivered to the ram and thus generate the cyclically-varying forces. An MTS FlexTest SE Controller was used as the control unit for this closed-loop system, and for an improved user interface, it was operated through a Hewlett Packard 2.66 GHz PC.

The MTS FlexTest controller maintains a constant testing frequency under which prescribed maximum and minimum loads are cycled. Phase I researchers, concerned whether dynamic resonance would be an issue, calculated the natural frequency of the test setup to be 6.7 Hz (Rios, 2007). The loading frequency, they concluded, should then be sufficiently distanced from this natural frequency to prevent dynamic resonance. During Phases I and II, fatigue tests were typically run at frequencies between 1-2 Hz.

### 2.3 Fatigue Testing Considerations

Constant amplitude fatigue loading can be defined by two parameters: the stress range ( $S_r$ ) and the mean stress ( $S_m$ ). During Phase I testing, 12-ksi was selected for the stress range and 16-ksi for the mean stress. A stress range of 12-ksi was seen as great enough to produce a finite life, but

not so large as to shorten life to the point of yielding questionable results. Indeed this stress range was large enough. The first Phase I specimens lasted less than 200,000 cycles, a mere half days testing.

Phase II specimens were designed in accordance with the conclusions of Phase I, namely that stiffening the connection could improve the overall fatigue life. Thus to produce a finite fatigue life within a reasonable testing schedule, it was decided for Phase II to test at a range of 18-ksi for all specimens except the stool-stiffened details, which were tested at a 12-ksi stress range. Mean stress was maintained at 16-ksi for Phase II, yielding testing stresses of 7-ksi minimum and 25-ksi maximum.

Unfortunately, this elevating of the stress range to 18-ksi did result in some undesirable side effects. Over the course of testing, three rod-eyes failed by fatigue fractures. See Figure 2.7 for a picture of these fractures. Following the third fracture, the setup was rebuilt with larger rod eyes, which, in addition to lowering the nominal stress with a larger area, were re-machined with radii to decrease the inherent stress concentration (See Figure 2.7). The radii of these larger rod-eyes were also micro-peened using a 3M TC 330 Roto-peener. Micro-peening introduces compressive residual stresses in an effort to further improve fatigue performance. Thus far, these modified rod-eyes have shown no fractures.

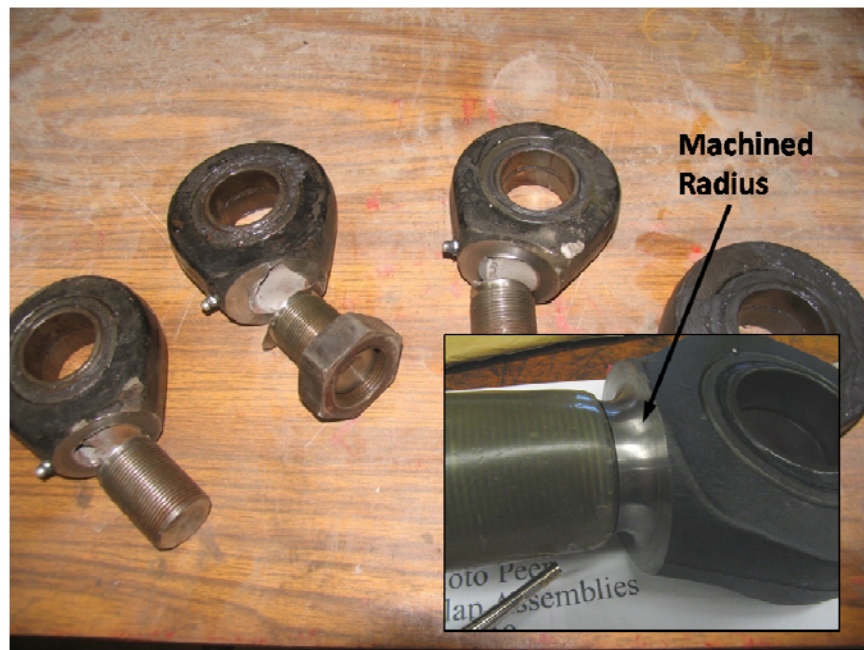


Figure 2.7 Fractured Rod-Eyes and Replacement

In addition to the reaction rod-eyes, top position anchor rods developed full depth fatigue cracks on several occasions. For each of these, the fatigue crack occurred at the first thread on the mast side of the outer loading box nut. In each instance, the test setup was shut down immediately, and the fractured rods were removed and replaced.

Threaded anchor rods and rod-eyes were not the only setup components to show signs of fatigue. During testing of the final set of Phase II specimens, the loading box developed a fatigue crack at the weld connecting the internal stiffener to the inside surface of the north attachment plate. See Figure 2.8 for an image of this crack. In the interest of testing program completion, the overall stiffness of the box was deemed satisfactory, and the final test was completed with the crack in place. At the conclusion of Phase II testing, the box was removed, and the cracked weld was air-gouged and re-welded.

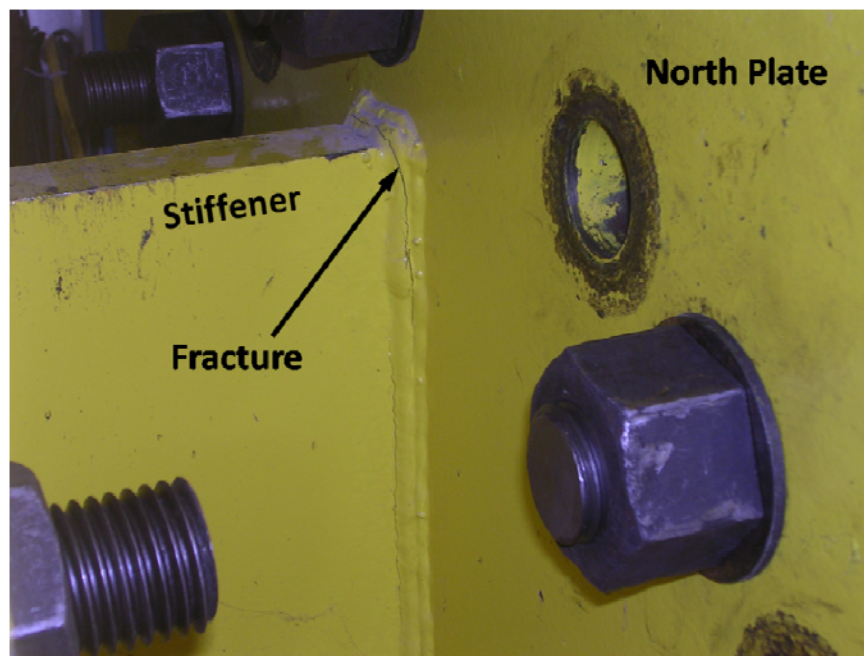


Figure 2.8 Loading Box Fracture

## 2.4 Testing Procedure

The high mast testing procedure had three distinct phases. The process began with specimen measurement and inspection. This was followed by the physical installation of the specimens into the test setup. Finally, necessary loads and displacements were determined, and the test was commenced.

### 2.4.1 Measurement and Inspection

All relevant dimensions of the specimens were measured and documented. This process was completed prior to installation to allow for easier access to the base plate. All dimensions are listed in Appendix B. Measured dimensions included:

1. Overall specimen length
2. Base plate thickness
3. Pole diameter measured to flats
4. Pole diameter measured to corners
5. Pole diameter at 12" from base (flats)
6. Pole wall thickness
7. Weld dimensions (long leg, short leg)
8. Collar length (if applicable)
9. Base plate access hole (if applicable)
10. Stool dimensions (if applicable)

This measurement process was done to both ensure that the specimens had been fabricated as specified and to confirm dimensions for the calculation of sectional properties and nominal loads. Pole diameter was measured at two locations to calculate the specimen taper. All dimensions for Phase II specimens were within specified tolerances.

Pole wall thicknesses were measured using either a Vernier caliper or an ultrasonic thickness gauge. The caliper could only be used if the base plate had been removed with an oxy-acetylene torch, so most thicknesses were measured ultrasonically. The gauge used was a Krautkramer USN 60 NDT device.

This measurement process also provided the opportunity to closely inspect the specimens for any misalignments. On several occasions, the specimens were found to have problems with the alignment of the base plate relative to the end plate. For these specimens, the two plates had not

been indexed properly with one rotated slightly relative to the other, 10 degrees at most. To still allow for testing, the end plates of these samples were re-drilled with properly indexed bolt holes.

#### 2.4.2 Installation Procedure

Due to the awkward shape and unbalanced weight of the horizontally-oriented high masts, the installation process was complex and often a trial-and-error operation. As a result, it was rarely completed the same way twice. Nevertheless, some guidelines for installation were observed over the course of testing, and these are detailed in Appendix A.

The installation procedure for Phase II modifies slightly the Phase I procedure (Rios, 2007), namely by recommending full removal of the pinned-end support during installation, a measure that allows for easier access to the load box for the incoming specimen.

Once a specimen failed, it was removed, flipped over, and used as a servant to allow for the continued testing of its replicate on the other side. Occasionally, this flipped specimen failed again before its replicate. In this event, another sample with similar stiffness was installed so testing could continue.

#### 2.4.3 Testing Loads and Displacements

All high mast specimens were tested under load ranges that created purely tensile stresses along the specimens' top fibers. The longitudinal tension stresses are largest at the weld toe connecting the specimen's base and pole shaft, the invariable location of fatigue cracking. At this spot, the calculated nominal bending stress is amplified by both the inherent flexibility of the connection and the notch effect of the weld toe. This notch effect, common to all fillet welds, was even more severe for welds with steep profiles or undercuts.

The simple elastic bending formula of  $\sigma = Mc/I$  was used to correlate top fiber nominal stresses and bending moments. In this formula,  $M$  is the bending moment at the location of the weld,  $I$  is the section's second area moment (moment of inertia or MOI) at that location, and  $c$  is the distance separating the section's top fiber and centroid. Moment ranges were calculated for the

prescribed maximum and minimum nominal stresses of 7 and 25 ksi and converted to loading ranges using the horizontal distance separating the loading location and weld toe. The moment  $M_1$ , shown in Figure 2.9, is the nominal moment used to calculate the desired load range.

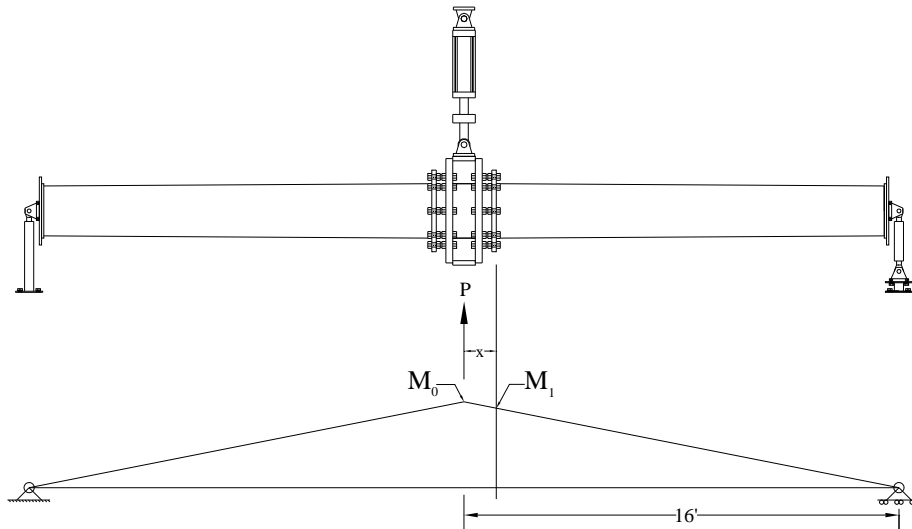


Figure 2.9 Moment Diagram for Calculating Testing Loads (Rios, 2007)

For a given symmetrically-applied load  $P$ , the maximum moment,  $M_0$ , induced in a simply-supported beam of length,  $L$ , occurs at the center and is valued at  $PL/4$ . This maximum moment drops linearly to either side of the beam's center (see Figure 2.9), thus the corresponding moment at some distance,  $x$  in feet, is a proportion of the maximum value:

$$M_1 = \frac{16 - x}{16} M_0 = \frac{16 - x}{16} \frac{PL}{4}$$

For the case of the high mast setup, the horizontal distance,  $x$ , depended on the stand-off length and base plate thickness, but was typically about a foot.

Sectional properties of the tested high masts were calculated assuming nominal dimensions. External collars and backing rings were not included in sectional calculations. Typically, these components measured less than a foot in length and were not physically long enough to participate in the bending response.

The drafting software AutoCAD 2007, through the use of its “massprop” function, was used to determine the MOI and top fiber distance,  $c$ , corresponding to specimen nominal dimensions. For the typical specimen, these were 1664-in<sup>4</sup> and 12.2-in, respectively. For purposes of comparison, the MOI formulation for thin-walled circular sections with 24-in diameters and 5/16-in thicknesses ( $0.39 \times d \times t^3$ ) yields 1631-in<sup>4</sup>.

Assuming a nominally-dimensioned specimen and an 18-ksi nominal stress range, the resulting testing loads were  $P_{\min} = 10.7$ -kips and  $P_{\max} = 38.3$ -kips. Given the fact that measured dimensions varied little, a majority of specimens were tested at or very near these loads. Full documentation of load ranges for all specimens is contained within Appendix C.

All high mast fatigue tests were executed under displacement control. While load control seems a more ideal choice, closed-loop systems tend to be unstable while in this testing mode. Note that, due to this decision, the measured dynamic loads will be less than what is specified due to inertial effects. The actual loads exerted on the specimens, however, will be correct provided the displacements are maintained.

Determining the testing displacement ranges was accomplished by manually moving the ram until the desired loads were observed. The corresponding displacements were recorded and testing was commenced with the ram cycling between them.

Testing would then proceed at a low frequency, 0.1 to 0.2 Hz, to allow the base plate and end plate connections to settle and self-adjust. This slippage would cause the load range to drop, so the setup was monitored closely during this time, and the displacement range was repeatedly adjusted to maintain the proper load range. Once the loads settled, the testing frequency was raised to its final value of 1-2 Hz, and the test would fully commence.



### 3 Test Specimen Design

#### 3.1 Introduction

The design choices for Phase II high mast connection details were made based on the conclusions of previous research at the University of Texas and elsewhere. This influencing work included Phase I testing of high masts (Rios, 2007), the concurrent testing of traffic signal mast arms at the University of Texas (Anderson, 2007), and finite element parametric studies performed on high mast models at Lehigh University (Warpinski, 2006).

The joint conclusion of these testing programs and parametric studies was that fatigue performance is directly tied to the rotational flexibility of the base plate connection. High flexibility leads to increased local bending of the pole wall immediately adjacent to the weld, which in turn elevates the stresses at the weld toe. Connection rotational flexibility is dependent on a large number of parametric variables. These include base plate thickness, base plate inner diameter, number of anchor rods, choice of connection and weld detail, and the presence of stiffening collars or stools.

The chief parametric variables in Phase I were base plate thickness, number of anchor rods, and the use of a stool or full penetration detail as alternatives to the typical fillet-welded socket detail. See Table 3.1 for the Phase I specimen matrix.

Table 3.1 Phase I Specimen Matrix (Rios, 2007)

Base Plate	Weld Detail	# Specimens	
		8 Rods	12 Rods
1.5-in	Fillet Welded Socket	2	2
2-in	Fillet Welded Socket	2	2
	Full Pen (WY)	2	
2-in (with stools)	Fillet Welded Socket	2	
3-in	Fillet Welded Socket	2	
	Full Pen (TX)		2

The most important conclusions of Phase I were that fatigue performance can be greatly improved by increasing the base plate thickness to 3-in, increasing the number of anchor rods from eight to twelve, and using a stiffer full penetration or stool detail in lieu of the conventional fillet welded socket (Rios, 2007).

In response to these results, all Phase II high masts, with the exception of the stool details, had 3-in base plates and used at least twelve anchor rods. Additionally, in response to the improved results for non-socket type details in Phase I, a majority of Phase II details incorporated the use of full penetration welds or stools.

The concurrent research on traffic signal mast arms at the University of Texas revealed that the use of a stiffening collar can improve fatigue performance in those structures (Anderson, 2007). For mast arms, these collars were placed around the shaft immediately adjacent to the arm's base plate. This finding led to the addition of collars to several Phase II high mast details to determine if they would have a similar favorable effect. The collar detail was patterned after the common TXDOT "ground sleeve" detail (TXDOT, 1995).

Analytical finite element research done at Lehigh University on socket connections indicated that pole wall thickness can also play a role in affecting fatigue performance (Warpinski, 2006). For this reason, wall thickness, originally held constant at 5/16-in during Phase I testing, was increased to 1/2-in for one set of specimens in the Phase II testing regimen.

With respect to the organization of Phase II high mast details, three categories have been selected to classify the tested specimens. These categories are fillet welded socket details, full penetration (groove-welded) details, and stool details. Note that for the first two detail groups, sockets and full penetrations, this classification scheme defines the details only by the way in which the specimens' pole shafts are connected to their base plates. This scheme does not have separate categories for specimens with collars and specimens without. Collars were used on both fillet welded socket and full penetration details.

This phase of high mast testing also considered different pole manufacturers. In Phase I, all specimens were manufactured by Valmont Industries, Inc. of Valley Nebraska. In Phase II, seven details were provided again by Valmont, and three more were provided by Pelco Products, Inc. of

Claremore, OK. One of these three Pelco details was identical to a Valmont detail and hence provided a basis for comparison of different manufacturers.

This chapter, following a brief explanation of the naming scheme used for test specimens, will begin with a discussion of typical specimen details, that is, the general characteristics inherent to all tested high mast specimens such as length and taper angle. It will then continue with descriptions of the different details themselves, separated by the aforementioned categories. Finally, tested details will be summarized in a specimen matrix.

### 3.1.1 Naming Scheme

The naming scheme used for high mast specimens in Phase II, similar to the scheme used in Phase I, provided a means for concisely summarizing key geometric details. It is explained through the following figure:

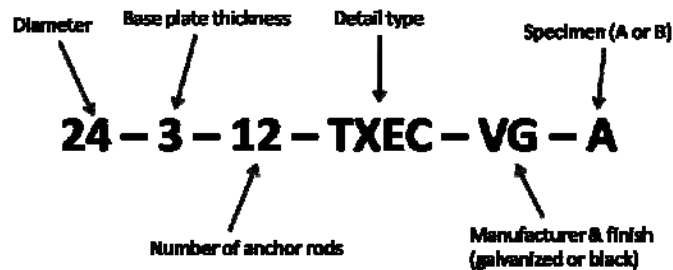


Figure 3.1 Specimen Naming Scheme

### 3.2 Typical Specimen Details

High mast specimens tested at the University of Texas were composed of three main components: base plate connection, pole shaft, and end reaction plate (see Figure 3.2). While the base plate connection was intentionally varied across the specimen catalog to observe fatigue performance, the latter two components were, for the most part, held constant. Exceptions included the thickening of the pole wall in one Valmont detail and pole shaft bend radii. All Pelco specimens were fabricated with much smaller radii than Valmont specimens (see discussion below).

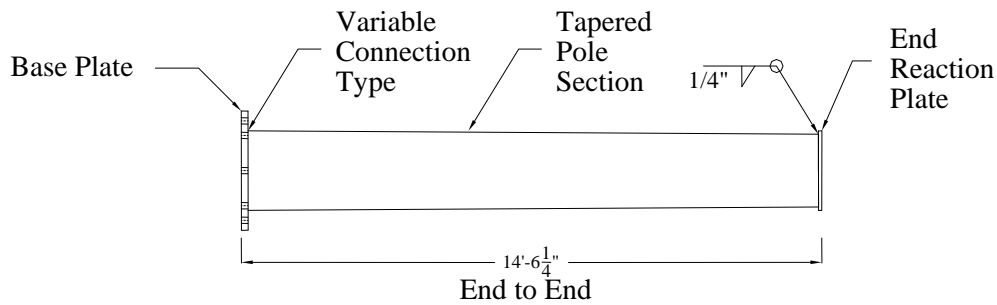


Figure 3.2 Specimen Typical Details (Rios, 2007)

Specimen length was dictated by the test setup length of 32-ft, which, as discussed in Section 2.2, was fixed. The specimen length of 14'-6 1/4" resulted after subtracting from the overall setup length the width of the loading box, the anchor rod stand-off lengths, and the end support lengths.

The pole shafts were sixteen-sided ("hexadecagonal") sections with base diameters, measured out-to-out across flat faces, of 24-in. The pole section was slightly tapered with a change in diameter per foot length of 0.14-in. This taper slope is comparable to those found on in-field masts. The pole wall thickness was maintained at 5/16-in for all specimens, except where deliberately increased to 1/2-in for a single specimen set.

All base plates had outer diameters of 36-in and bolt circle diameters of 30-in. Inner diameters for base plates varied depending on the detail type. In socket-type details, the base plate inner diameter was equal to the pole shaft outer diameter; in full penetration details, it could be smaller. Base plate bolt holes were sized at 1-7/8-in to fit 1-3/4-in threaded anchor rods. A typical base plate schematic is shown in Figure 3.3.

The bends of the polygonal section, which are formed over a shaped mandrel with a press-brake device, varied depending on the manufacturer. All Valmont specimens were fabricated with 4-in typical bend radii. The specimens from Pelco, however, had typical bend radii less than 1/2-in due to a slightly different forming process. According to an engineer from Valmont, it is actually quite difficult to form poles with radii as large as 4-in. The required press brake forces are somewhat large.

A parametric study in this research project investigated the issue of bend radii and the findings are presented in Chapter 6. The analytical results suggested that, for pole sections with sixteen

sides, the difference in stress concentration factor between 4-in bend radii and 1/2-in bend radii is not great. For this reason, the variation among manufacturers should not be a confounding issue.

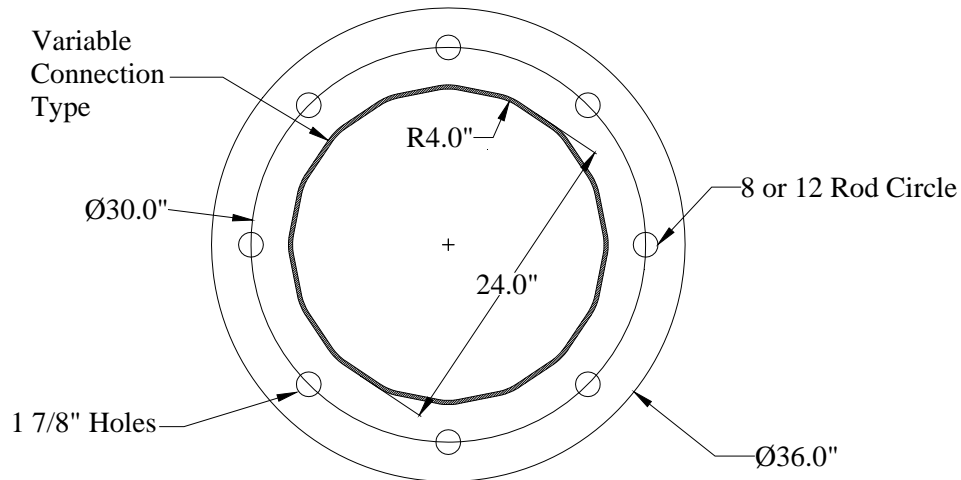


Figure 3.3 Typical Base Plate and Pole Section

With the exception of one specimen set, all high masts were tested with a bend, rather than a flat face, in the top position. This orientation was considered to be more detrimental to fatigue performance given that the bending stresses, which naturally flow toward the anchor rod, will be focused through the shaft's bend, thereby amplifying the stress concentration (see Figure 3.4). A single specimen set with the stool detail was fabricated with a flat face at the top for the express purpose of testing this assumption (24-3-12-STL30-VG, see Section 3.5).

Additionally, all masts were positioned with their longitudinal weld seam in the top position (see Figure 3.4). This too was seen as a more fatigue-critical scenario given that inherent imperfections in the weld metal, especially at the intersection of this weld and the circumferential base plate fillet weld, provide for ample crack initiation sites.

All Phase II specimens were galvanized. Previous findings at the University of Texas suggested that this corrosion-resisting procedure, which is used on almost all in-field steel traffic structures, can reduce fatigue performance (Koenigs, 2003). Galvanizing was thus specified for all specimens in Phase II for fidelity to realistic masts.

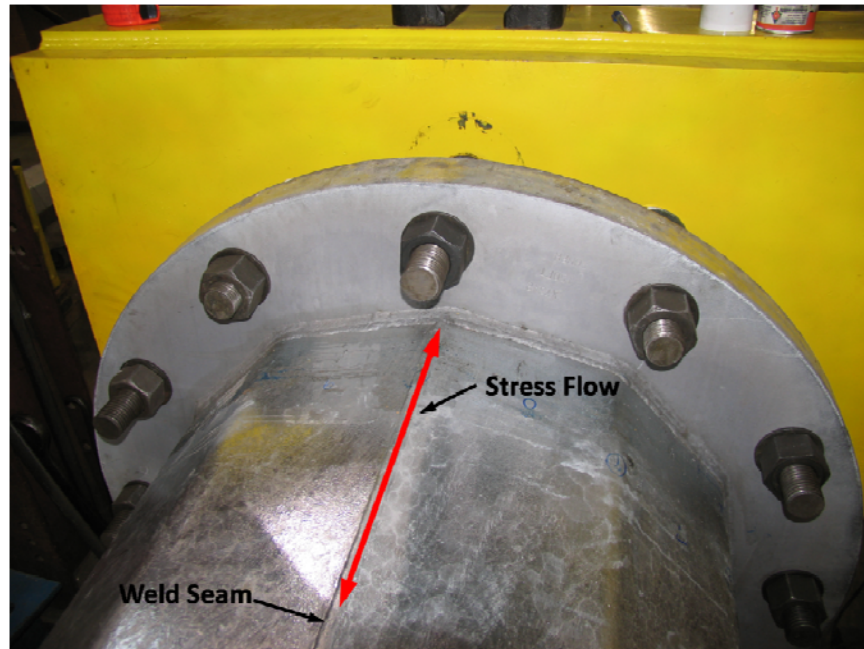


Figure 3.4 Bend and Weld Seam Orientation

Two identical, matched-pair specimens were tested for each type of connection detail (specimens A and B). The test setup naturally required symmetric stiffness, and hence identical specimens, for uniform distribution of load. Furthermore, given that fatigue strength is inherently probabilistic in nature, testing two matched pair specimens, each to failure, yielded more data points and increased experimental confidence.

### 3.3 Socket Details

Due to its relative simplicity, the socket detail is the most common type of base plate connection among pole-type traffic structures. Fabrication is straightforward as the base plate is cut with an inner hole sized to fit an inserted pole shaft, and the two are connected with dual fillet welds. See Figures 3.5 and 3.6 for details of this connection. In spite of its widespread use, this detail has been shown to exhibit relatively poor fatigue behavior, repeatedly performing below an AASHTO E' level (Rios, 2007).

Of note in this detail is the backside equal leg fillet placed within the base plate. This “seal weld,” common in socket details, provides a small degree of structural stiffness to the connection

and also seals the seam between the wall and base plate. It is important to seal this seam to prevent galvanizing slag from becoming entrapped and leading to accelerated corrosion.

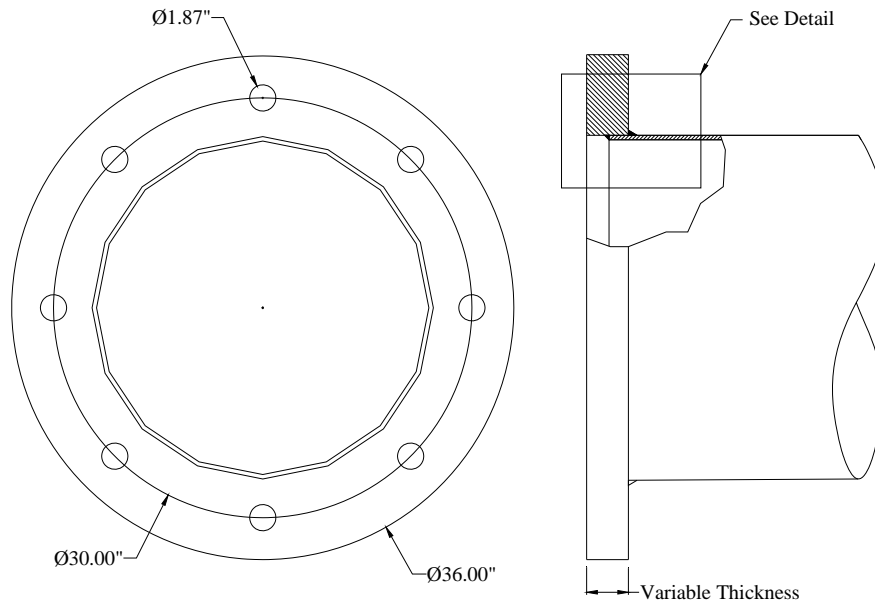


Figure 3.5 Socket Connection (Rios, 2007)

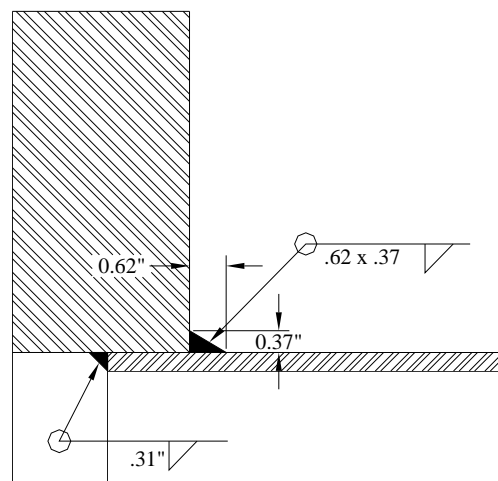


Figure 3.6 Socket Connection Detail (Rios, 2007)

In Phase II, this connection detail was tested with the addition of an external collar. The collar acts as an external stiffener, bracing the portion of the pole wall most prone to local bending and stress concentration. The collar used was 12-in long and 3/8-in thick and was attached to the pole

shaft with unequal leg fillet welds. See Figures 3.7 and 3.8 for schematics of this socket external collar (SEC) connection.

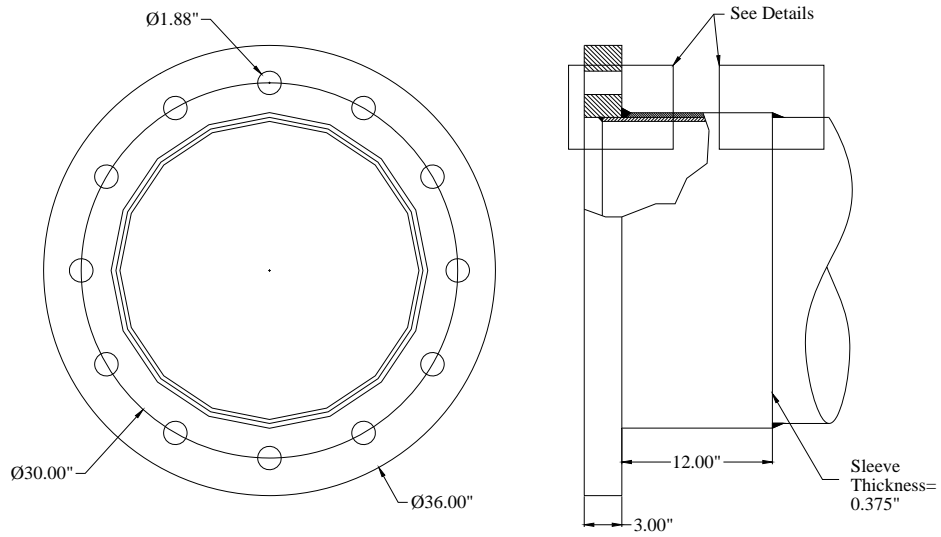


Figure 3.7 Socket External Collar Connection

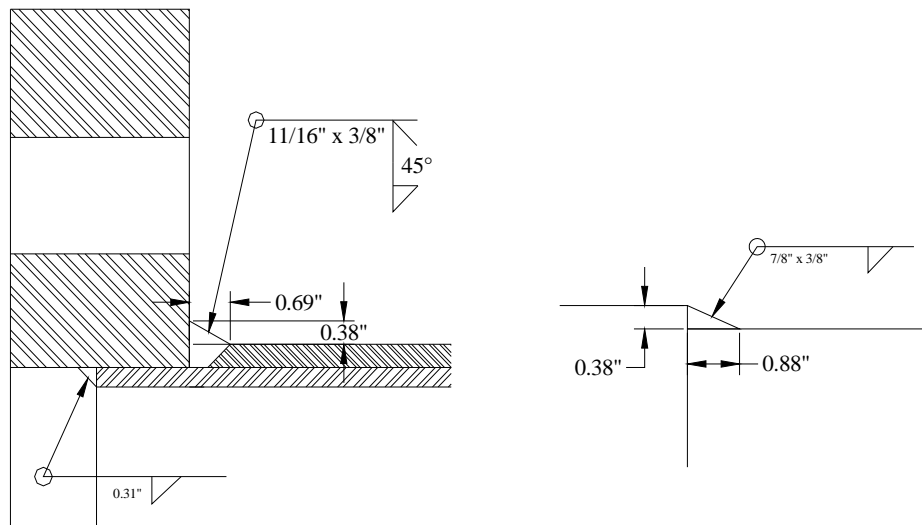


Figure 3.8 Socket External Collar Connection Details



This SEC connection detail was tested for both manufacturers, Valmont and Pelco. The two details were identical with one exception. The Pelco specimens had sixteen anchor rods rather than twelve (Note that only a twelve-rodded detail is shown in Figure 3.7). Analytical research on anchor rods has shown that varying this detail has negligible effect on stress concentrations for base plates thicker than 2-in (See Chapter 6). Therefore, comparisons of fatigue performance between the two manufacturers should not be compromised by this difference.

### 3.4 Full Penetration Details

The use of full penetration welds in high mast details leads to inherently stiffer connections when compared to fillet-welded sockets. Typical full penetration details are shown in Figures 3.9 and 3.10. The names used for these details are unique to this project and do not indicate any special relationship to the states in question.

The increased stiffness of full penetration details is a product of two improvements made over the conventional socket detail. First, the load path is made more direct by providing full continuity of weld material between the pole wall and base plate. In both designs shown below, this is done by beveling the pole wall, filling the resulting cavity with weld material, and topping this cavity with a fillet weld. The second way connection stiffness is improved in full penetration details is by allowing a smaller inner diameter for the base plate hole. For these types of details, the only limit on base plate hole size is the practical issue of access. The welder must have adequate room to place the inner fillet welds.

The chief difference between the two full penetration details shown below is the presence of a backing ring in the Wyoming detail. The backing ring allows for the creation of a root opening between the pole wall and base plate, thus increasing the size of the cavity to be filled with weld material and reducing the probability of lack of fusion at the weld's root. This backing ring also stiffens the connection by acting as an internal collar.

As was the case with the socket specimen base plate, the seam created by the backing ring needs to be sealed against corrosive intrusion. This is done by fillet welding the top of the ring to the inside of the pole shaft. In addition to closing the seam, this fillet weld also increases the backing ring's structural participation, boosting, if just slightly, the overall stiffness of the connection.

However, this also means the seal weld will attract stress flow, which renders it potentially susceptible to fatigue cracking. In all analytical models of this connection, however, the seal weld had a lower hotspot stress than the base plate weld (See Chapter 6).

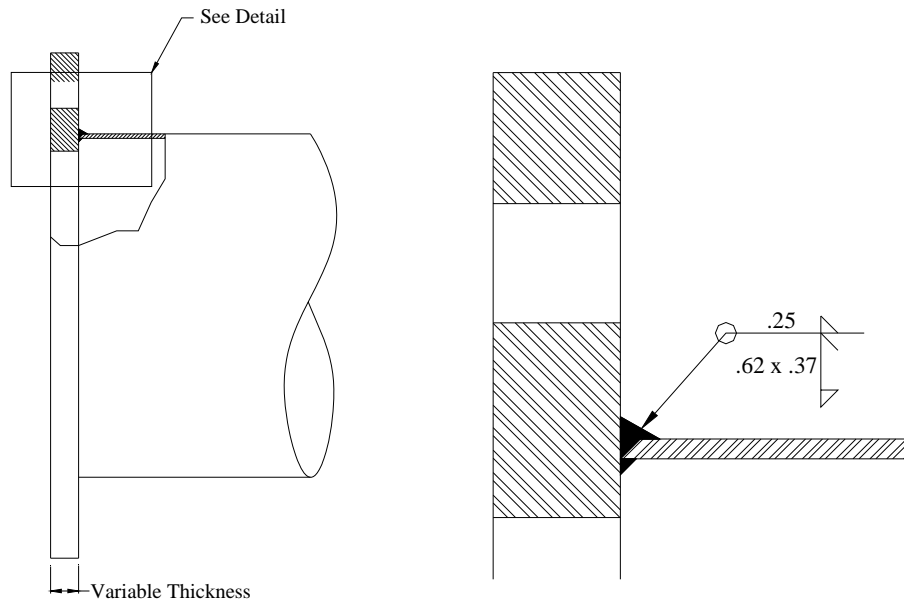


Figure 3.9 Texas Connection Detail

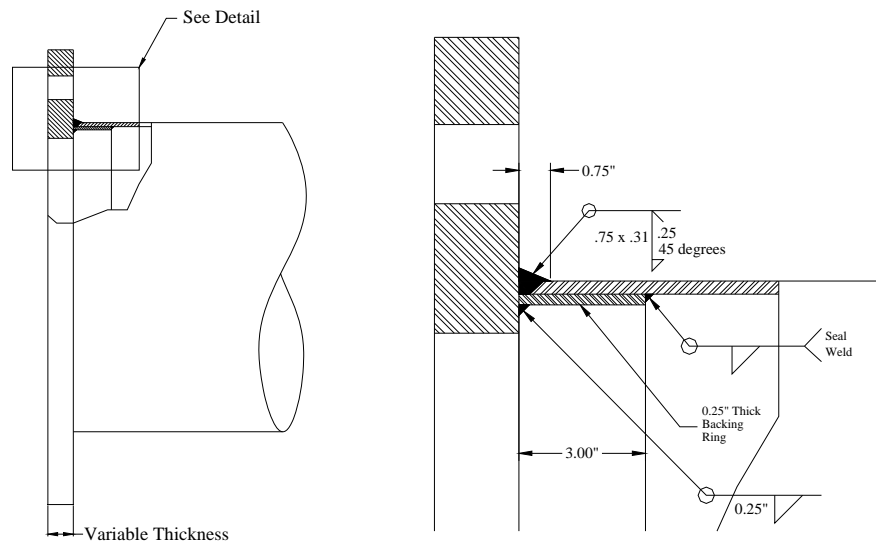


Figure 3.10 Wyoming Connection Detail

Phase I researchers tested one set each of Wyoming and Texas details (See Table 3.1), each with 22.5-in base plate holes. The favorable results from these tests led to further testing of full penetration details in Phase II. For this phase, these details were improved by reducing the size of the inner base plate hole and/or adding external collars.

In Phase II, two full penetration details were manufactured by Pelco, and three full penetration details were manufactured by Valmont. The Pelco details had reduced inner base plate holes and were unstiffened (no collars). Of the three Valmont details, two had external collars and one had a thickened shaft wall. These details were: Texas External Collar (TXEC), Wyoming External Collar (WEC), and Wyoming Thick Wall (WTh).

The Pelco details were identical to the details shown in Figures 3.9 and 3.10 (WY and TX), and had 3-in base plates, 12.5-in inner base plate holes, and sixteen anchor rods.

The Texas External Collar detail combined a Texas type full penetration weld (no backing ring) with an external collar. See Figures 3.11 and 3.12 for schematics of this connection.

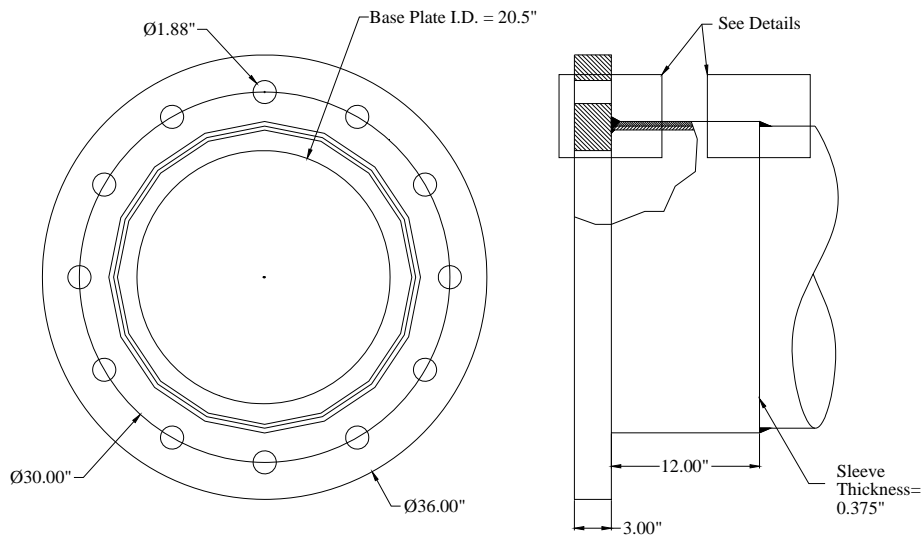


Figure 3.11 Texas External Collar Connection

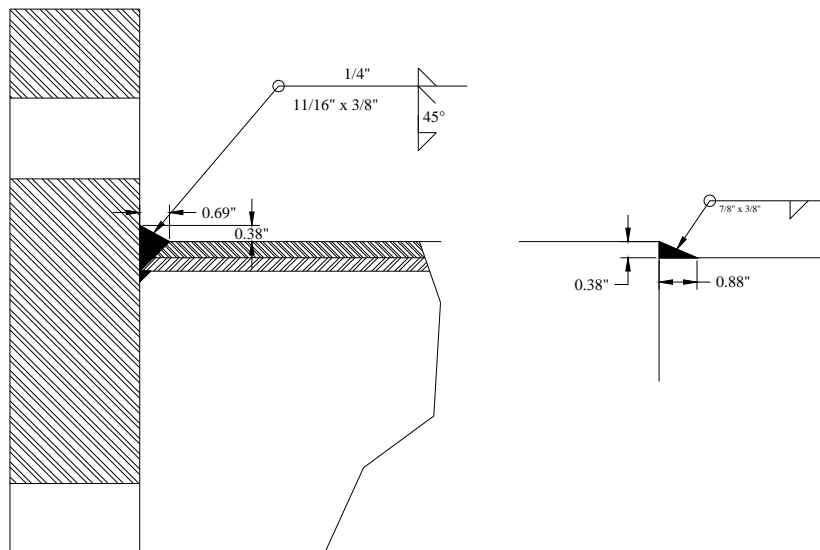


Figure 3.12 Texas External Collar Connection Details

The Wyoming External Collar (WEC) detail improves connection stiffness over the TXEC detail by both adding a backup ring and reducing the base plate inner diameter from 20.5-in to 12.5-in. See Figures 3.13 and 3.14 for details of this connection. Dimensions of the external collar are the same for both specimens.

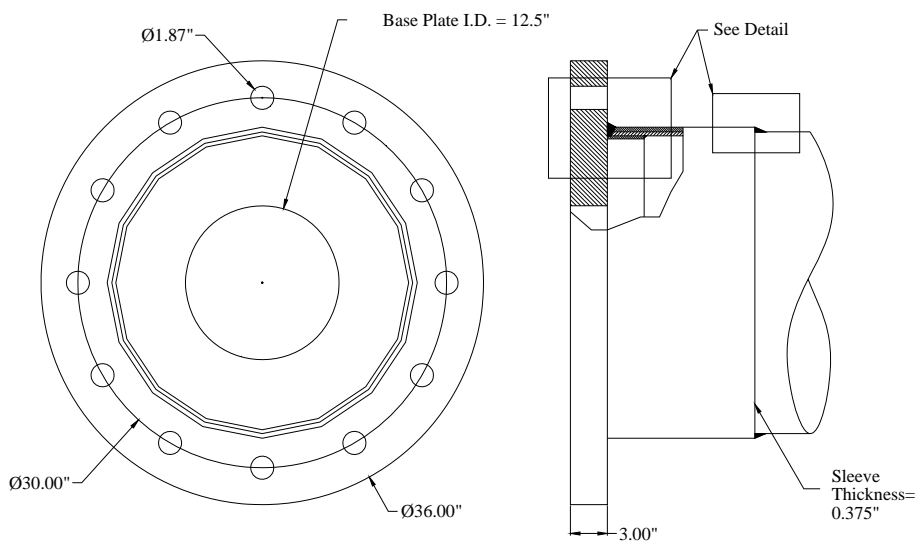


Figure 3.13 Wyoming External Collar Connection

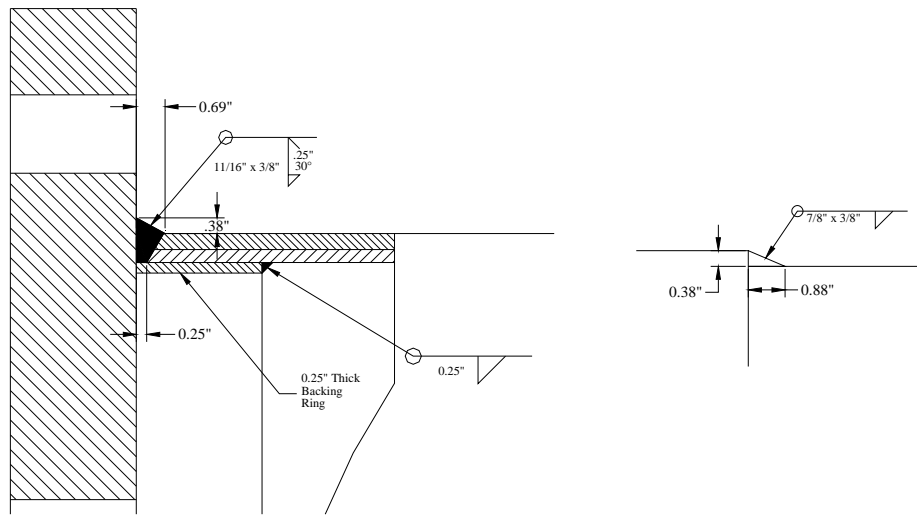


Figure 3.14 Wyoming External Collar Connection Details

The Wyoming Thick Wall (WTh) connection detail takes a conventional Wyoming detail with no external collar and increases the pole wall thickness from 5/16-in to 1/2-in to observe the resulting effects on fatigue life. Like the WEC detail, it has a reduced base plate inner diameter of 12.5-in. See Figures 3.15 and 3.16 for schematics of this connection.

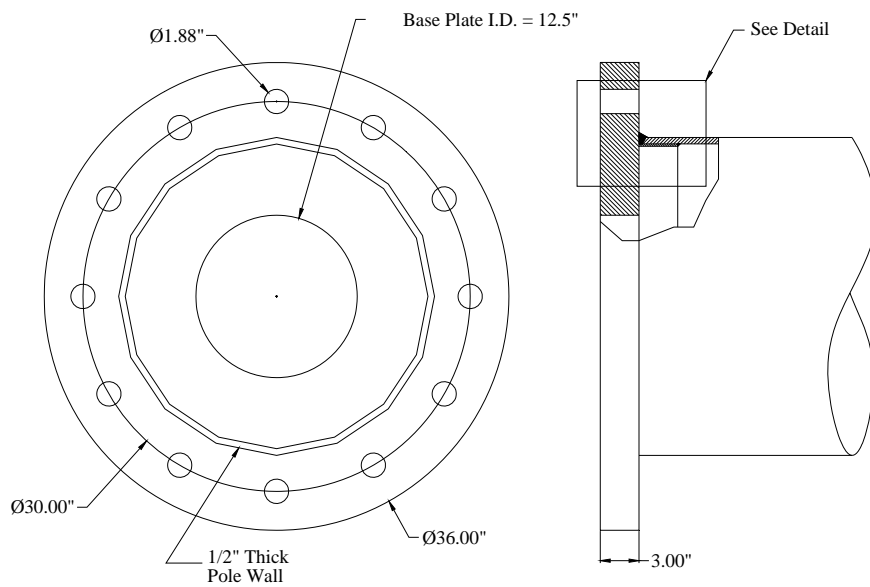


Figure 3.15 Wyoming Thick Wall Connection

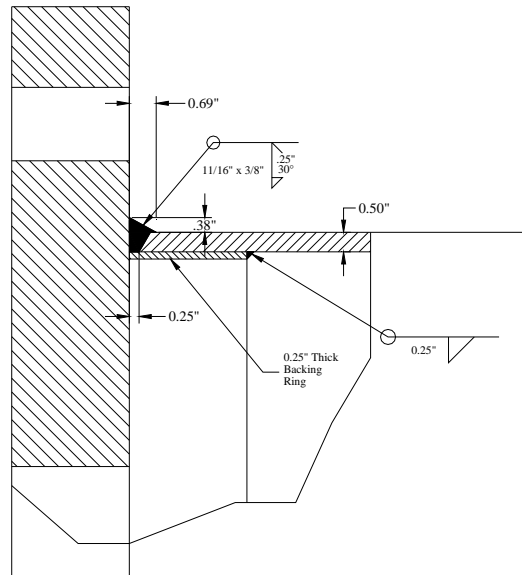


Figure 3.16 Wyoming Thick Wall Connection Detail

### 3.5 Stool-Stiffened Details

In Phase I of high mast testing, a prototype mast detail stiffened with U-shaped ribs was tested (Rios, 2007). The idea for this specimen came from a similarly-detailed mast arm design tested at the University of Texas (Koenigs, 2003). See Figure 3.17 for pictures of both these details. Note that, for this type of high mast connection, the base plate is connected to the pole shaft with a fillet welded socket detail.

This stiffened high mast detail performed well in Phase I, approaching an AASHTO Category E, and it was decided to give it further study during Phase II. For this round of testing, however, the individual cap plates mounted on each set of ribs were exchanged for a continuous ring. It was hoped that through this modification, stresses would be distributed more evenly.

Three sets of stool-stiffened details were tested in Phase II. All had 2-in thick base plates and socket-type base plate-to-pole connections. The differences between these specimens were in their anchor rod numbers and base plate-to-pole shaft orientations. One set had a reduced number of rods, eight rather than twelve. This was done to further investigate the role this variable plays in fatigue performance, particularly in the case of a stool-stiffened connection.

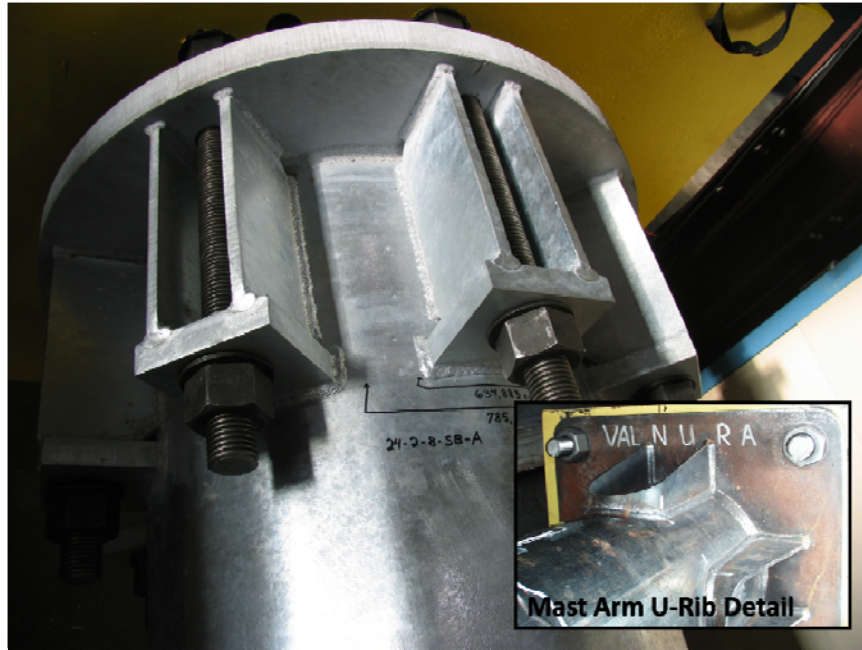


Figure 3.17 Phase I Stool Stiffened Detail

The remaining two sets of stool-stiffened connections both had details with twelve anchor rods, but differed in their orientation of the shaft fold. For one of these sets, the pole shaft was rotated 30-degrees relative to the base plate. This rotation resulted in a flat polygonal face, rather than a bend, in the top position. This was done to test the hypothesis that this orientation is inherently less severe for fatigue. See Figures 3.18, 3.19, and 3.20 for details of these connections.

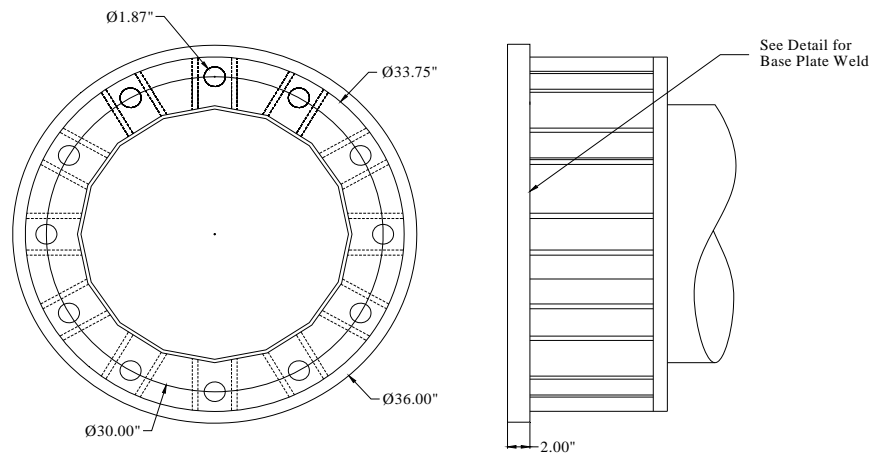


Figure 3.18 Continuous Stool Connection (8-Rod Detail Not Shown)

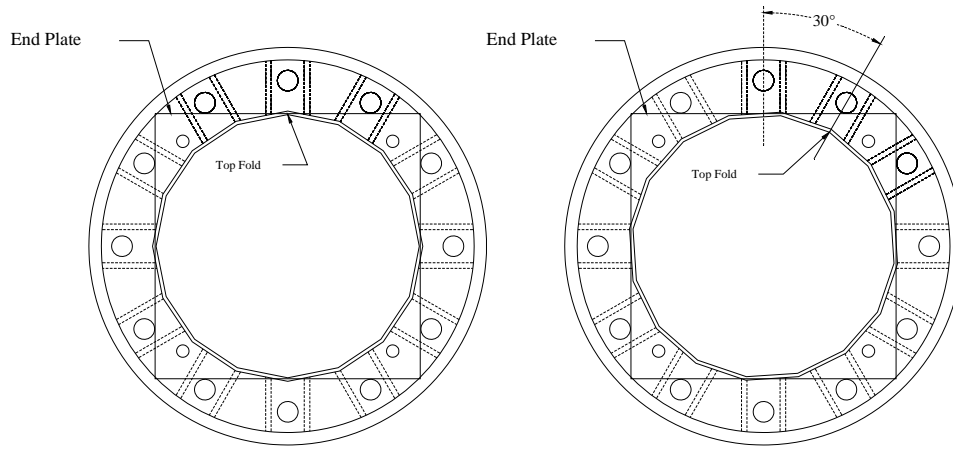


Figure 3.19 Continuous Stool And 30-degree Offset Connections

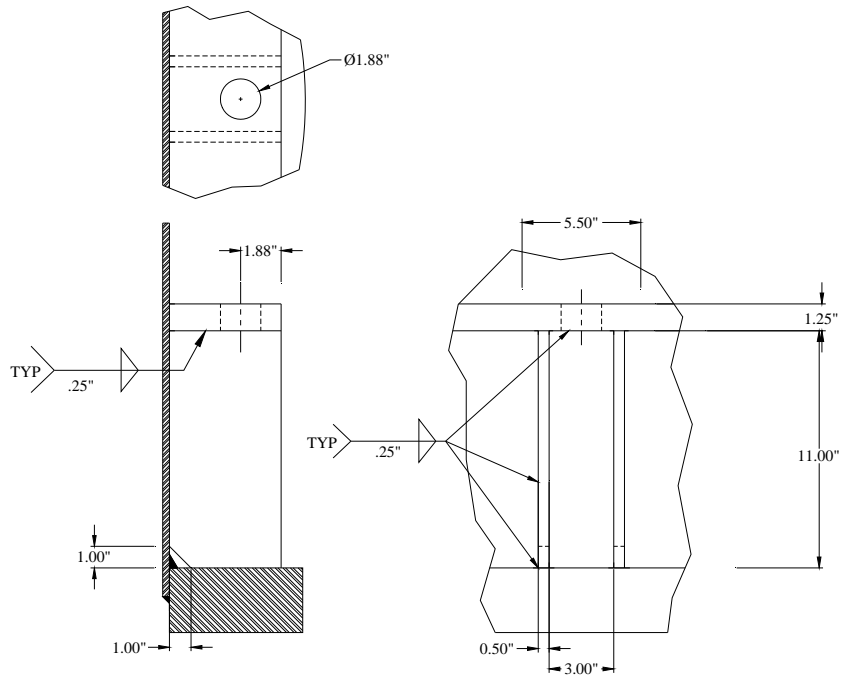


Figure 3.20 Continuous Stool Connection Detail



### 3.6 Summary of Tested Details

The tested details are summarized below.

Table 3.2 Summary of Phase II Specimens

Specimen Name	Connection Detail Name	Manufacturer	Base Plate-to-Pole Weld Type	Stiffening Device	Wall Thick. (in)	Base Plate Thick. (in)	Anchor Rods	Base Plate Inner Diam. (in)	Number of Specimens
24-3-12-SEC-VG	Socket Ext. Collar	Valmont	Fillet Weld	Collar	0.3125	3	12	n/a	2
24-3-12-TXEC-VG	Texas Ext. Collar	Valmont	Full Pen. Weld	Collar	0.3125	3	12	20.5	2
24-3-12-WEC-VG	Wyoming Ext. Collar	Valmont	Full Pen. Weld	Collar	0.3125	3	12	12.5	2
24-3-12-WTh-VG	Wyoming Thick Wall	Valmont	Full Pen. Weld	None	0.5000	3	12	12.5	2
24-2-8-STL-VG	Continuous Stool	Valmont	Fillet Weld	Stool	0.3125	2	12	n/a	2
24-2-12-STL-VG	Continuous Stool	Valmont	Fillet Weld	Stool	0.3125	2	12	n/a	2
24-2-12-STL30-VG	Cont. Stool (30 deg)	Valmont	Fillet Weld	Stool	0.3125	2	8	n/a	2
24-3-16-SEC-PG	Socket Ext. Collar	Pelco	Fillet Weld	Collar	0.3125	3	16	n/a	2
24-3-12-WY-PG	Wyoming	Pelco	Full Pen. Weld	None	0.3125	3	16	12.5	1
24-3-12-TX-PG	Texas	Pelco	Full Pen. Weld	None	0.3125	3	16	12.5	1

## 4 Experimental Results

### 4.1 Introduction

All high mast specimens were fatigue tested in the Ferguson Lab test setup. Nine detail types were considered among two manufacturers, Valmont and Pelco. A total of fourteen Valmont specimens and four Pelco specimens were tested. Note that the four Pelco specimens represented three different details, thus two of these specimens did not have replicates. All Valmont details had replicate specimens. See Table 3.2 for a full specimen testing matrix.

All specimens were tested to failure except one of the Valmont TXEC specimens, which did not crack within a reasonable time frame and was declared a runout (see discussion in Section 4.4). Failure was consistently defined as a 10% loss in overall stiffness (combined stiffness of two back-to-back masts) resulting from a growing fatigue crack in one or both of the specimens.

Given that the cyclic fatigue loading was executed in displacement control, this failure definition was equivalent to a 10% drop in the measured forces. The MTS controller was able to continually monitor these forces and automatically terminate the test when the 10% threshold was crossed. This failure definition typically resulted in cracks ranging from about 1-ft to 2-ft in length (see examples in Figures 4.2 - 4.4).

Once a specimen developed a full-length crack, testing of its un-fractured replicate was continued by reinstalling the fractured specimen in a 180-degree rotated orientation. Once reinstalled, the fractured specimen's crack would be below its neutral axis (now a region of compression), and the fracture surfaces would simply bear against each other. This process would return the fractured specimen to its original flexural stiffness and provide for symmetric load distribution.

The manner in which all fractures initiated and grew was consistent, though the fracture locations varied depending on the detail (see Section 4.2). All fractures initiated at the top of the poles at a weld toe adjacent to the pole shaft (for example, in Figure 4.1, toes of either the base plate weld or collar weld), then propagated down through the shaft wall (and collar, if present). Crack growth was in the characteristic radial pattern, so once extending fully through the shaft wall, the fracture would grow along the weld toe, propagating circumferentially from either side of the

initiation point. See Figure 4.1 for a schematic illustrating potential fracture locations and the weld detail for a fractured socket external collar connection.

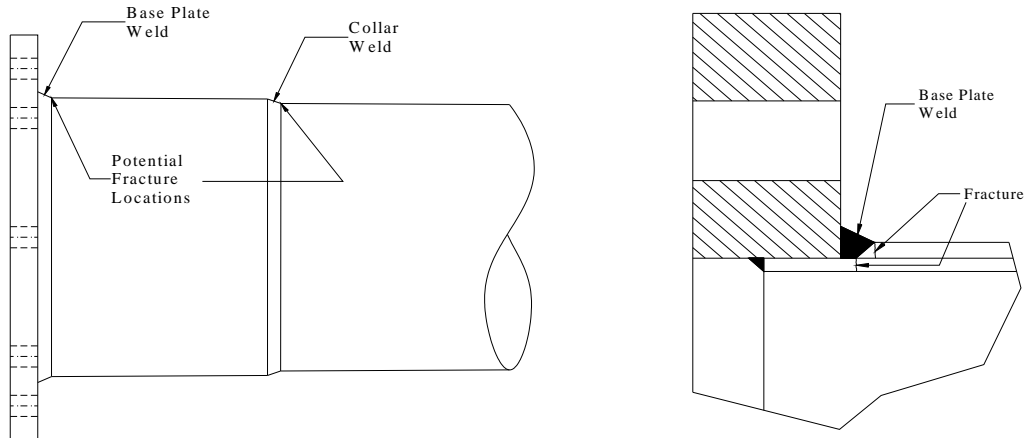


Figure 4.1 Potential Fracture Locations and Weld Detail for SEC Connection

Following a brief discussion of the various fracture locations among the specimens, the experimental results for all fatigue tests in Phase II will be presented. Results are organized according to the same detail categories of Chapter 3:

- Socket Detail (SEC was the only Phase II socket detail)
- Full Penetration Details
- Stool-Stiffened Details

In the forthcoming sections, nominal stress ranges and fatigue lives (number of cycles to failure) are tabulated for the failed specimens. Additionally, the fatigue coefficient,  $A$ , is calculated and tabulated for each failure. This coefficient allows for a direct comparison among details with different nominal stress ranges and is derived from the Paris power law describing the general fatigue response of metals. The fatigue coefficient is directly proportional to the performance of a test specimen. It is calculated as follows ( $S_r$  = nominal stress range,  $N$  = fatigue life):

$$A = N \times S_r^3$$

Each specimen's fatigue coefficient is also correlated to an AASHTO fatigue category. These categories range from E' to A and are defined in Table 4.1. These design fatigue categories are based on empirical testing of established connections and represent lower bounds of the data.

Table 4.1 AASHTO Fatigue Categories

AASHTO Fatigue Category	Design Fatigue Coefficient, A
A	$250 \times 10^8$
B	$120 \times 10^8$
C	$44 \times 10^8$
D	$22 \times 10^8$
E	$11 \times 10^8$
E'	$3.9 \times 10^8$

Following the presentation of individual results for all Phase II specimens, fatigue results for both phases of high mast testing will be discussed and summarized in S-N fatigue life plots.

#### 4.2 Fracture Locations

Among unstiffened specimens (no external collars or stools), the invariable location of cracking was the toe of the fillet weld which connected the base plate and pole shaft (called the “base plate weld”). Figure 4.2 shows a typical fracture of this type. Phase II unstiffened details included Wyoming (WY), Texas (TX), and Wyoming Thick Wall (WTh).

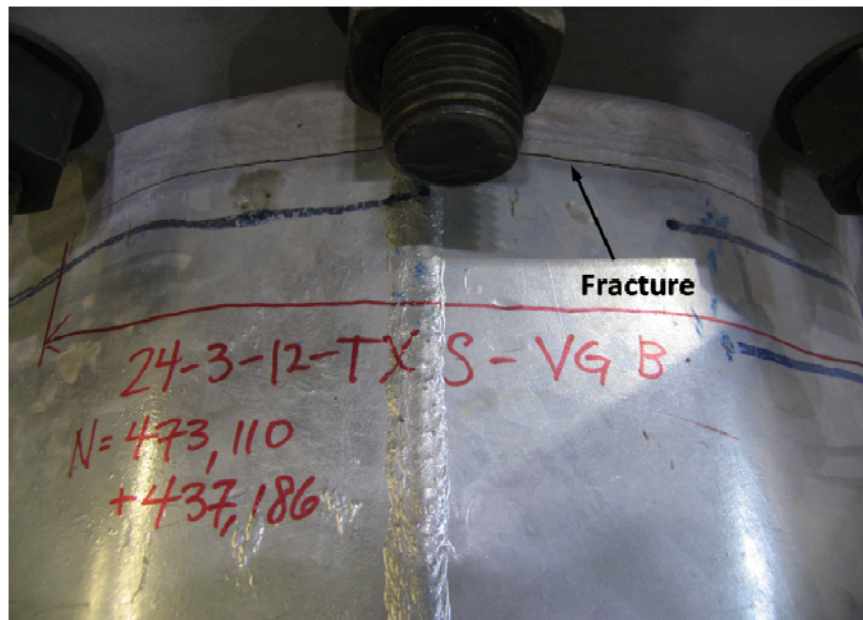


Figure 4.2 Base Plate Weld Fracture

For specimens with external collars, the fracture locations varied. Depending on the relative stress concentrations in the connection, initiation could occur at either the base plate weld toe (similar to the crack in Figure 4.2) or the collar weld toe, as shown in Figure 4.3.

All Valmont Socket External Collar (SEC) and Texas External Collar (TXEC) specimens developed fractures at the toes of their base plate welds, which would suggest that the hotspot stress at this location exceeded that at the top of the collar in both of these details, a fact confirmed by the analytical models (See Chapter 6).

The Pelco SEC specimens, which were nearly identical to the Valmont SEC specimens, both formed cracks at their collar welds instead (see Figure 4.3 for an image of this crack location). It was discovered that these specimens, unlike the Valmont specimens, had been improperly fabricated with equal leg fillet welds at their collars, which heightened the hotspot stresses there. See Section 4.6.1 for a detailed discussion of this issue.

Both Wyoming External Collar (WEC) specimens developed fractures at their collar welds. This connection detail is inherently stiffer than the SEC and TXEC details due to its backing ring and reduced base plate inner diameter. This high level of stiffness moves the critical hotspot from the base plate weld to the top of the collar. See Figure 4.3 for an image of this crack location.

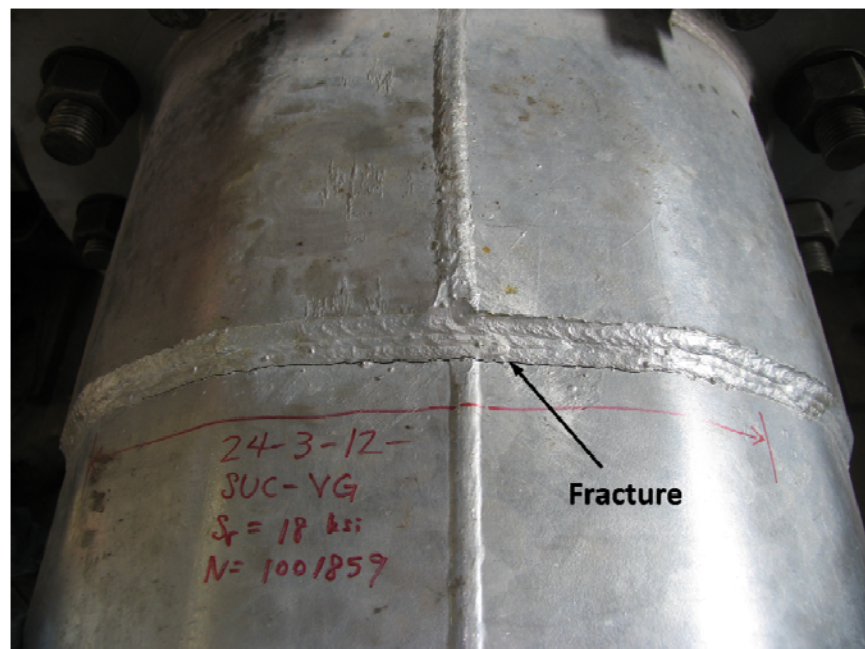


Figure 4.3 Collar Weld Fracture

All stool-stiffened specimens developed fractures at the fillet weld toe along the top of the stool (See Figure 4.4). Similar to the WEC detail's collar effect, the presence of the stool in these details increases the rotational stiffness of the connection and shifts the hotspot, and hence crack, away from the base plate.

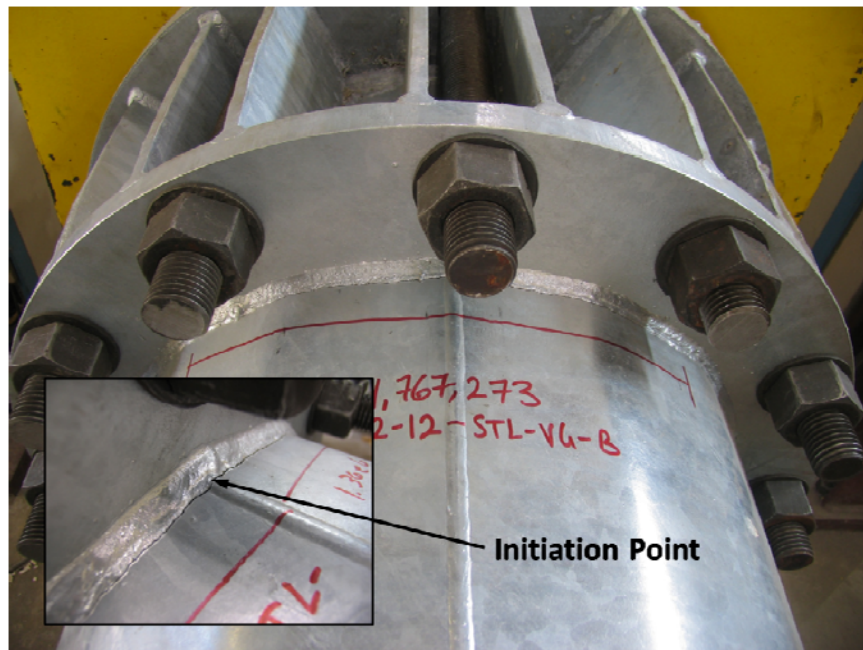


Figure 4.4 Stool Detail Fracture

#### 4.3 Results for Socket Details

The only socket details tested in Phase II were the SEC connections from each manufacturer, Pelco and Valmont. These details were identical except for number of anchor rods. Pelco's detail had sixteen, and Valmont's had twelve. An analytical study on anchor rods revealed that, for base plates thicker than 2-in, there is no stress concentration difference between specimens with twelve and sixteen rods (see Chapter 6). Both of these details had 3-in nominal base plates.

Both Valmont specimens developed fractures at the toes of their base plate welds (as in Figure 4.2). Both Pelco specimens developed fractures at their collar weld toes (as in Figure 4.3). The cause of this disparity was mentioned briefly in the previous section and will be discussed further



in Section 4.6.1. All fractures initiated at the tops of the specimens then propagated through the shaft wall and along the weld toe in both directions.

See Figure 4.5 for a section of a Valmont SEC weld. The surface of this cut, which shows both the weld profile and through-thickness fracture, has been polished and etched with a nitric acid solution to reveal the weld fusion lines. A similar section of a Pelco specimen was not available.

All specimens were tested at a nominal stress range of 18-ksi. The Valmont specimens developed fractures within around 400,000 – 500,000 cycles. The Pelco specimens did not last as long and failed at about 100,000 cycles. Fatigue lives are summarized in the following table:

Table 4.2 Fatigue Results for Socket Detail Specimens

Specimen	Nominal $S_r$	Life, N	A ( $\times 10^8$ )	AASHTO Category	Crack Location
24-3-12-SEC-VG-A	18	540,520	31.5	D	Base plate WT
24-3-12-SEC-VG-B	18	345,542	20.2	E	Base plate WT
24-3-16-SEC-PG-A	18	137,693	8.0	E'	Collar WT
24-3-16-SEC-PG-B	18	95,799	5.6	E'	Collar WT

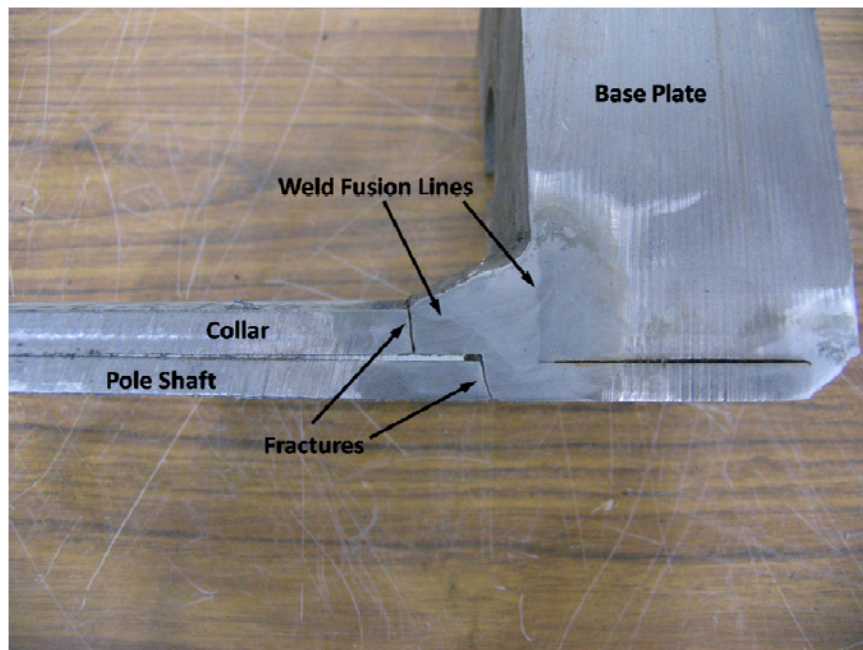


Figure 4.5 Section of Valmont Socket External Collar Connection

#### 4.4 Results for Full Penetration Details

Full Penetration details included the Texas External Collar (TXEC), Wyoming External Collar (WEC), and Wyoming Thick Wall (WTh), Texas (TX), and Wyoming (WY) details. The first three were Valmont details, and the latter two were Pelco details. See Table 3.2 for a matrix summarizing important geometric characteristics of these details. The nominal stress ranges and locations of fatigue cracking for all these details varied.

The Valmont TXEC specimens, the first specimens of the testing program, were cycled at a stress range of 12-ksi. This turned out to be a relatively low stress range for the stiffer details of Phase II, so the first specimen (B) did not begin cracking until about 4.0 million cycles, which at 1.5 Hz, represented 30 days of continuous testing. In the interest of program completion, specimen A was not tested further and was declared a runout specimen. Runouts, not corresponding to an actual failure, simply represent a lower bound for fatigue life.

Cracking in specimen 24-3-12-TXEC-VG-B initiated at the base plate weld toe and propagated through both the collar and shaft wall before growing circumferentially along the weld toe. See Figure 4.6 for a polished and etched section of this specimen's weld. Note that the inner surfaces of both the pole shaft and collar were fused by the heat of the band saw, and their interface is not visible. It is therefore marked with a dashed line.

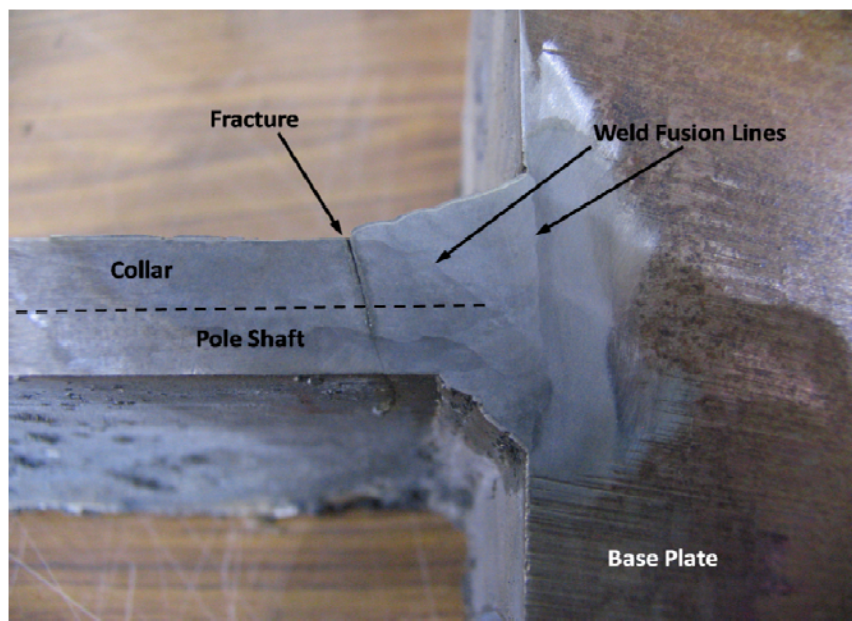


Figure 4.6 Section of Texas External Collar Connection



Following the testing of TXEC details, the nominal stress range was raised to 18-ksi for specimens of comparable rotational stiffness. Specimens with the WEC detail were tested at this elevated stress range, and both developed cracks within about 1.5 million cycles. Cracking initiated not at the base plate weld, but at the top of the collar weld for both specimens (as shown in Figure 4.3). Figure 4.7 shows a polished and etched section at the collar weld, the location of cracking. Notice that this weld is indeed an unequal leg fillet.

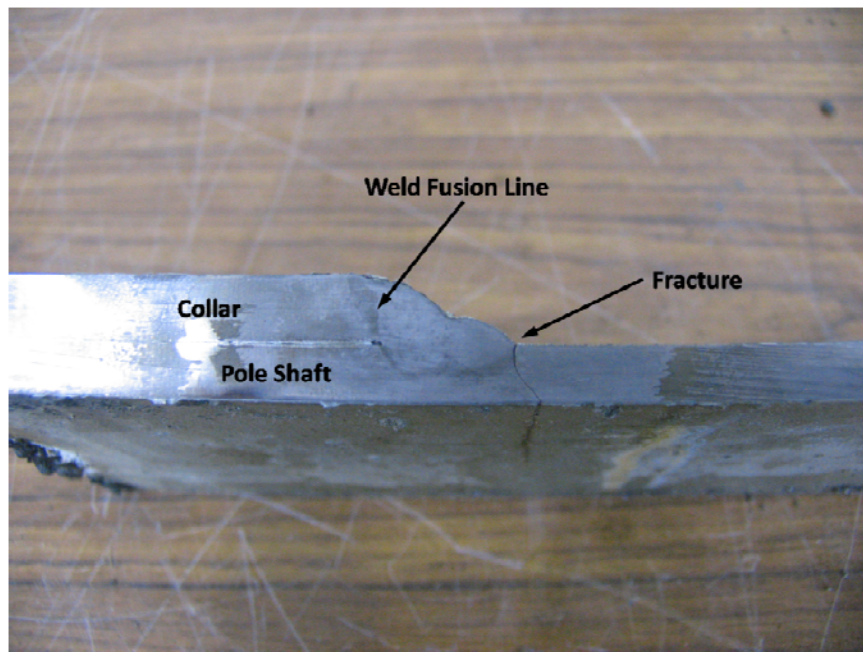


Figure 4.7 Section of Collar Weld in Wyoming External Collar Connection

The Valmont WTh specimens were tested at a nominal stress range of 11.4-ksi. Given that the section modulus for this thick-walled pole is 60% greater than those of the SEC and WEC poles, the hydraulic ram did not have the requisite load capacity for an 18-ksi stress range. The 11.4-ksi stress range resulted from applying the same load range used in the SEC and WEC details. Fatigue cracking for both specimens of this detail type initiated and grew along the base plate weld toe (as shown in Figure 4.2)

This decision to test the thick-walled specimens at the same load range as thin-walled specimens revealed an important quality of thicker-walled masts, namely, the fact that they reduce nominal stresses by offering larger section moduli. In-service high mast towers will also be subjected to

relatively constant load ranges, so by thickening the wall, nominal stress can be reduced and, theoretically, fatigue life increased. High mast poles are routinely fabricated and installed in sections, thus a designer could specify an increased wall thickness for only the bottom section and improve an entire mast's fatigue performance.

The two unstiffened full penetration details provided by Pelco, Texas and Wyoming, did not have replicates and were tested together. They had identical base plate thicknesses (3-in) and identical inner base plate diameters (12.5-in), and their only difference was the presence of a backing ring in the WY detail. It was thus decided that the stiffnesses of these details were symmetric enough to test them together.

Each of the Pelco full penetration specimens were tested at a nominal stress of 18-ksi and developed fractures at their base plate weld toes (as in Figure 4.2). Images of their fractured weld profiles are not included.

Fatigue results for all Phase II full penetration details are summarized in the following table.

Table 4.3 Fatigue Results for Full Penetration Details

Specimen	Nominal $S_r$	Life, N	A ( $\times 10^8$ )	AASHTO Category	Crack Location
24-3-12-TXEC-VG-A	12	4,034,441 <sup>1</sup>	69.7	C	Base plate WT
24-3-12-TXEC-VG-B	12	4,034,441	69.7	C	Base plate WT
24-3-12-WEC-VG-A	18	1,330,470	77.6	C	Collar WT
24-3-12-WEC-VG-B	18	1,001,859	58.4	C	Collar WT
24-3-12-WYTh-VG-A	11.4	862,107	12.8	E	Base plate WT
24-3-12-WYTh-VG-B	11.4	680,613	10.1	E'	Base plate WT
24-3-16-TX-PG	18	238,372	13.9	E	Base plate WT
24-3-16-WY-PG	18	366,092	21.4	E	Base plate WT

1 - Runout Specimen

#### 4.5 Results for Stool-Stiffened Details

All specimens for the three stool-stiffened details were tested at a nominal stress range of 12-ksi. Fatigue lives for all six specimens ranged from about 1 to 2 million cycles. Cracking for each specimen initiated at the fillet weld above the stool and propagated circumferentially along the weld toe (as in Figure 4.4). Figure 4.8 shows a polished and etched section at the crack location of one of the six specimens. See Table 4.4 for a summary of results for all stool-stiffened specimens.

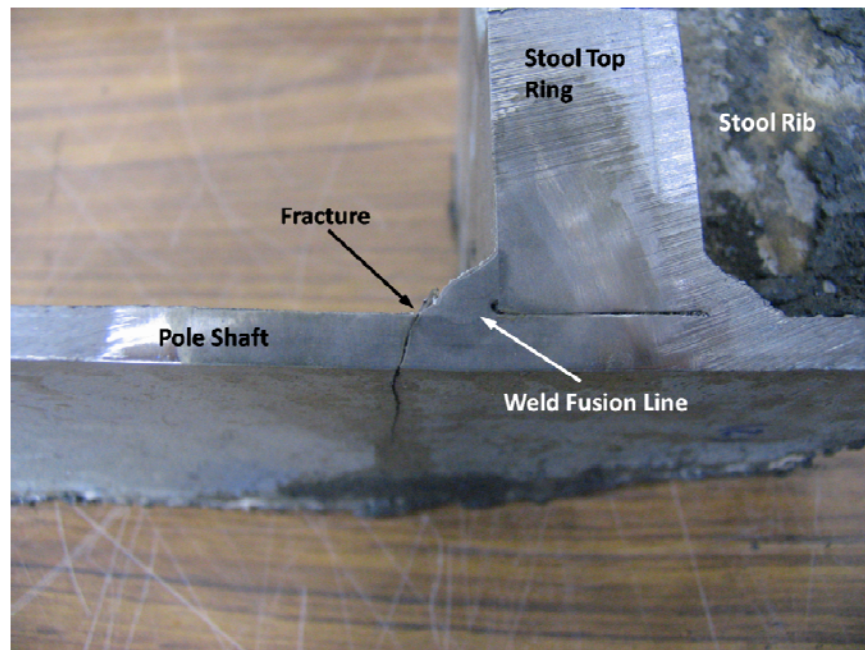


Figure 4.8 Section of Stool Detail Fillet Weld

Table 4.4 Fatigue Results for Stool-Stiffened Details

Specimen	Nominal $S_r$	Life, N	A ( $\times 10^8$ )	AASHTO Category	Crack Location
24-2-12-STL-VG-A	12	2,160,059	37.3	D	Stool WT
24-2-12-STL-VG-B	12	1,680,547	29.0	D	Stool WT
24-2-12-STL30-VG-A	12	2,068,561	35.7	D	Stool WT
24-2-12-STL30-VG-B	12	1,389,066	24.0	D	Stool WT
24-2-8-STL-VG-A	12	1,240,413	21.4	E	Stool WT
24-2-8-STL-VG-B	12	1,357,965	23.5	D	Stool WT

#### 4.6 Results Summary and Discussion

This section will begin with a summary and discussion of all Phase II results. Following this, the results from Phase I will be incorporated where applicable, and separate summaries for different detail types will be presented and discussed.

Fatigue data in this section will be plotted on typical S-N plots. These plots show the relationship between fatigue life (along the abscissa) and nominal stress range (along the ordinate) and are usually graphed in log-log form. All plots include the AASHTO fatigue design categories (A-E') with their respective constant amplitude fatigue limits (these are the horizontal portion of each fatigue category line).

The S-N chart in Figure 4.9 summarizes all Phase II fatigue data for specimens from both manufacturers. The single TXEC runout specimen is marked with a small arrow, which indicates that it would have plotted with greater life, had it been tested to failure.

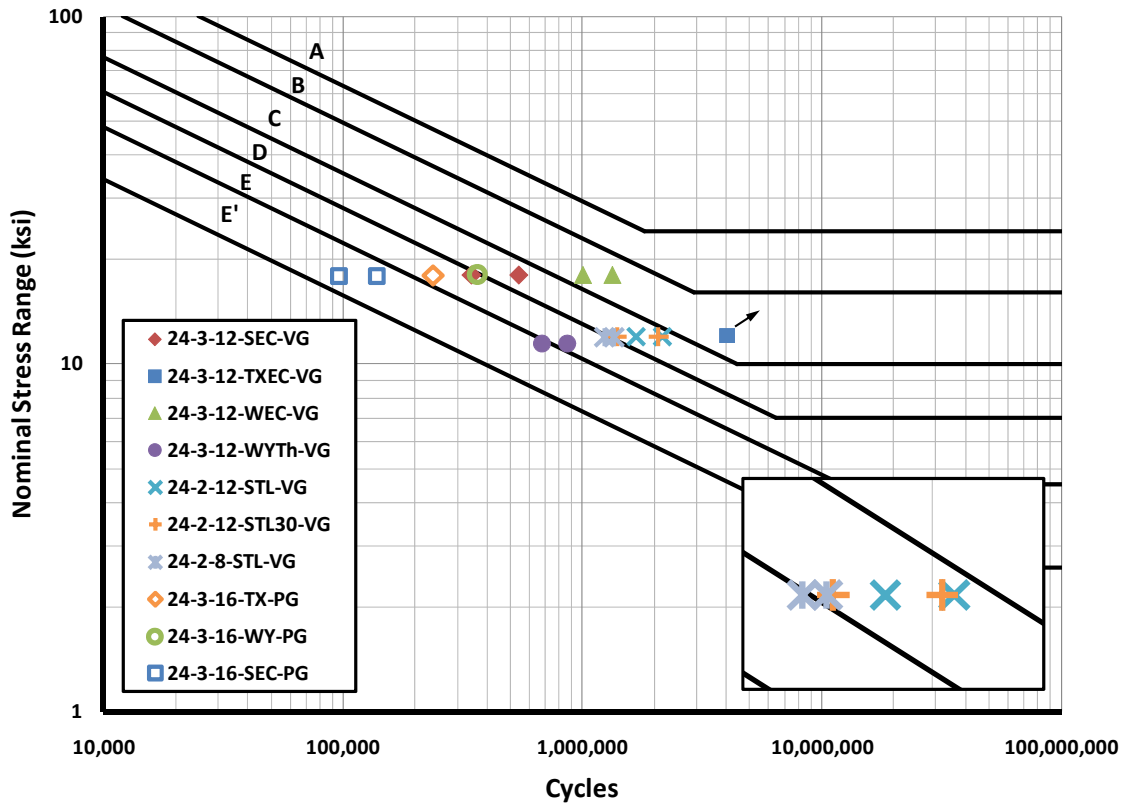


Figure 4.9 Phase II Fatigue Test Results

The Valmont WEC and TXEC details showed the highest performance among all specimens, reaching an AASHTO category C level. These full penetration details, already stiff by virtue of their weld type and reduced base plate hole, are made even stiffer by adding external collars and thus have the highest fatigue performance.

Performances of the two SEC details from different manufacturers were not equivalent. The Valmont SEC specimens attained roughly a Category D level performance, whereas the identical Pelco SEC specimens tested to only a category E' level. Both of these performed better than the unstiffened socket details from Phase I (see Figure 4.11), but their disparity is questionable.

The most plausible cause for this performance difference was revealed by a close examination of the collar weld in the Pelco specimens. Based on AASHTO guidelines, this weld had been specified as an unequal leg fillet sized at 3/8-in x 7/8-in (long leg along the pole shaft). The Valmont specimens had been correctly fabricated with this weld; however, the Pelco specimens had not. Their collar welds were equal leg fillets.

Multiple measurements of the Pelco specimens revealed an average collar weld size of 0.5-in x 0.5-in. See Figure 4.10 for a profile of the collar weld in one of the Pelco specimens. The surface in this image has been etched to contrast the weld and base metals.

Note that the image in Figure 4.10 shows a portion of the shaft wall that was deformed in the galvanizing process due to the expansion of entrapped air between the collar and shaft. This bulge occurred in only one of the Pelco SEC specimens and does not appear to be related to their poor performance.

Early mast arm fatigue research at Lehigh University found that the use of an equal leg fillet weld heightens the stress concentration factor at the top of the arm relative to an unequal leg fillet weld (Miki, 1984). The reduced angle of incidence of the unequal fillet is the cause for this reduction. The use of equal leg fillet welds in the Pelco SEC specimens explains their reduced fatigue life.

Given this explanation for the performance disparity among SEC details, there does not appear to be a significant sensitivity to pole manufacturer, at least when considering masts fabricated by Valmont Industries, Inc. and Pelco Products, Inc.

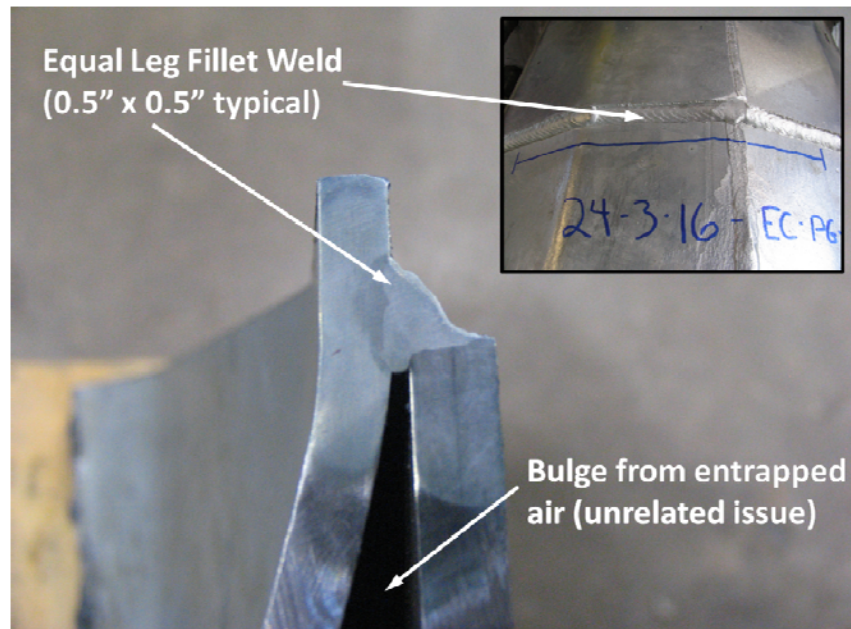


Figure 4.10 Typical Collar Weld in Pelco SEC Connection

In Figure 4.9, the Pelco WY detail slightly outperformed the Pelco TX detail, which is most likely attributable to the presence of its backing ring. Additionally, these two details, which both had 5/16-in thick walls, performed roughly comparable to the Valmont WTh detail, which had 1/2-in thick walls. This suggests that wall thickness potentially plays a reduced role in controlling fatigue performance when compared to other variables.

It is possible, however, that Valmont's WTh specimens failed prematurely. Based on analytical modeling of this connection detail, its SCF was calculated to be 1.8, which is among the lowest of all Phase I and II details. When the fatigue lives of this detail's specimens were plotted against hotspot stress, they were the most significant outliers among all the tests (see Figure 6.9), plotting well below the rest of the data.

This fact suggests that these specimens may have had poorer than average welds leading to lower than expected fatigue life. Unfortunately, sections of these specimen's welds are not available to verify this hypothesis. Thick-walled high mast specimens need to be tested further to characterize how their performance is related to the thickness of their shaft walls.

The three stool-stiffened details in Phase II, all of which had 2-in base plates, performed consistently relative to each other and showed a performance roughly comparable to the Valmont

SEC detail, but still below that of the two collar-stiffened full penetration details (TXEC and WEC).

The negligible difference in results between the STL and STL30 details suggests that the orientation of pole shaft bend has little bearing on fatigue performance. However, it is important to note that this finding is specific to sixteen-sided specimens with bend radii as large as those in the details tested (4-in typical).

The slight improvement in performance shown by the twelve-bolted STL specimens over the eight-bolted STL specimens mirrors the Phase I findings concerning anchor rods in socket specimens, though the benefit in these Phase II stools is smaller.

In Phase I, fatigue performance was greatly improved for socket details of both 1.5-in and 2.0-in base plates when the number of anchor rods was increased from eight to twelve. This fatigue life improvement was on the order of 100-200 % (see Figure 4.10). For the Phase II STL details, however, the average fatigue life improvement is only about 30% when the number of anchor rods is increased. These new Phase II results suggest that increasing the number of anchor rods has a reduced benefit when the base plate connection is already stiffened through other means. This finding was confirmed analytically and will be discussed in Chapter 6, Analytical Results.

#### 4.6.1 Phase I and II Socket Details

Figure 4.11 presents an S-N plot of fatigue data for all socket details from both phases (specimens separated in legend according to phase). Note that, under the Phase I naming scheme, “S” refers to a simple fillet-welded socket detail (Rios, 2007). See Chapter 3, Figures 3.6 and 3.7 for schematics of this connection.

The inclusion of Phase I data in Figure 4.11 reiterates the chief findings for Phase I socket details: fatigue performance is strongly tied to both the number of anchor rods and the base plate thickness. Increasing either will clearly improve performance. However, the Phase I simple sockets still performed very poorly, not even reaching a Category E' level, which is their AASHTO classification.

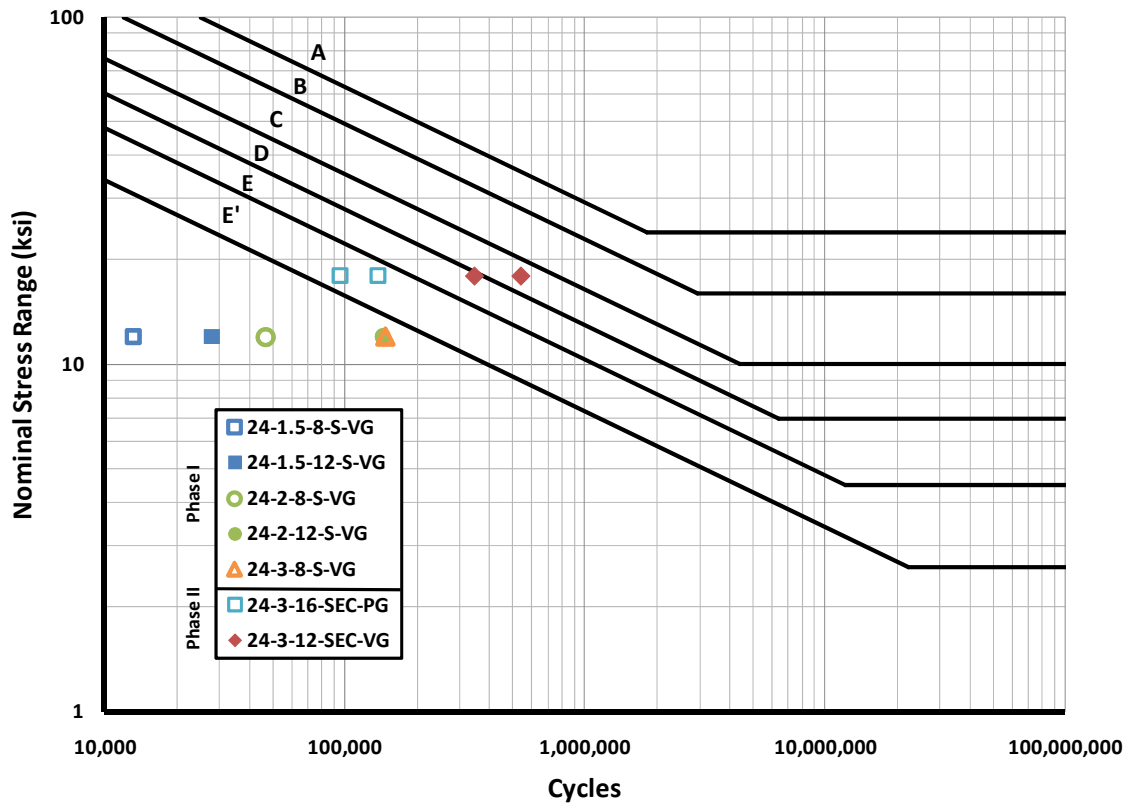


Figure 4.11 Socket Results for Phases I and II

Though both sets of Phase II SEC specimens outperformed all the unstiffened sockets from Phase I, the Pelco SEC's can be ignored due to their improper fabrication. Comparing the Valmont SEC specimens to the unstiffened sockets reveals the great benefit of adding an external collar to a standard socket detail.

The Valmont SEC detail can be most directly compared to the 24-3-8-S specimens from Phase I due to a common base plate thickness. The two details do have a different number of anchor rods, but this parametric variable has been shown analytically to have a reduced effect for base plates 3-in and thicker (see Chapter 6, Analytical Results). Therefore, the improvement in performance shown by the Valmont SEC detail, which corresponds to a ten-fold increase in fatigue coefficient, can be most directly attributed to the addition of an external collar.



#### 4.6.2 Phase I and II Full Penetration Details

Figure 4.12 presents an S-N plot of all Phase I and II fatigue data for full penetration type connections. Note that the base plate inner diameters of these specimens are not all equal. All Phase II diameters were 12.5-in except for the case of the TXEC detail, for which the diameter was 20.5-in. The Wyoming and Texas details in Phase I had 22.0-in inner diameters.

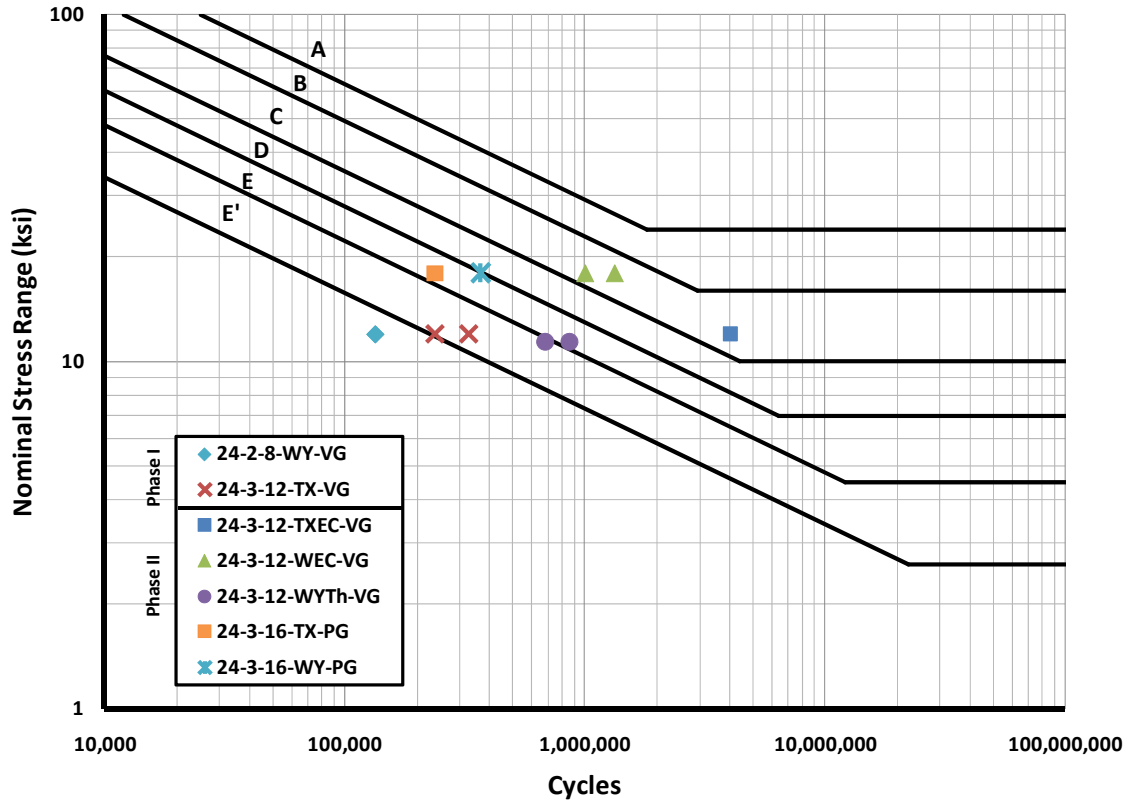


Figure 4.12 Full Penetration Results for Phases I and II

Comparing the Pelco unstiffened full penetration details from Phase II to the Valmont unstiffened full penetration details from Phase I reveals the benefit of reducing the inner base plate hole size. This reduction greatly boosts the base plates bending stiffness and improved performance by at least one fatigue category.

As with the socket results presented in Figure 4.11, the data in Figure 4.12 clearly show the benefit of adding external collars to high mast base connections. Results for the Phase II TXEC

specimens can be directly compared to results for the Phase I TX specimens. Base plate inner diameters for these two details vary by only a small degree (22.0-in in the TX detail, 20.5-in in the TXEC detail), thus the only large difference is the external collar present in the TXEC specimens. Average fatigue life is improved by a factor of fourteen due to its addition. Additionally, the Valmont WEC detail can be compared to the Pelco WY detail, as the only difference between these is the external collar in the WEC specimens. Average fatigue life increases by a factor of three.

#### 4.6.3 Phase I and II Stool Details

All Phase I and II fatigue data for stool-stiffened details are plotted in Figure 4.13. Under the Phase I naming scheme, “SB” refers to the “stool base” connection (Rios, 2007). For an image of this connection detail, see Chapter 3, Figure 3.17.

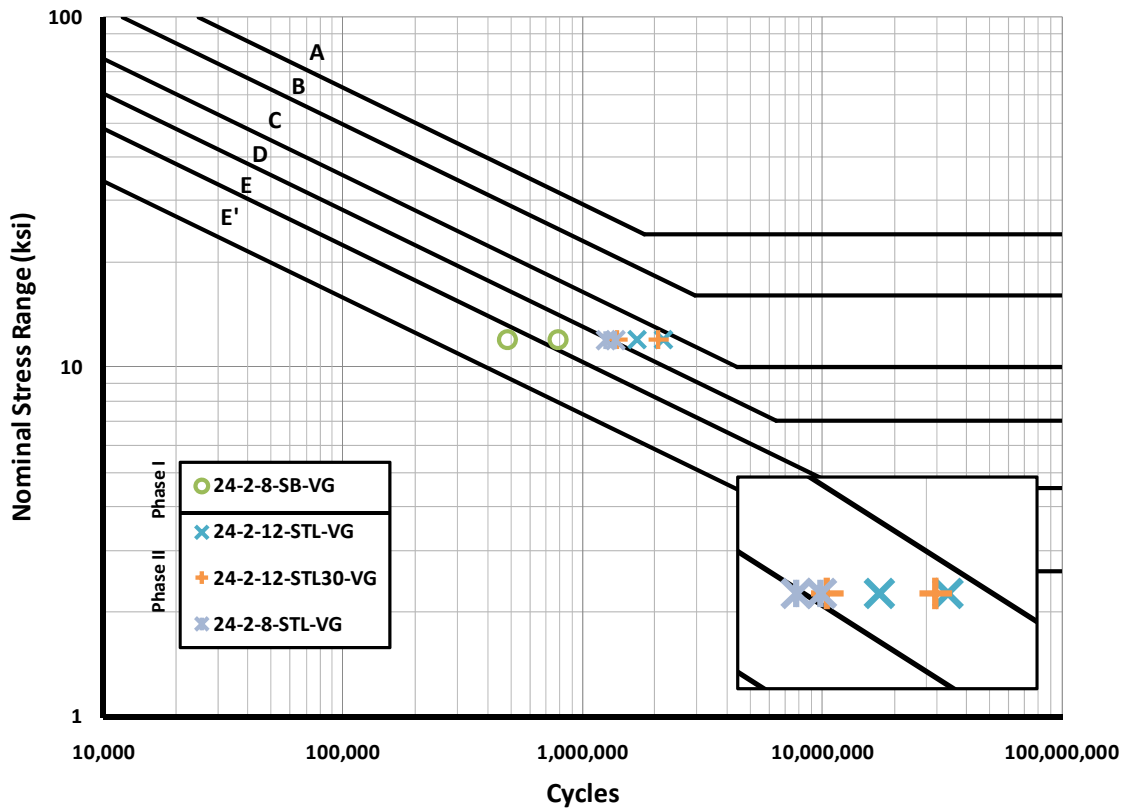


Figure 4.13 Stool Results for Phases I and II

The chief difference between the stool base connection from Phase I and the continuous stool connection (STL) from Phase II is the way in which the stiffening ribs of this connection are supported at their tops. In the SB connection, each set of ribs has an individual steel cap plate. In the STL detail, however, the vertical ribs are supported by a continuous steel ring. During Phase II, this continuous ring was added for a more uniform stress distribution and a possible improvement in performance.

To examine the effect of exchanging the individual cap plates for a continuous ring, a direct comparison can be made between the eight-bolted SB detail from Phase I and the eight-bolted STL detail from Phase II. The STL specimens do show a slight improvement in performance over the SB specimens, marked by a rough doubling of average fatigue life. This is not a strong improvement, but it is most likely attributable to the use of a continuous ring in the STL connection, as this is the only difference in the two details.

## 5 Finite Element Modeling

### 5.1 Introduction

High mast base plate connections were modeled using the commercial finite element software Abaqus. As with the experimental specimens, the analytical models included only the bottom 14-feet of the pole shaft in addition to the base plate connection. The models were constructed using a combination of shell and solid elements, and to shorten computation time, were analyzed in half-space using a symmetric boundary condition.

By modeling high mast connections analytically, the catalog of knowledge was greatly expanded beyond the eighteen physical details tested in Phases I and II. The results were valuable for two important reasons. In addition to providing stand-alone relative comparisons of connections, they were also combined with experimental data, which until that point had only been indexed to nominal stress.

The un-fractured finite element models were loaded and analyzed elastically to obtain hotspot stresses at the base plate connections. Hotspot stresses, which can be highly mesh-dependent, were determined using two accepted extrapolation techniques. These will be discussed in Section 5.2. Stress concentration factors (SCF) were then obtained by normalizing hotspot stresses with the appropriate nominal stresses.

The stress concentration factor, a measure of nominal stress amplification, provided a relevant stand-alone basis for comparing fatigue performance of the various details. Additionally, the SCFs of experimentally-tested specimens were multiplied by appropriate nominal stresses to construct a hotspot stress S-N plot. Fatigue data, when plotted against hotspot stress instead of nominal stress, tends to collapse the data points into a single curve (sometimes called an “X curve”), providing a unique relationship between hotspot stress and fatigue life.

The current chapter, following a discussion of hotspot stresses and extrapolation techniques, will describe the development of the base high mast model. Once verified, this base model was used for a parametric study in which key geometric details were altered to observe the resulting effect on SCF. This parametric study will be discussed in Chapter 6, Analytical Results.

## 5.2 Hotspot Stresses

A hotspot stress represents the elevated stress state in a solid object resulting from abrupt changes in the local geometry. In high mast connections, hotspots are typically found at the toe of the weld connecting the base plate and shaft (as shown in Figure 5.1). Hotspot stresses result from a combination of small-scale geometric irregularities like weld toe notches and larger-scale features like base plate geometry. A hotspot is typically the initiation point for fatigue cracking.

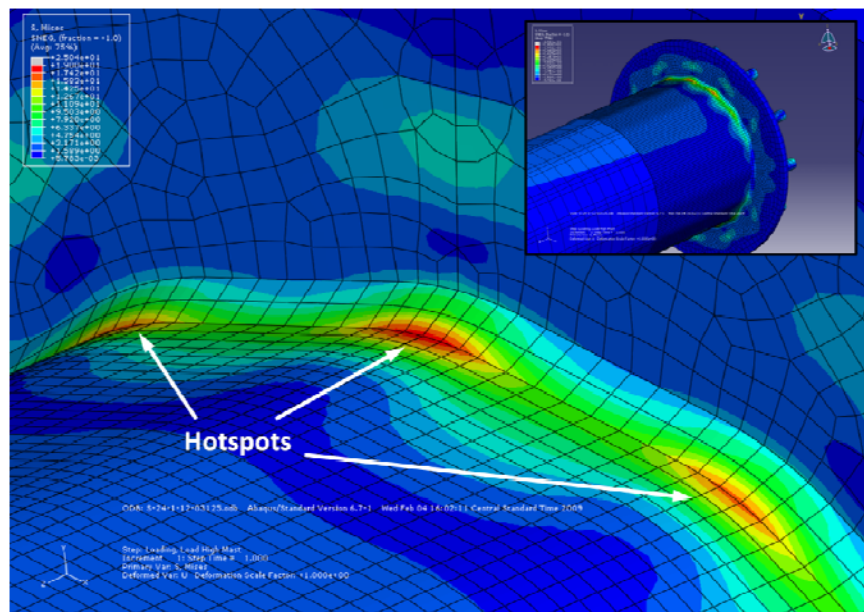


Figure 5.1 High Mast Hotspots

Hotspot stresses are typically referenced to the nominal stress for the location in question, and the ratio of the two is the stress concentration factor. Nominal stresses are calculated using simple mechanics equations like those for axial stress ( $\sigma = P/A$ ) and bending stress ( $\sigma = Mc/I$ ). High mast nominal stresses, being the product of a flexural load, were calculated using the equation for simple bending,  $Mc/I$ .

An oft-quoted example of stress concentration is for an axially-loaded plate with a hole cut in its middle. In this example, the stress concentration factor is 3, which indicates that the presence of the hole triples the remotely-applied nominal stress. In other words, the axial stresses immediately adjacent to the hole are three times what they are away from the hole.

Stress concentrations in high mast base plate connections are a product of two geometric features. The first, which is larger in scale, is the rotation of the base plate and the resulting double curvature in the shaft wall. Figure 5.2 shows this double curvature and the resulting surface stresses. Due to this bending, surface stresses first dip below the nominal stress profile then peak at the location of the weld toe. Note the close agreement of surface stresses with the simple bending formulation ( $M/I$ ) beyond the 6-in mark.

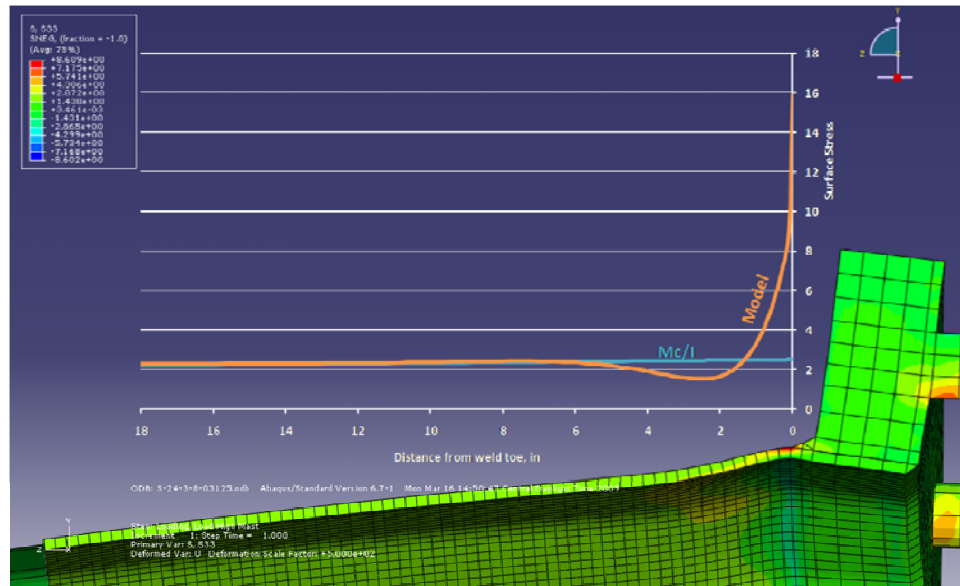


Figure 5.2 High Mast Local Curvature and Surface Stresses

The second geometric feature contributing to stress concentration is the shape of the fillet weld, which is an effect more local in scale than the larger geometric effect of base plate rotation. The weld's contribution (also termed the “notch effect”) is inherent to all structural fillet welds and is dependent on the profile of the weld. For welds with steep angles or undercuts (which can result from poor weld fusion), this notch effect can be very large. For this reason, AASHTO specifies fillet welds to have unequal leg lengths. This reduces the toe's angle of incidence and the SCF.

Figure 5.3 shows an expanded view of the same stress profile from Figure 5.2. Note the two regions on the “Model” stress profile. The elevated stresses in Region 1 are due to the macro-effect of base plate rotation and the resulting double curvature. The abrupt nonlinear stress peak in Region 2, however, is due to the micro-effect introduced by the weld toe.

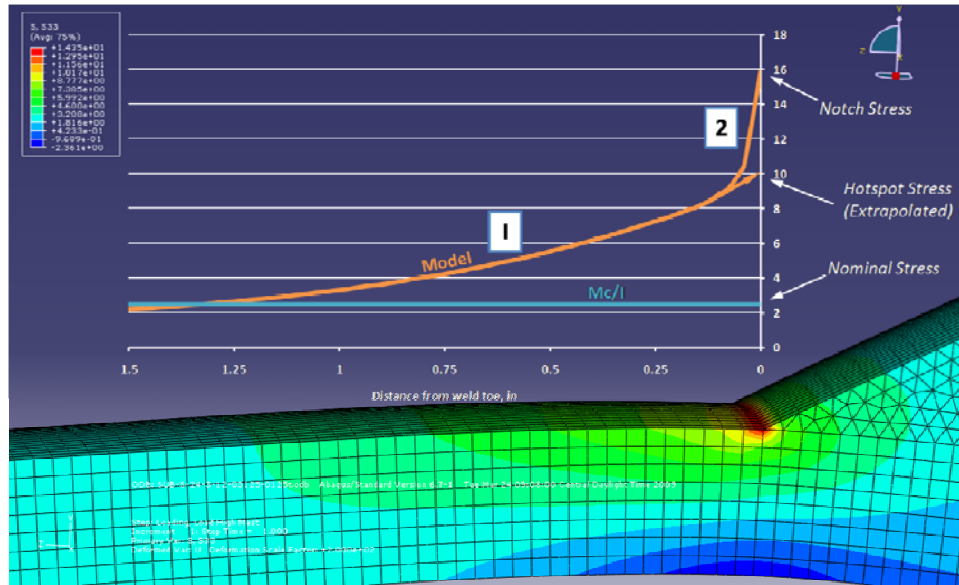


Figure 5.3 High Mast Surface Stresses (Expanded View)

The weld toe notch stress is very difficult to capture analytically. If the toe is modeled as a perfectly sharp corner as it is in the model shown above, the stress there is technically a singularity and asymptotically approaches infinity. The elements of the model cannot reflect this singularity and will give a finite value (16 ksi, in the figure). As the mesh refinement increases, so will the notch stress, thus any observable value is mesh-dependent.

To accurately capture a finite notch stress that is mesh-independent, the weld toe must be modeled with a small, non-zero radius, which requires a very fine mesh and great computation time. Furthermore, for the notch stress to be accurate, the modeled radius needs to be representative of real weld toes, which can have highly variable profiles.

For these reasons, welds in this study were simply modeled as sharp corners and their contributions to hotspot stress were neglected. In other words, hotspot stresses included only the contribution from the double curvature effect. In Figure 5.3, this is done with a straight-line extrapolation of the Region 1 curve. This value for hotspot stress has been shown to be mesh-independent provided the mesh in the weld toe region is composed of elements smaller than 25% of the wall thickness ( $t/4$ ). Mesh refinement will be discussed in Section 5.3.3.

The notch effect (and notch stress), which obviously still plays a role in initiating fatigue cracks, is implicitly included by combining analytical hotspot stresses with experimental data in the form

of an X-curve. This X-curve can then be used for fatigue life estimates of similarly-detailed connections, provided their hotspot stresses are found in the same manner as those found in the construction of the curve.

Hotspot stresses in this analytical study were calculated using two accepted numerical techniques. The first, which is a simple extrapolation of surface stresses similar to what is shown in Figure 5.3, is published by the maritime classification agency Det Norske Veritas (DNV) in its “Recommended Practice” for “Fatigue Design of Offshore Steel Structures” (DNV, 2008).

The second technique, termed the “structural stress” technique, obtains a hotspot value by resolving through-thickness stresses into simple membrane and bending components. This technique was developed by P. Dong of the Center for Welded Structures Research (Dong, 2001).

Brief descriptions of each technique will follow. Over the course of analytical modeling, the two techniques provided hotspot stresses that were invariably within 1-5% of each other (Structural Stress hotspots almost always exceeded DNV hotspots).

### 5.2.1 DNV Extrapolation Technique

The DNV technique obtains a hotspot stress by projecting surface stresses to the weld toe via a straight-line extrapolation. The pick points anchoring the extrapolation line are located at distances from the weld toe of  $0.5t$  and  $1.5t$ , where  $t$  is equal to the wall thickness. See Figure 5.4 for a visual description of this technique. Surface stresses should be maximum principal stresses, which, for the high mast models, were also the z-component normal stresses (S33 component stresses in Abaqus).

For convenience, element nodes should coincide with the  $0.5t$  and  $1.5t$  pick points; thus the mesh size should be some factor of the wall thickness. Normal S33 stresses can simply be taken from the model at these points and related to the extrapolated hotspot stress using the following linear extrapolation formula:

$$\sigma_{HS} = 1.5 * \sigma_{0.5t} - 0.5 * \sigma_{1.5t}$$



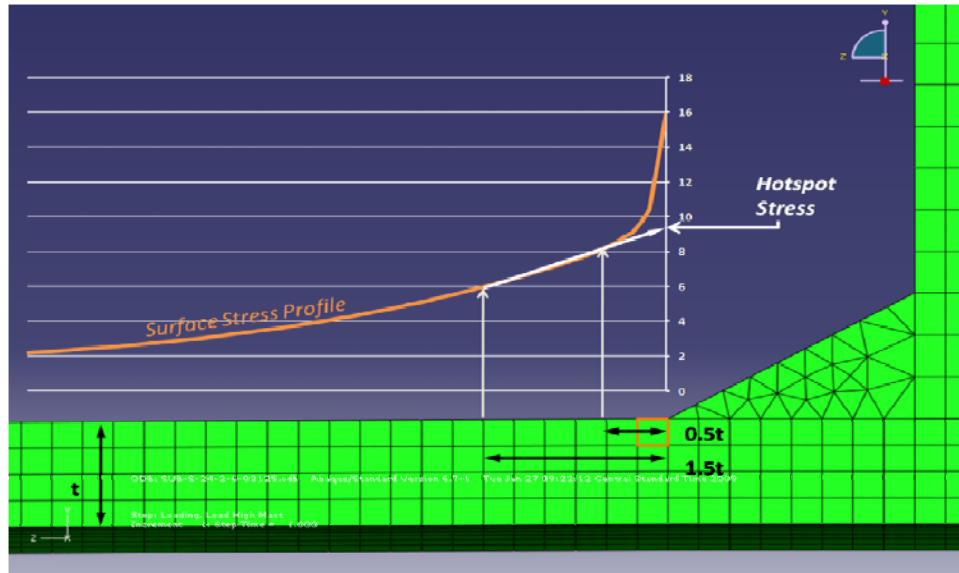


Figure 5.4 DNV Extrapolation Technique

### 5.2.2 Structural Stress Technique

This technique considers through-thickness normal and shear stresses rather than surface normal stresses. It calculates a weld toe hotspot stress by resolving the nonlinear normal stress distribution (Figure 5.5a) into a statically-equivalent linear distribution (Figure 5.5b), known as the structural stress distribution.

The membrane ( $\sigma_m$ ) and bending ( $\sigma_b$ ) components of the structural stress distribution are found by imposing equilibrium at a nearby reference plane (see Figure 5.6). This plane is chosen such that it is sufficiently far from the weld toe to ensure that normal and shear stresses are well behaved and more amenable to calculation of a mesh-independent hotspot value. The membrane component is found by imposing force equilibrium in the x-direction:

$$\sigma_m = \frac{1}{t} \int_0^t \sigma_x(y) dy$$

The bending component,  $\sigma_b$ , can then be found by imposing moment equilibrium at the reference plane. The reference plane distance,  $\delta$ , is arbitrary but should be within a distance of about  $2t$ .

Moment summation is taken about a point directly below the weld toe (note that the following formulation assumes positive shear stresses act downward):

$$\sigma_m \frac{t^2}{2} + \sigma_b \frac{t^2}{6} = \int_0^t \sigma_x(y)y dy + \delta \int_0^t \tau_{xy}(y) dy$$

In the Structural Stress technique, hotspot stress is then defined as the addition of the resolved membrane and bending components of the linear distribution:

$$\sigma_{HS} = \sigma_m + \sigma_b$$

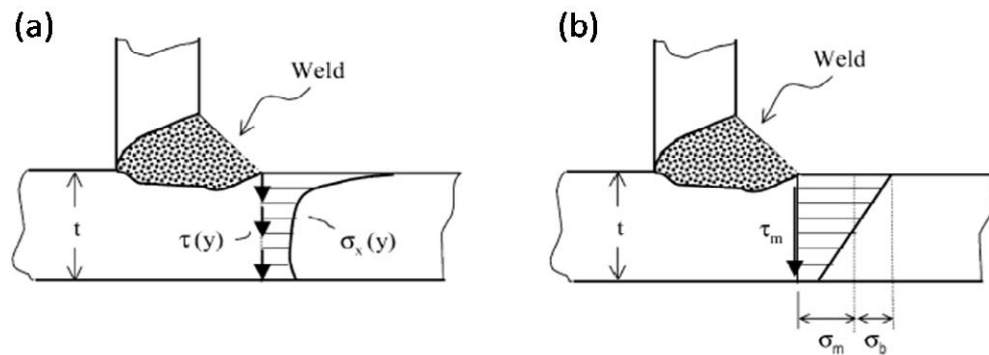


Figure 5.5 (a) Local through-thickness stresses (b) Structural stress definition (Dong, 2001, reprinted with permission)

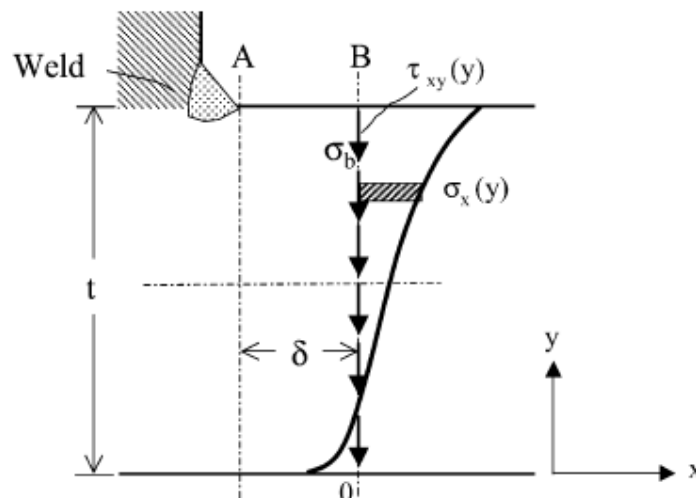


Figure 5.6 Structural Stress Calculation Procedure (Dong, 2001, reprinted with permission)

### 5.3 Base Model Development

A base analytical model was developed and verified before the parametric study was initiated. This development provided the opportunity to finalize model characteristics such as mesh refinement, boundary conditions, and element types.

The base model had a standard socket connection and possessed the following geometric details: 174-in length, 24-in diameter, 5/16-in wall thickness, 3-in base plate. For a schematic of this type of detail, see Chapter 3. Additionally, all anchor rods, of which there were twelve, were 1.75-in in diameter.

This section will discuss the major steps and decisions that contributed to the development of the base model, and will begin with the process for model construction.

#### 5.3.1 Model Construction

The base model was made up of two macro-components: a connection assembly composed of solid elements and a pole shaft assembly composed of shell elements (See Figure 5.7). Each of these two macro-parts was created in the Abaqus Assembly module by merging separate micro-parts. The micro-parts themselves had been created in the Part module through simple extrusion, rotation, sweeping, and cutting techniques.

This merging process greatly improved mesh quality and also simplified the model (leading to faster computation). The alternative to merging would have been joining the boundary nodes of the individual micro-parts (which can be done in the Abaqus Interaction module).

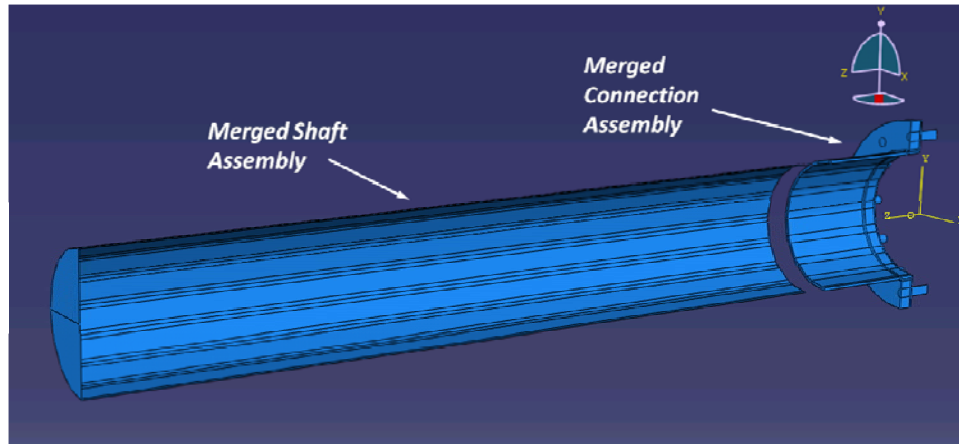


Figure 5.7 Base Model Merged Assemblies

The micro-parts merged to create the connection assembly included the base plate, a solid portion of the pole shaft, the fillet weld, and the anchor rods (See Figure 5.8). Note that different techniques for modeling the anchor rods were investigated in a boundary condition study that will be discussed in Section 5.3.2. The micro-parts merged to create the pole shaft assembly were the extruded shaft and the end plate. Computation time was greatly reduced by modeling a majority of the pole shaft using shell rather than solid elements.

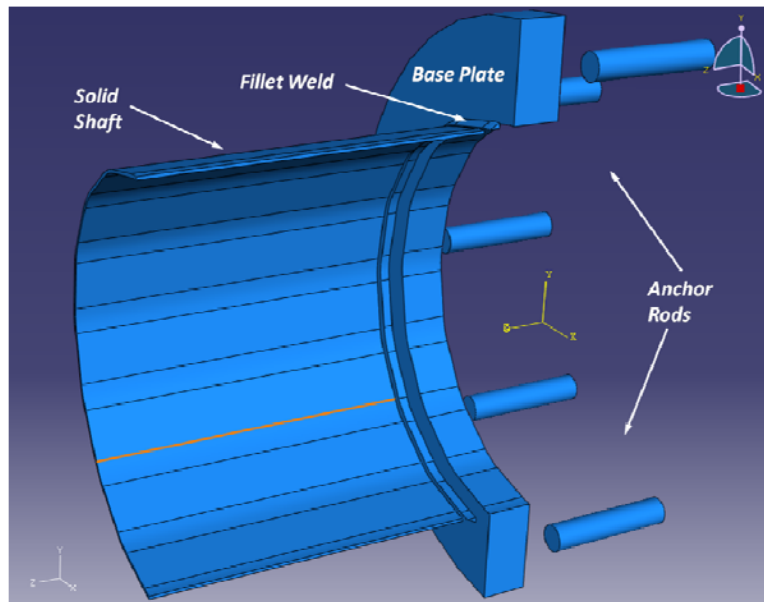


Figure 5.8 Merged Connection Assembly Micro-parts

The process of merging separate parts in the Abaqus Assembly module removes all former internal boundaries, so a seam had to be reinserted into the merged base assembly to create the discontinuous interface between the pole shaft and base plate (See Figure 5.9). Seams (and internal cracks, for that matter) can be created in the Abaqus Interaction module. This process was repeated during the parametric study for models with external collars and backing rings.

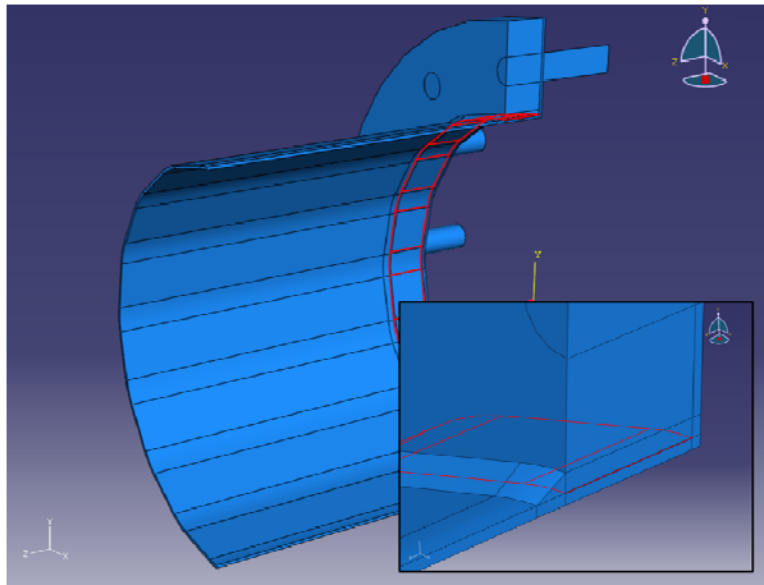


Figure 5.9 Internal Seam

Contact relationships were defined for the internal surfaces of these imposed seams. Abaqus does not offer a unique type of contact element for surfaces that impact each other during analysis. Instead, it allows for the creation of a user-defined contact relationship that is assigned to the two contact surfaces (each composed of normal elements) in the Interaction module. Note that, for the analysis to then correctly account for contact, it must account for geometric nonlinearity.

The base model pole shaft was initially tapered with the same small taper angle of the experimental specimens (0.14 in/ft). However, a subsequent trial run comparing the base model and an identical un-tapered model revealed only a 1% difference in hotspot stress. For this reason, all models constructed for the parametric study were un-tapered. This allowed for much simpler and faster construction of the models.

### 5.3.2 Load and Boundary Conditions

A downward-acting point load was applied to the center of the model's end plate to create a bending moment at the weld toe section (See Figure 5.10). The value of this load was arbitrary as the resulting hotspot stress was normalized by the appropriate nominal stress. For simplicity, a 1- kip load was chosen.

A symmetric boundary condition (BC) was used for the model's single plane of symmetry (the Y-Z plane), which permitted the use of half the elements as a fully-intact model, thereby reducing the computation time. This boundary condition functioned by simply restricting x-direction displacements for all nodes along this plane (See Figure 5.10). Note that the resulting stresses and displacements for a half-model are twice what they would be for a full mast. Thus, to be correct, all model stresses were divided by two following analysis.

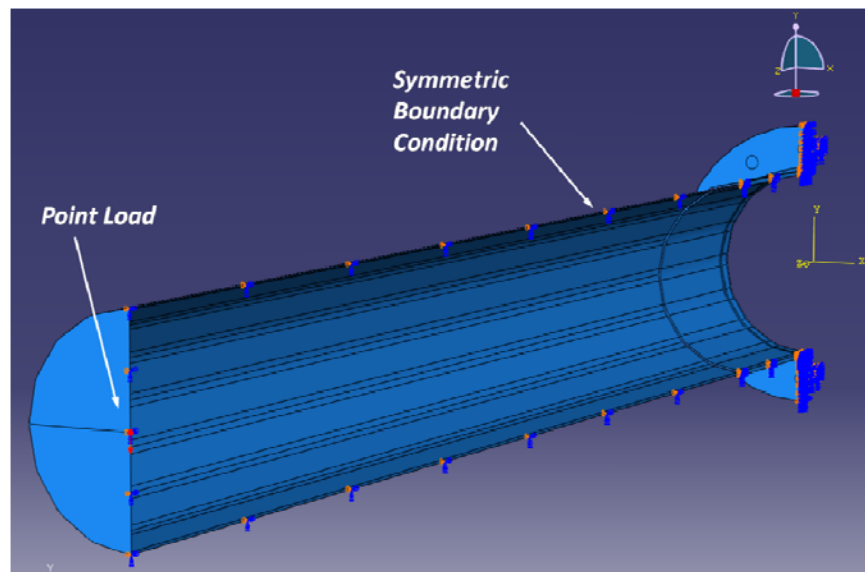


Figure 5.10 Point Load and Symmetric BC

The anchor rods were modeled to be continuous with the base plate, and, consistent with the experimental setup, were given 4.5-in standoff lengths. Their far ends were restrained with full nodal fixity, simulating the restraint of the load box attachment points in the experimental setup. Figure 5.11 shows this anchor rod boundary condition.

Before finalizing this method, a brief study was carried out which investigated modeling the rods, nuts, and base plate as separate entities. In this alternative method, contact relationships were

defined for all interfaces and a preload was assigned to the anchor rod to simulate the tightening of the base plate nut. The complexity of this method resulted in very long computation times, and moreover, results were inconsistent and mesh dependent. For these reasons, the simpler, continuous method described above was used for the base model and all subsequent parametric models.

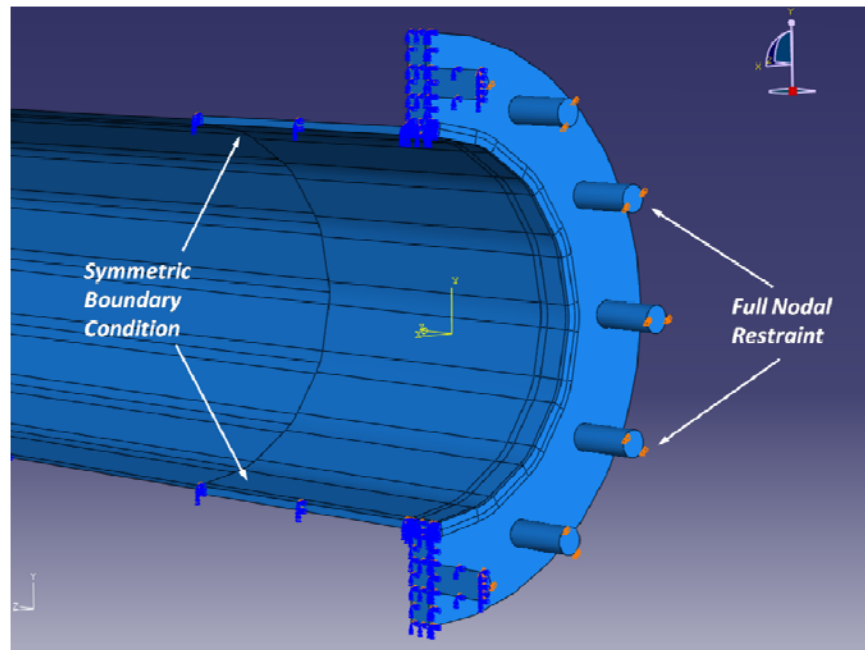


Figure 5.11 Boundary Conditions

### 5.3.3 Meshing

Both the DNV and Structural Stress methods recommend meshing the hotspot region with solid elements of size equal to the wall thickness,  $t$  (DNV, 2008) (Dong, 2001). For confirmation of this, a mesh refinement study was carried out investigating element sizes of  $t$ ,  $t/2$ ,  $t/4$ ,  $t/6$ , and  $t/8$ . The results of this study are shown in Figure 5.12.

Though the Structural Stress method yields mesh independent SCFs for all mesh sizes, the DNV method does not show mesh independence until a  $t/4$  mesh or finer. Following this study, all models were meshed with elements of size  $t/4$ . Note that this level of refinement did require submodeling, which will be discussed in Section 5.3.4.

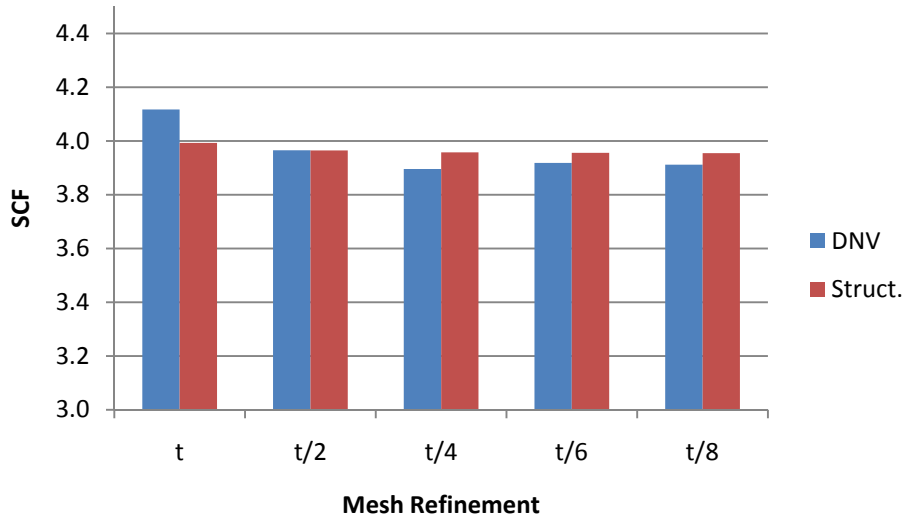


Figure 5.12 Mesh Refinement Study

The hotspot stress at the weld toe was much less sensitive to the level of mesh refinement in regions far from the hotspot. These included the base plate, anchor rods, pole shaft beyond 2-ft, and the end plate. The hotspot value at the weld toe proved to be unaffected provided the elements in these regions were sized below  $3t$  for solids and  $6t$  for shells (where  $t$  is the pole shaft thickness). See Figure 5.13 for a visual summary of high mast model meshing.

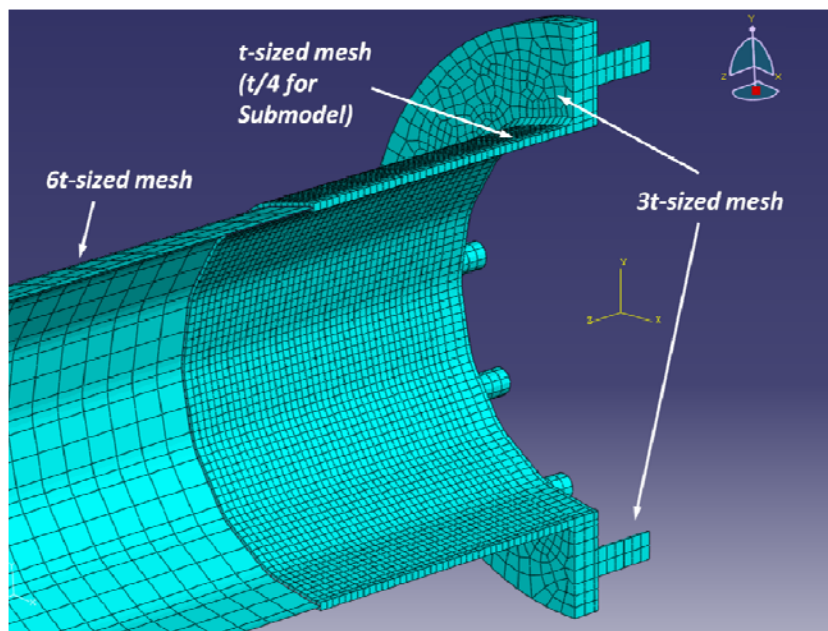


Figure 5.13 Base Model Mesh



Though neither document presenting the hotspot techniques addressed the issue of element type, the Abaqus “Getting Started” manual recommends the use of twenty-noded quadratic elements for regions with high stress gradients (Abaqus, 2006). These complex elements are alternatives to the simpler eight-noded elements that are sufficient in most FEA applications.

This recommendation was tested by running identical models with both types of elements. The model comprised of quadratic elements yielded smoother displacement profiles and was also more successful at capturing mesh-independent stresses in the hotspot region. Subsequently, all analytical models were constructed with quadratic elements.

These elements are known as C3D20R-type elements in the Abaqus element library and have been successfully used in other analytical investigations of tubular structure base plate connections (Ocel, 2006).

Hexahedral (“brick”) shapes were used for all elements, with the exception of those composing the welds. Due to the small angle of the weld toe, mesh quality was compromised when the weld was modeled with brick elements, thus wedge shapes were used instead. Note that quadratic wedge type elements have fifteen nodes rather than twenty.

All elements were of the “reduced-integration” type (eight Gaussian integration points per element rather than twenty-seven). The difference between reduced-integration elements and full-integration elements was also investigated by analyzing models with each type. No change in hotspot stress was observed, though the reduced-integration model was quicker.

#### 5.3.4 Submodeling

The  $t/4$  mesh refinement necessary for a mesh-independent hotspot stress was not possible in a full high mast model. This refinement resulted in an unreasonable number of elements and far too great a computation time to be practical. For this reason, the technique of submodeling was used to model the hotspot region.

A submodel functions by taking a small portion of a global model and re-analyzing it with a finer mesh. This is done by assigning the submodel’s boundary nodes a specific submodeling

boundary condition. This boundary condition uses the global model's displacement results for nearby nodes to "drive" the submodel boundary nodes to the same positions. This technique was used for all parametric models in addition to the base model.

The global model was always analyzed first with a  $t$ -sized mesh in the hotspot region. Following this, the global results were used to drive the submodel, which was meshed with elements of size  $t/4$ . See Figure 5.14 for an image of a typical submodel.

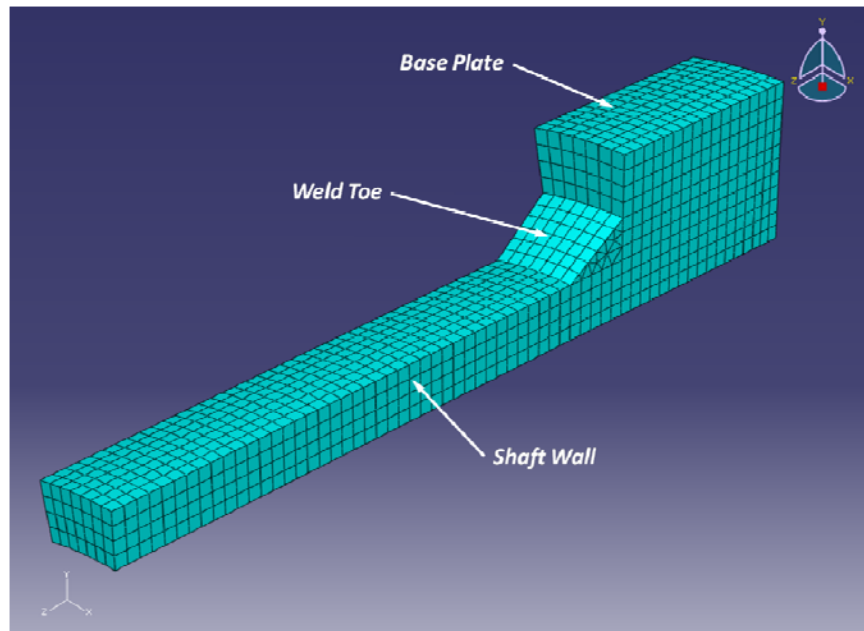


Figure 5.14 Typical Submodel

### 5.3.5 Model Verification

The high mast base model was verified by running a small parametric study identical to one completed by M. Warpinski in her analytical study of high mast socket connections (Warpinski, 2006). These parametric studies varied the base plate thickness (for a single wall thickness, 0.1875-in) and observed the resulting effect on stress concentration factor. See Figure 5.15 for the results of these two studies.

Though the absolute values for SCF, which can be sensitive to boundary conditions, hotspot extrapolation techniques, and other modeling assumptions, were not necessarily equal in the two

studies, they were close, and more importantly, the overall trends were the same. This fact, in effect, substantiates the base model and the assumptions that were made in its construction.

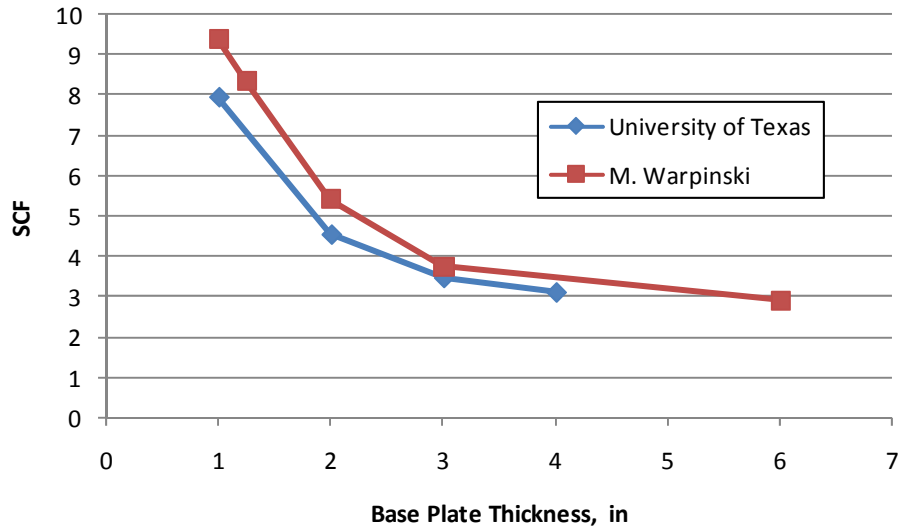


Figure 5.15 Base Model Verification

## 6 Analytical Results

### 6.1 Introduction

Once the base finite element model was constructed and verified, it was used for two analytical investigations. First, a series of parametric studies were executed to explore the effects of various geometric details on stress concentrations. These included: wall thickness, shaft diameter, number of anchor rods, base plate inner diameter, collar length, and shaft bend radius.

Following this, a study was initiated in which finite element models were created for all experimentally-tested connection details from both phases (with the exceptions of the stool details and Pelco details). The SCFs derived from these models were used to determine experimental hotspot stresses for the tested specimens. The fatigue results from Chapter 4, when plotted in a log-log format against hotspot rather than nominal stress, collapsed into a linear cluster of data with a regression slope reasonably close to the expected value for steel.

Hotspot stresses for all analytical models were determined in accordance with the two numerical methods presented in Section 5.2: the DNV extrapolation method and the Structural Stress linearization method. These two hotspot methods yielded very consistent results, with their calculated values differing by only 1-5%. All reported hotspot stresses in this chapter are an average of the values from each method. See Appendix D for a summary of these hotspots.

For unstiffened details (those without collars or backing rings), a single hotspot existed at the base plate weld toe. The stress concentration factor was then defined as the ratio of that location's hotspot stress to its nominal stress, where the latter is calculated assuming the simple bending formula,  $Mc/I$ .

For stiffened models, such as those with collars, multiple hotspot locations could exist (see Figure 6.1). For these models, the stress concentration factor was defined by the largest of the hotspots (also called the "critical hotspot"), but was still normalized by the nominal stress at the base plate weld. Note that the calculations for section modulus at the base plate weld ignored the presence of collars and backing rings and considered only the pole's section.

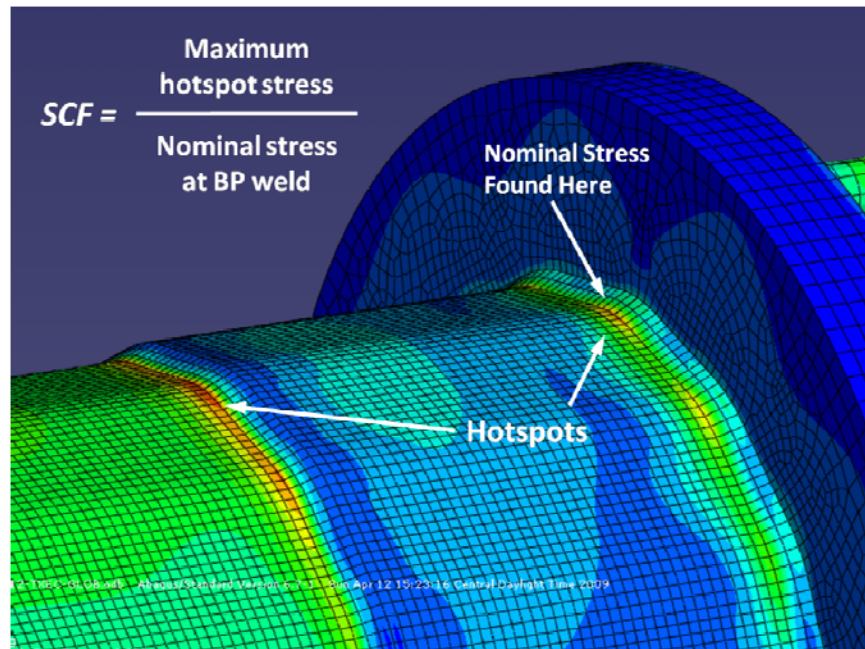


Figure 6.1 Analytical Model with Multiple Hotspot Locations

This SCF definition was consistent with the experimental procedure. All experimental specimens were tested at loads which created a desired nominal stress at the base plate weld toe, even when fracture initiation occurred elsewhere, such as the top of the collar. By relating the analytical models' maximum hotspots to their base plate weld nominal stresses, their SCFs could be used with the experimental data to determine the proper hotspots corresponding to the actual location of fracture initiation.

The forthcoming sections will present all analytical results, including the results from parametric studies and the hotspot results for experimental specimens. Discussion and recommendations will be included where applicable.

## 6.2 Parametric Studies

A series of high mast geometric variables were investigated parametrically to determine how their alteration affected stress concentrations. Five studies were performed, and in total, forty-three high mast models (and their submodels) were analyzed to support these studies.

In addition to their primary parametric variables, several of these studies also varied base plate thickness to observe interaction. Note that wall thickness and shaft diameter, two separate parametric variables, were combined into a single study to jointly consider the effect of altering the pole’s section geometry. The parametric studies are summarized in Table 6.1.

Table 6.1 Parametric Study Matrix

Parametric Study	Among:		Primary Variable Range	Total Models
	Detail(s)	Base Plate(s)		
<i>Wall Thickness and Shaft Diameter</i>	Socket	1-in to 4-in	5/16-in, 1/2-in	16
			24-in, 36-in	
<i>Anchor Rod Number</i>	Socket and Texas	2-in to 4-in	6 (S) or 8 (TX), 12, 16	18
<i>Base Plate Inner Diameter</i>	Texas and Wyoming	3-in	10-in, 16-in, 22-in	6
<i>Collar Length</i>	Socket External Collar	3-in	3-in, 6-in, 12-in, 18-in	4
<i>Shaft Bend Radius</i>	Socket	3-in	0.5-in, 2-in, 4-in	3

### 6.2.1 Wall Thickness and Shaft Diameter Study

This study investigated the effects on SCFs of modifying the pole shaft section geometry in socket connections. The pole’s section was modified by changing only the wall thickness and shaft diameter, not the section shape. Only a sixteen-sided hexadecagonal section with 4-in bend radii was considered. Two wall thicknesses, 5/16-in and 1/2-in, and two shaft diameters, 24-in and 36-in, were considered across the 1-in to 4-in range of base plate thicknesses. Number of anchor rods was held constant at twelve. See Figure 6.2 for a schematic of the analyzed connection. Though this study investigated only socket-type details, the implications can reasonably be extended to other high mast detail types.

Comparisons within this particular study will be made on the bases of both hotspot stress and SCF. Theoretically, the two will change independently because modifying the pole shaft section will usually change the nominal stress. In the other studies, where the pole shafts (and hence, nominal stresses) were constant, changes in hotspot stress mirrored changes in SCF, and only one was needed for comparisons.

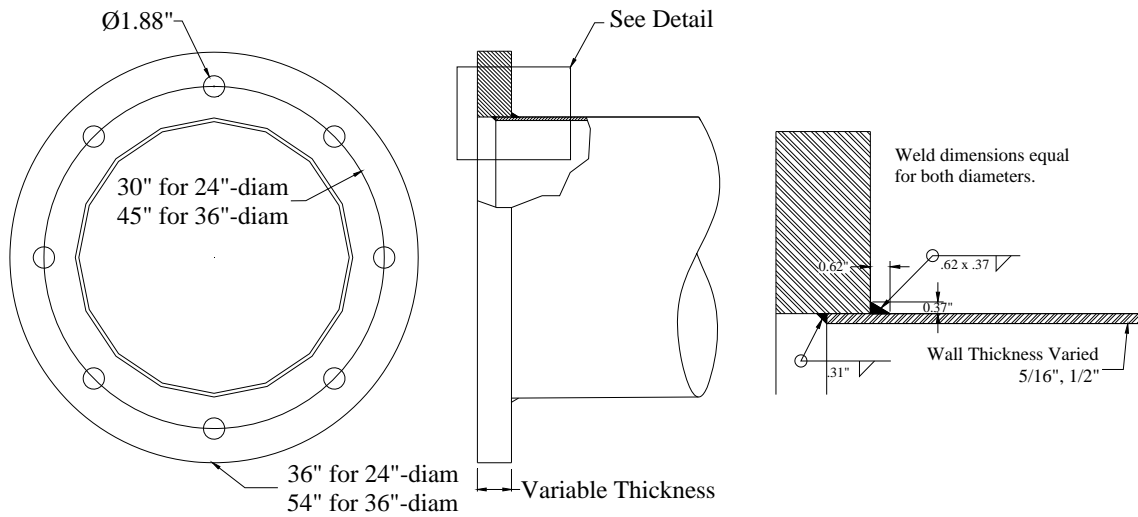


Figure 6.2 Connection Detail for Wall Thickness and Shaft Diameter Parametric Study

Hotspot stresses for all models in this study are presented in Table 6.2 and are plotted versus base plate thickness in Figure 6.3. These hotspot stresses were all produced by a 1-kip point load acting at the end of models 175-in long, thus the applied bending moment at the base plate weld was constant for all models, and hotspots can be compared directly.

The hotspot results for this study reveal that increasing the section modulus of a mast, either by thickening its shaft wall or increasing its diameter, reduces its hotspot stress. This reduction in hotspot can potentially lead to improved fatigue performance, although this assumes that the moments causing fatigue stresses remain constant with changes in the shaft section. This may not be true in the case of vortex shedding.

Table 6.2 Hotspot Stresses for Wall Thickness and Shaft Diameter Parametric Study

Diam, in	Wall, in	Section Mod, in <sup>3</sup>	Hotspot Stress, ksi, for BP Thickness, in =			
			1	2	3	4
24	5/16	137	11.2	6.3	4.5	3.8
	1/2	218	6.9	4.1	2.9	2.3
36	5/16	312	9.4	4.9	3.1	2.3
	1/2	497	5.7	3.3	2.1	1.5

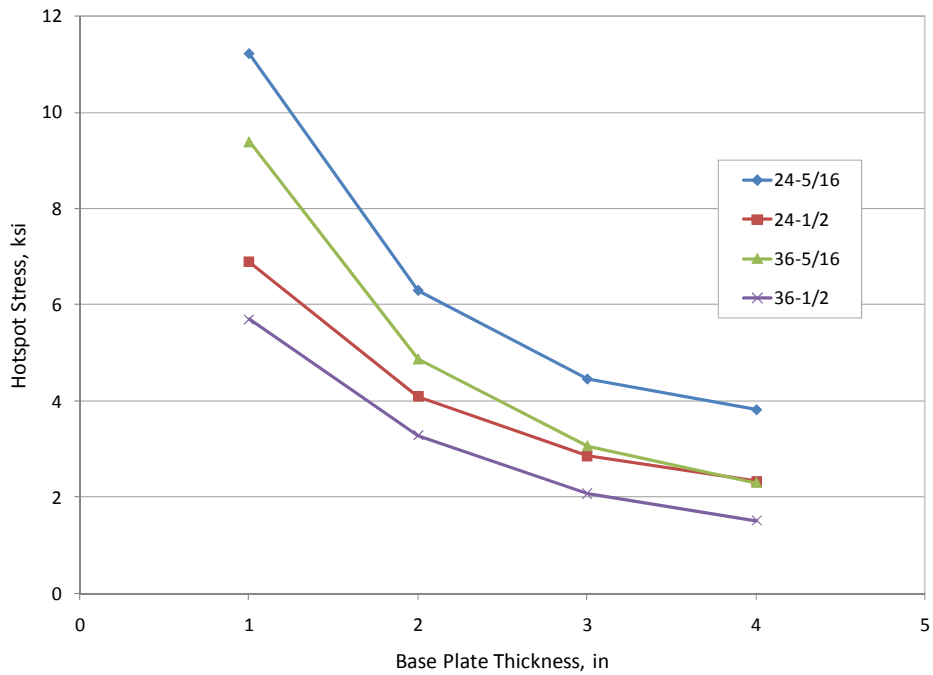


Figure 6.3 Hotspot Stresses for Socket Details in Wall Thickness and Shaft Diameter Study

The individual hotspot reductions from increasing either the wall or diameter are not necessarily equal, however, and the relative difference is dependent on base plate thickness. For the 1-in thick base plate, the hotspot reduction from thickening the wall (40%) is much greater than the hotspot reduction from enlarging the diameter (16%). The difference then diminishes as the base plate is increased to 4-in, and the two reductions equalize.

Hotspot stresses are reduced in masts of larger section moduli for the same reasons nominal stresses are reduced. For a given bending moment, a mast with a larger section modulus has better bending resistance and provides more cross-sectional area through which stresses can flow, thus lowering hotspots.

Models in this study were also compared on the basis of stress concentration factor (SCF). See Table 6.3 and Figure 6.4 for these results.



Table 6.3 SCFs for Wall Thickness and Shaft Diameter Parametric Study

Diam, in	Wall, in	Section Mod, in <sup>3</sup>	$\sigma_{nom}$	SCF for BP Thickness, in =			
				1	2	3	4
24	5/16	137	1.25	9.0	5.1	3.6	3.1
	1/2	218	0.78	8.8	5.2	3.6	3.0
36	5/16	312	0.55	17.1	8.9	5.6	4.2
	1/2	497	0.34	16.5	9.5	6.0	4.4

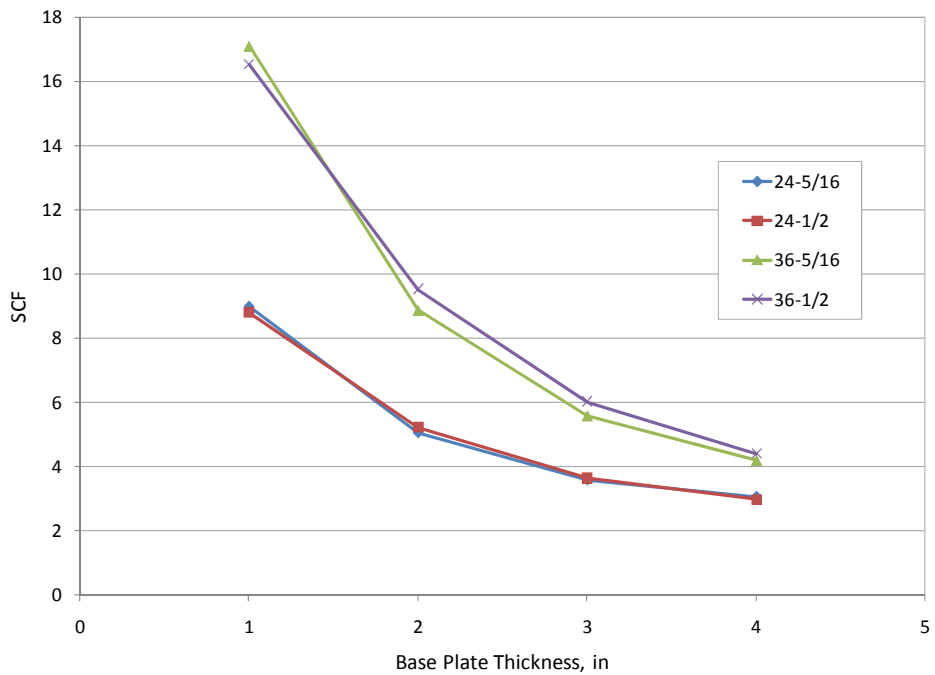


Figure 6.4 SCFs for Socket Details in Wall Thickness and Shaft Diameter Parametric Study

Three important relationships between SCF and connection geometry are visible in Figure 6.4. The first is a strong SCF sensitivity to base plate thickness. However, this correlation has been well-documented elsewhere and will not be discussed here (Ocel, 2006) (Warpinski, 2006). The other two relationships are between SCF and either shaft diameter or wall thickness.

The shaft diameter has a visibly large effect on the stress concentration factor. Figure 6.4 reveals that the 36-in models have the largest SCFs, even though they showed the lowest hotspots in Figure 6.3 (for a given base plate and wall thickness). This reveals that the inherent hotspot

reduction in poles of enlarged diameter is met with a far greater nominal stress reduction. Thus the ratio of the two (the SCF) actually increases as diameter increases.

Though an increased diameter always results in an elevated SCF, the relative heightening of SCF depends on the base plate thickness. The effect is greatest for base plates of 1-in and reduces as they are thickened to 4-in. These increases in SCF range from about 90% in 1-in base plates to about 40% in 4-in base plates.

Given that stress concentration in high mast connections is largely a product of base plate flexibility, this diameter sensitivity can be explained by considering the change in relative flexibility between the pole shaft and base plate when the shaft diameter is increased. For a given base plate thickness, an increase in shaft diameter reduces the relative stiffness contribution of the base plate and renders it less resistant to the bending moment imposed on it. It therefore does a poorer job in restraining the double curvature of the pole shaft wall, leading to higher local bending and higher stress concentration. Additionally, for enlarged diameters, the base plate must be cut with a larger hole, which further reduces its stiffness.

This relative stiffness explanation is justified by a visible scaling effect in Figure 6.4. Observe that, for a 36-in diameter mast to achieve a similar SCF range as a 24-in diameter mast, its base plate needs to be thickened by about 1-in. This reveals that the SCF can be maintained if both the pole shaft and base plate are enlarged simultaneously.

The other important relationship visible in Figure 6.4 is the effect of pole wall thickness on the stress concentration factor. Relative to shaft diameter, pole wall thickness plays a much smaller role in affecting the SCF, with differences due to thickness ranging from only 2-3% in the 24-in masts and 3-8% in the 36-in masts.

This insensitivity to wall thickness reveals that the hotspot reduction from thickening the shaft wall (shown in Figure 6.3) is met with a proportional reduction in nominal stress, thus rendering the SCF, which is the ratio of the two, relatively unchanged. For both diameters and all base plates, these two reductions consistently range between 35-40%.

It is intuitive that an increase in pole wall thickness should reduce the nominal stress due to an elevated section modulus. It is also intuitive that increasing the wall thickness should reduce the hotspot stress. Thicker pole walls are stiffer and thus better at resisting the local double curvature

responsible for elevating the surface stresses. Evidently, for the tested details, these two reductions are proportional.

#### 6.2.1.1 Verification of Findings and Conclusions

These findings concerning the effects of modifying the pole shaft section are in good agreement with analytical investigations of traffic poles at both the University of Texas and the University of Minnesota. However, they diverge slightly from analytical high mast work carried out by M. Warpinski at Lehigh University. In that study, a slightly greater SCF dependency on wall thickness is observed than what is presented above (Warpinski, 2006).

The effect of increasing the shaft diameter was explored by R. Duraisamy at the University of Texas. Using Abaqus to model circular mast arms with socket details, Duraisamy also concluded that increasing the shaft diameter, in her case, from 6.5-in to 11-in, increased the SCF (Duraisamy, 2005).

Like the results presented above, the relative increase in Duraisamy's SCFs depended on the base plate thickness. For her mast arms, increases in SCF due to an enlarged diameter ranged from 36% for 1-in base plates to 8% for 3-in base plates (Duraisamy, 2005). These increases are less than what was seen in the current study, but this can be attributed to the size effect of comparing 24-in and 36-in high masts to mast arms less than 12-in in diameter. Additionally, these mast arms' base plates were rectangular, and the high masts' are circular.

Duraisamy also investigated the wall thickness effect by modeling two 10-in diameter mast arms, one with a 0.179-in wall and the other with a 0.239-in wall. Both were on socket detailed models with 1.5-in base plates. The difference in stress concentration factor between these two mast arms was only 6%.

This result is in agreement with an earlier research study performed at the University of Texas in which 10-in mast arms of wall thicknesses equaling Duraisamy's were modeled with 1.5-in and 2.0-in base plates. In that study, differences in stress concentration factor due to alteration of wall thickness were very small, ranging between only 1-3% (Koenigs, et al 2003).

J. Ocel, in a PhD dissertation at the University of Minnesota, presents results in very close agreement with the current findings. He found a strong SCF dependency on shaft diameter, modeling diameters of 15-in, 20-in, and 25-in, but virtually no relationship between SCF and wall thickness. For his range of diameters, Ocel found a consistent rise in SCF of about 20% per 5-in increase in diameter. Then, when considering wall thicknesses of 0.26-in, 0.46-in, and 0.66-in for his 20-in model, SCFs were within 4% of each other, revealing little dependence (Ocel, 2006).

In an analytical investigation of 24-in multi-sided high masts at Lehigh University, however, M. Warpinski found a slightly greater SCF dependency on wall thickness than what was cited by Ocel and what is seen in the current study. Considering wall thicknesses of 5/16-in and 1/2-in for a 1.25-in base plate, she observed a 16% increase in SCF when the wall was thickened (Warpinski, 2006).

These independent findings, when considered alongside the current observations, suggest that the wall thickness relationship to SCF can possibly be sensitive to individual modeling assumptions and other unknown factors. What is consistent, however, is that the SCF dependency on wall thickness is less than those of other parametric variables such as shaft diameter and base plate thickness. Additionally, a thickened wall shaft is consistently found to reduce hotspot stresses, a finding that is confirmed by Warpinski (Warpinski, 2006).

Two major recommendations can be formed following this parametric study. The first concerns the scaling effect of high mast poles with enlarged diameters. When a high mast diameter is increased, perhaps for reasons of strength design, its base plate needs also to be thickened to maintain the relative stiffness between the two and prevent excess stress concentration. The amount by which the base plate needs to be thickened is open to a designer's judgment.

The second conclusion to draw from this study relates to the issue of wall thickness. Though this variable's physical influence on stress concentration is debatable in light of the research, thickening the pole shaft wall appears to always reduce hotspot stresses, which can lead to improved fatigue performance. A designer can elect to increase only the wall thickness of the bottommost section in a spliced high mast assembly and thus improve the performance of the entire mast without incurring too great an increase in cost.

### 6.2.2 Anchor Rod Study

The second parametric study investigated the effect of varying the number of anchor rods to observe the relationship with stress concentration factor. Hypothetically, increasing the number of anchor rods should act to stiffen the connection in the same way thickening the base plate does. Experience as shown that a stiffened connection results in less bending of the base plate and reduced hotspot stresses.

In Phase I of experimental testing, fatigue performance was greatly improved for socket detail specimens of 1.5-in and 2.0-in base plates when the number of anchor rods was increased from eight to twelve. In Chapter 4, this improvement was noted to be on the order of 100-200%. In Phase II, however, the fatigue life improvement for stool details in which the number of anchor rods was increased from eight to twelve was only about 30%.

This reveals that for details which are already quite stiff, such as the stool-stiffened details, there is an upper limit on the additional stiffness to be gained by adding more rods. For the more flexible sockets in Phase I, boosting the number of anchor rods represented a larger stiffness contribution relative to the overall stiffness of the connection, and hence fatigue life was greatly improved.

Two detail types, Socket and Texas (full penetration), were considered for this parametric study. The latter had a reduced base plate inner diameter of 16-in, and was thus inherently stiffer. Additionally, several base plate thicknesses, 2-in, 3-in, and 4-in, were considered for both connection types to further investigate the anchor rod effect for base plates of different stiffnesses.

For a schematic of the socket connection, see Figure 6.2, but note that this figure shows a twelve-rod connection. For a schematic of the Texas connection detail see Figure 6.5 below. Note that all models for both details had 5/16-in shaft walls and 24-in shaft diameters.

Three different anchor rod sets were considered for each detail type. For the socket details, anchor rod sets of six, twelve, and sixteen were considered. For the Texas details, anchor rod sets of eight, twelve, and sixteen were considered. See Table 6.4 and Figure 6.6 for the SCF results of this parametric study.

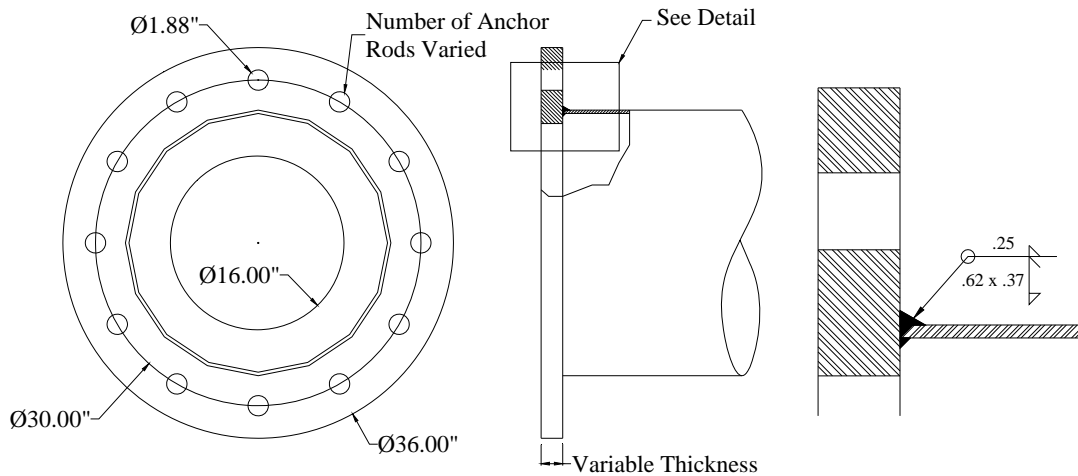


Figure 6.5 Texas Connection Detail for Anchor Rod Parametric Study

Table 6.4 Results of Anchor Rod Parametric Study

Detail	Anchor Rods	SCF for Base Plate Thickness:		
		2-in	3-in	4-in
Socket	6	5.9	3.9	3.2
	12	5.0	3.6	3.1
	16	4.7	3.5	3.0
Texas	8	3.4	2.4	2.0
	12	3.2	2.3	2.0
	16	3.1	2.3	2.0

The results of this study reveal that the number of anchor rods plays a relatively small role in affecting stress concentration factor, especially when compared to other more significant variables like base plate thickness and detail type.

Of the six connection details presented, only the 2-in Socket, which is also the most flexible, shows a significant effect from varying the number of anchor rods in its connection. Its stress concentration factor drops by 15% as the number of rods is increased from six to twelve. It then drops another 6% as four more rods are added. The effect from increasing the number of anchor rods is virtually negligible in the remainder of the details.

These results confirm what has been observed in experimental testing. In both phases, only socket details with base plates of 1.5-in or 2.0-in have shown any significant fatigue life

improvement when the number of anchor rods is increased. If the base plate is already quite stiff, due to greater thickness, a reduced inner diameter, or the presence of an external collar or stool, it will not see as large a reduction.

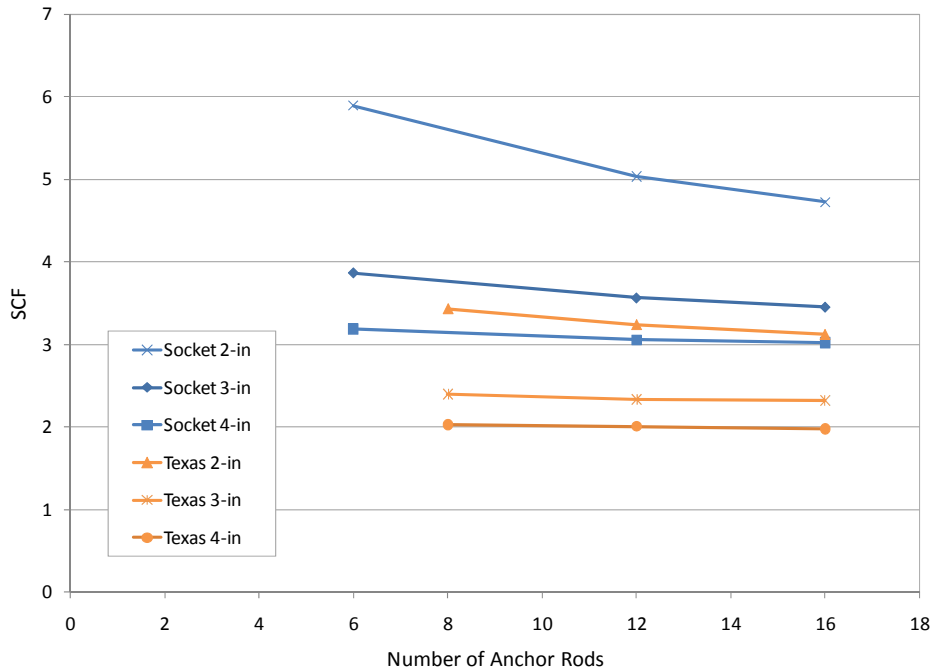


Figure 6.6 Results of Anchor Rod Parametric Study

In conclusion, as it is already advisable for designers to specify base plates as 3-in or thicker for all detail types, the number of anchor rods is not significant, at least where fatigue of the pole shaft is considered. More anchor rods may be necessary when considering their own fatigue resistance or where strength is an issue, but if not, the number of rods can be reduced to eight or twelve, thus cutting fabrication time and expense. This recommendation is echoed by an analytical study from Lehigh University (Warpinski, 2006).

### 6.2.3 Base Plate Inner Diameter Study

This parametric study considered the effect on SCF of varying the diameter of the inner base plate hole. This variable applies only to full penetration type details and not sockets. The inner diameter of the base plate in socket details must be equal to the outer diameter of the pole shaft and therefore cannot be varied. This hole must still be provided in full penetration details for three reasons: welder access to the inner fillet welds, wiring of the high mast's lighting system, and draining of molten zinc during galvanizing.

The hypothesis of this study is that, by reducing the size of the inner hole, the base plate of full penetration details will be made stiffer and will more effectively restrain the local bending of the shaft wall that leads to high hotspot stresses.

Both Texas and Wyoming details were considered. See Figure 6.5 for a schematic of the Texas detail, but note that this figure shows a 16-in inner base plate diameter. For a schematic of the Wyoming detail, see Figure 6.7 below. The chief difference between the Texas and Wyoming details is the presence of a fillet-welded backing ring in the Wyoming. All models had 24-in diameters, 5/16-in shaft walls, 3-in base plates, and were connected with twelve anchor rods.

Base plate inner diameters of 10-in, 16-in, and 22-in were considered in this study. SCF results are presented in Table 6.5 and Figure 6.8.

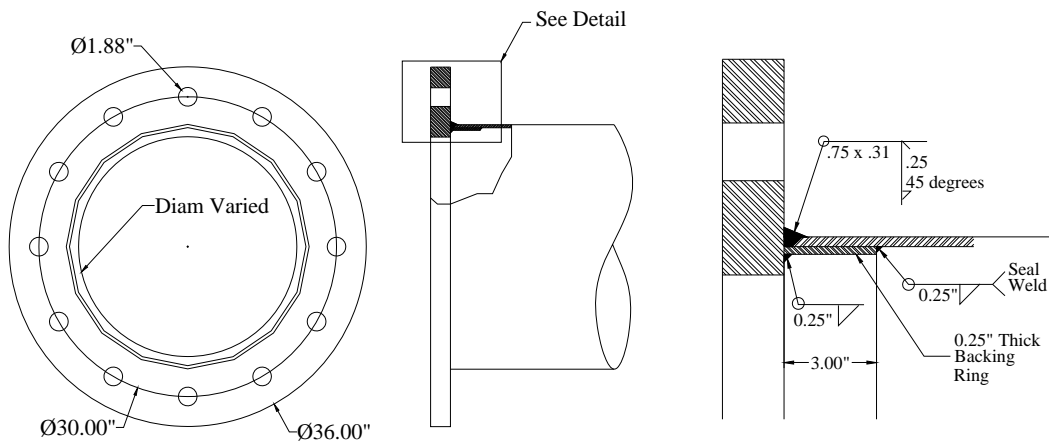


Figure 6.7 Wyoming Detail for Base Plate Inner Diameter Study



Table 6.5 Results of Access Hole Parametric Study

Detail	SCF for BP Inner Diameter:		
	10-in	16-in	22-in
Texas	2.1	2.3	3.1
Wyoming	1.6	1.9	2.6

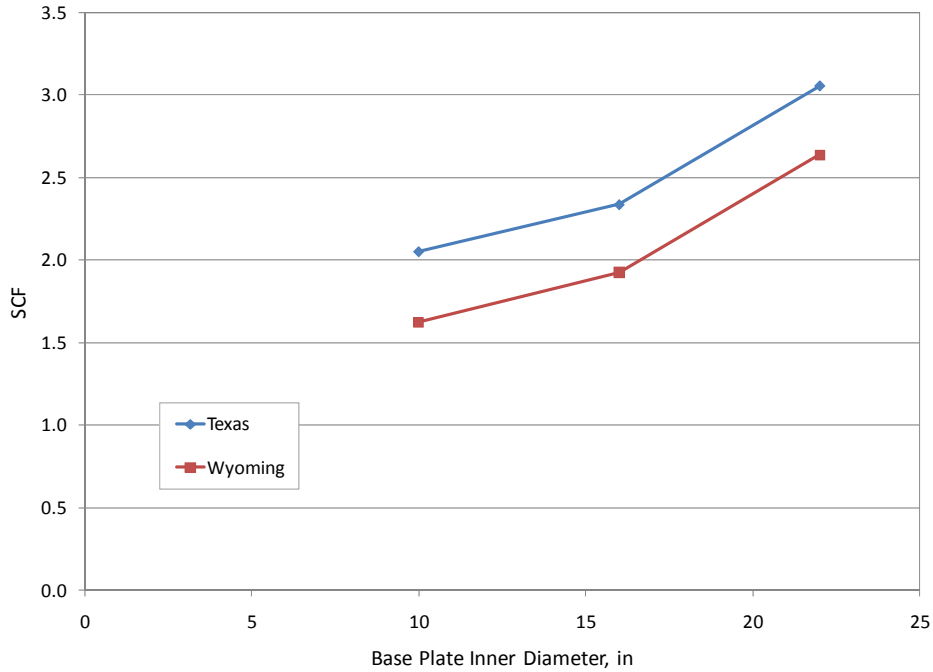


Figure 6.8 Results of Base Plate Inner Diameter Parametric Study

In light of the results, the hypothesis is indeed correct. The stress concentration factor is reduced (and hence, so are hotspot stresses) as the hole size is reduced. However, there appears to be a leveling of the benefit. The greatest reduction in SCF, which is about 25%, comes with the initial decrease in hole diameter from 22-in to 16-in. As the hole size is then decreased to 10-in, the reduction in SCF tapers to only about 10%.

This study also reveals the favorable role played by the Wyoming detail’s backing ring in reducing hotspot stresses. On average, the Wyoming models exhibit stress concentration factors 20% lower than those of the Texas models, and the only geometric difference between these two details is the presence of the backing ring. This attachment acts as an internal collar restraining

the shaft wall and suppressing the local double curvature largely responsible for creating hotspot stresses.

All critical hotspots for the Wyoming models were at the base plate weld, though the top of the backing ring, which is fillet welded to the inside of the pole shaft, also represents a potential hotspot location. The backing ring specified in this detail is only 3-in in length.

Considering the results of this study, it is recommended that base plate holes be made as small as practically possible in full penetration type details. Given that base plates are cut from plate steel, designers can very easily specify a smaller inner diameter. The only important consideration for this design decision is that welders still have adequate access to place quality internal welds.

#### 6.2.4 Collar Length Study

This parametric study considered the Socket External Collar (SEC) connection and sought to investigate whether the stress concentration factor was dependent on the length of the collar. See Figure 6.9 for a detail of this connection.

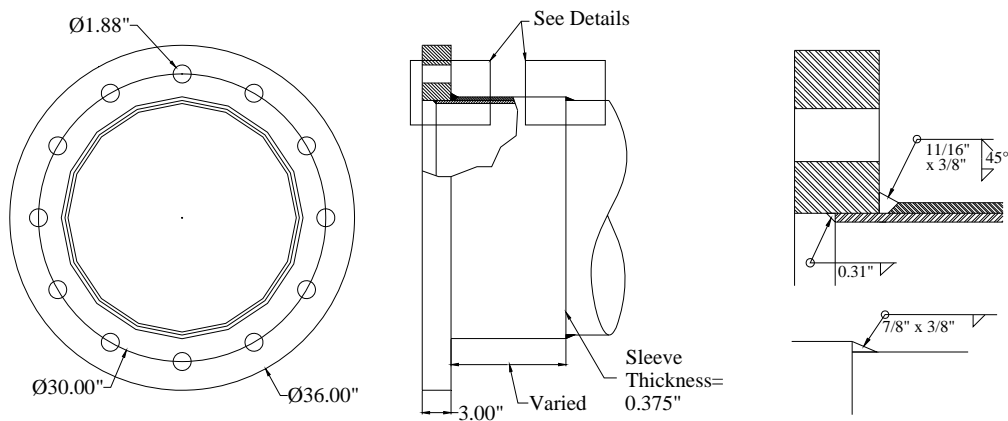


Figure 6.9 Socket External Collar Connection Detail

The largest hotspot stresses for all models in this study occurred at the base plate weld toes, though each model also had a smaller hotspot at the top of its collar. The lower stresses at the

end of the collar agree with experimental results. For the properly fabricated Valmont SEC specimens, fracture initiated at the toe of the base plate weld, not the collar weld.

In addition to this detail's specified collar length of 12-in, three other lengths were considered: 3-in, 6-in, and 18-in. See Table 6.6 and Figure 6.10 for all SCF results.

Table 6.6 Results of Collar Length Study

Collar Length	SCF
3-in	2.2
6-in	2.1
12-in	2.1
18-in	2.2

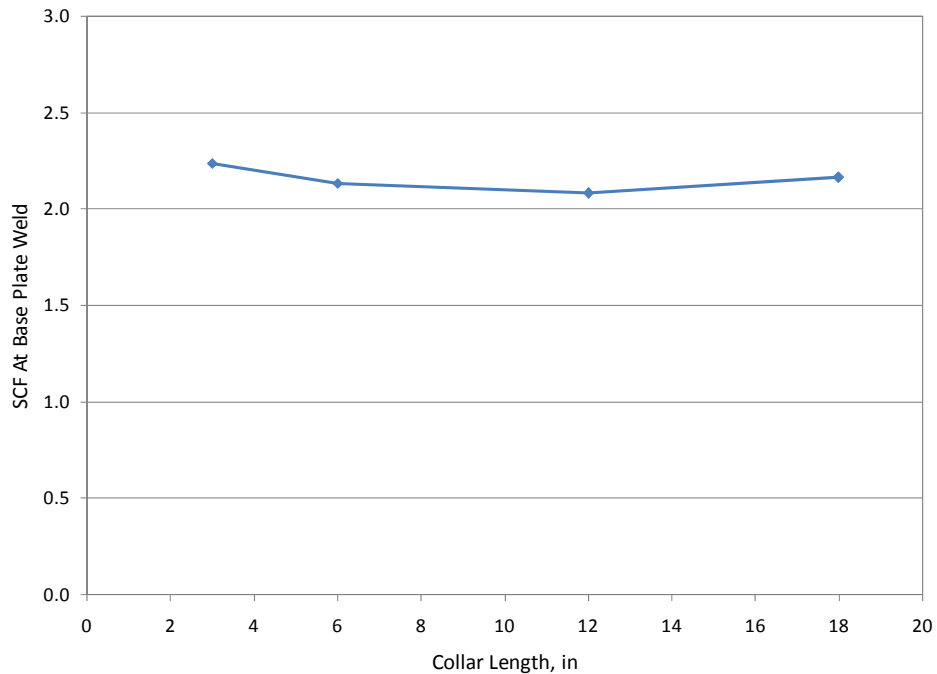


Figure 6.10 Results of Collar Length Study

The results show that the stress concentration factor at the base plate weld toe of SEC details has virtually negligible dependence on the length of the collar. More importantly, these SCFs, when compared to the SCF of an unstiffened 3-in socket, which is about 3.6, suggest that the very presence of the collar is of far greater importance than its length. Adding a collar to a 3-in socket detail reduces its SCF by 40%, regardless of the collar's length.

Following this study, and also in light of experimental evidence, it is recommended to provide collars on all socket details to improve their fatigue performance. The length of the collar is up to the discretion of the designer, but is recommended to be between 3-in and 18-in based on the results of this study.

### 6.2.5 Shaft Bend Radius Study

This parametric study considered the internal radii of the bends in the pole shaft and their effect on stress concentration. These bends are created as the pole shaft is formed in a press brake. The specified bend radius was 4-in for all Valmont experimental specimens, and those that were measured confirmed this. However, radii can vary greatly among manufacturers due to differences in fabrication methods. In addition to 4-in, radii of 2-in and 0.5-in were considered in this study. All models were sixteen-sided with 5/16-in walls and had socket-type details with 3-in base plates, 24-in diameters, and twelve anchor rods. See Figure 6.2 for a schematic.

Hypothetically, it was thought that by reducing the bend radii, the poles' vertices would become sharper and act as stress risers, elevating hotspots and also SCFs (the nominal stress changes are small for poles with these different radii). See Table 6.7 and Figure 6.11 for the SCF results.

Table 6.7 Results of Bend Radius Study

Bend Radius	SCF
0.5-in	3.8
2-in	3.7
4-in	3.6

In light of the data presented in Figure 6.11, sharper bend radii do appear to attract slightly more stress leading to elevated SCFs, but the difference is not great. When the bend radius was reduced from 4.0-in to 0.5-in, the SCF increased by only about 6%. In light of these results, no significant recommendation can be made concerning pole shaft bend radii.

At the University of Minnesota, Ocel found that sharpening the shaft's bend radii elevated SCFs to a greater degree than what is seen here, but that was for eight and twelve-sided sections (Ocel, 2006). A sixteen-sided section is much closer to a circle than either a eight or twelve-sided mast, and the changes in bend radius considered here (0.5-in vs. 4-in) are not great.

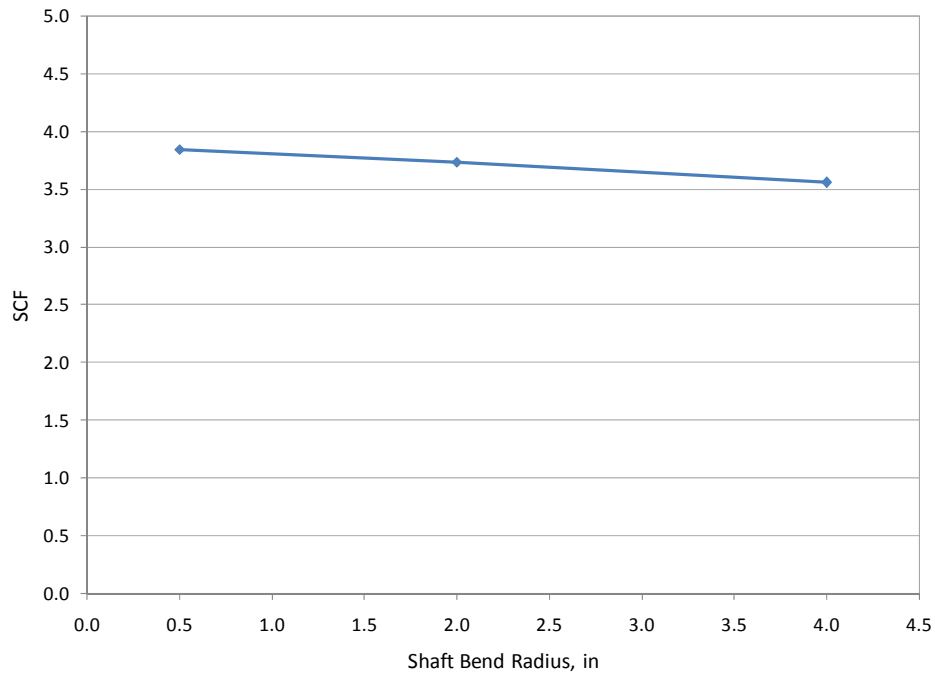


Figure 6.11 Results of Bend Radius Study

### 6.3 Hotspot Results for Experimental Specimens

Finite element models of most Phase I and Phase II connection details were created and analyzed for this portion of the analytical research. Due to their high level of complexity and for lack of adequate time, the stool details from both phases were not included. The Pelco details were also not included in this study. All hotspots, which were determined according to the two numerical methods presented in Chapter 5, were normalized by each model's top fiber nominal stress at the location of the base plate weld to produce stress concentration factors.

Stress concentration factors and experimental hotspot stresses of the tested details are presented in Table 6.8. This table also includes each detail's experimental results, including fatigue lives and fatigue coefficients, which were originally presented in Chapter 4. Fatigue coefficients, which are calculated according to Equation 4.1, provide for direct comparison between details tested at different stresses.

Table 6.8 Experimental and Analytical Results for Phase I and II Specimens

	Detail	Experimental Results					Analytical Results	
		$\sigma_{nom}$ (ksi)	$N_A$	$N_B$	$N_{avg}$	$A_{nom}$ ( $\times 10^8$ )	SCF	$\sigma_{hotspot}$ (ksi)
Phase I Details	24-1.5-8-S	12	13,193	13,193	13,193	0.2	7.1	84.8
	24-1.5-12-S	12	27,977	27,977	27,977	0.5	6.1	73.5
	24-2-8-S	12	46,772	46,772	46,772	0.8	5.4	64.3
	24-2-12-S	12	143,214	143,214	143,214	2.5	5.0	60.0
	24-3-8-S	12	147,550	147,550	147,550	2.5	3.7	44.7
	24-2-8-WY	12	133,819	133,819	133,819	2.3	4.5	54.0
	24-3-12-TX	12	236,154	327,487	281,821	4.9	3.1	37.2
Phase II Details	24-3-12-TXEC	12	4,034,441	4,034,441	4,034,441	69.7	1.7	20.4
	24-3-12-SEC	18	540,520	345,542	443,031	25.8	2.1	37.8
	24-3-12-WEC	18	1,330,470	1,001,859	1,166,165	68.0	1.8	32.4
	24-3-12-WTh	11.4	862,107	680,613	771,360	11.4	1.8	20.5

The fatigue coefficients,  $A_{nom}$ , which directly quantify the fatigue performance of the above details, are plotted versus analytical stress concentration factor in Figure 6.12 below. When plotted in log-log space, there is very good linear correlation between the two quantities, revealing that analytical SCF is a good predictor of a detail’s potential fatigue performance.

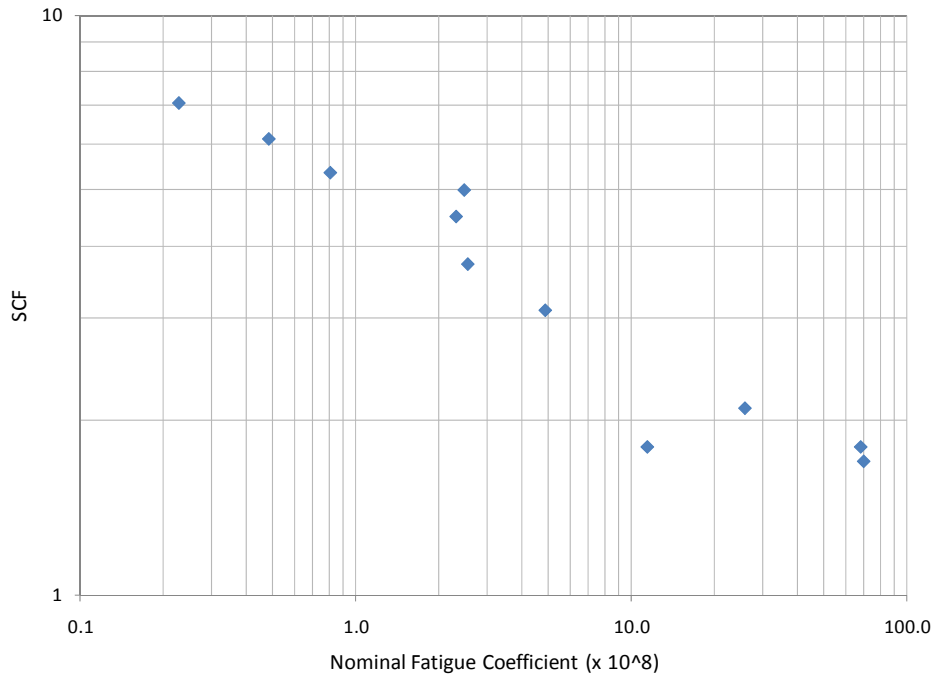


Figure 6.12 Experimental Fatigue Performance vs. Analytical SCF

The data presented in Table 6.8 can also be visualized by plotting, for each set of specimens, average experimental fatigue life versus hotspot stress, where the latter is found by multiplying the experimental nominal stress by the analytical stress concentration factor. See Figure 6.13 for this plot.

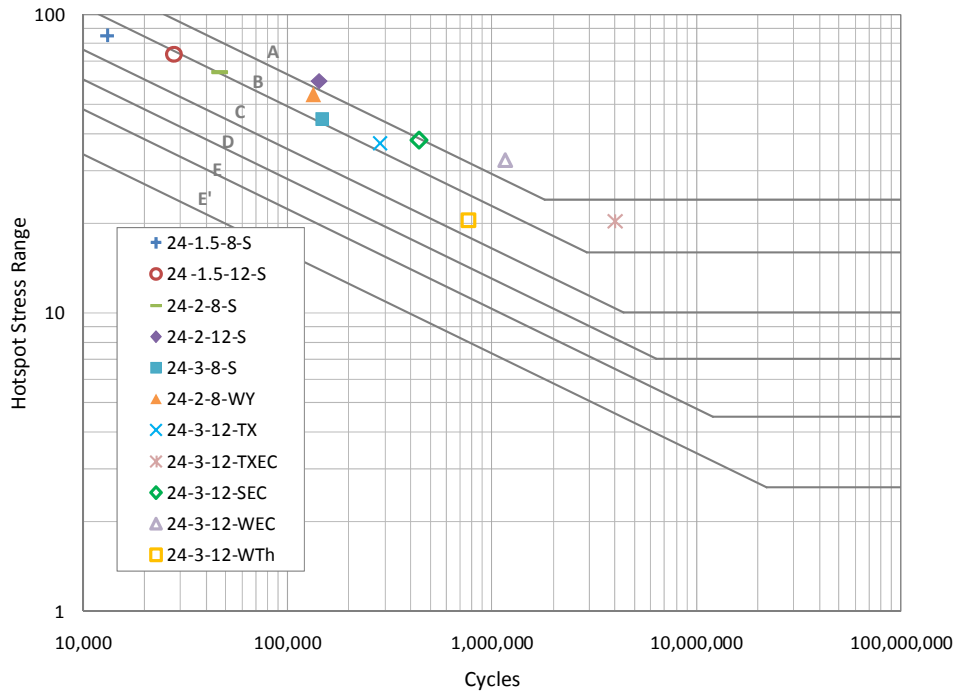


Figure 6.13 Experimental Fatigue Life vs. Hotspot Stress

The data points in Figure 6.13 plot in a reasonably well-defined linear cluster (also called an “X-curve”) that congregates above the Category C line. This indicates that the calculated geometric SCFs are reasonably accurate and implicitly verifies the analytical procedure.

It is expected that the details should all plot in the Category C/B region. Category C is the AASHTO fatigue category for unground fillet welds not subject to any macro-geometric amplification, and its fatigue category line is a lower bound of established test data. By considering the high mast connections’ geometric hotspot stresses rather than nominal stresses, stress amplification due to connection flexibility is essentially removed, leaving behind a Category C detail.

The Wyoming Thick Wall (WTh) data points plotted the farthest below the cluster, which may indicate that their failures were premature. This could be caused by welds with excessive

imperfections or poor profiles. Unfortunately, no sections of their welds are available to verify this hypothesis.

The regression slope for this cluster of data is -0.26, which is a 24% difference from the expected value for steel of -0.33.



## 7 Conclusions and Recommendations

This chapter will summarize the conclusions and recommendations that followed this research study. Chapter 4 presents additional discussion concerning the analytical results and Chapter 6 presents additional discussion and recommendations concerning the experimental results.

This chapter will be divided into three sections: Experimental Conclusions, Analytical Conclusions, and Recommendations.

### 7.1 Experimental Conclusions

- High mast fatigue performance is drastically improved through the addition of external collars to existing high mast connections (these collars are also known as “ground sleeves”). This benefit is consistent for both socket details and full penetration details.
- Full penetration details see a strong improvement in fatigue performance when their base plate inner diameters are reduced. This reduction is not possible in socket details due to the fundamental construction of their connection.
- Fatigue performance is very much dependent on the shape of the weld at potential fracture locations, and the use of unequal fillets is necessary. The socket external collar specimens fabricated by Pelco Products performed worse than identical Valmont specimens due to the use of equal leg fillet welds.
- The experimental data do not show a strong benefit in fatigue performance from thickening the shaft wall. However, the results are not totally conclusive, and this variable needs further experimental study. Other experimental studies have found a modest fatigue life improvement from thickening the pole shaft wall (Ocel, 2006).

- Varying bend radii in sixteen-sided poles does not appear to play a strong role in affecting experimental fatigue performance. Pelco's poles, which have 0.5-in radii, did not show significantly different performance than Valmont's, which have 0.4-in radii.
- Stool-stiffened details with continuous rings show a slight improvement in performance over stool details with individual cap plates. This improvement is due to a more uniform distribution of stress.
- The AASHTO fatigue classification scheme needs revision as it is both unconservative for many socket details and oversimplified in general. Current category assignments do not account for base plate thickness, base plate inner diameter, or the presence of collars. These variables have all been shown to strongly affect fatigue performance.

## 7.2 Analytical Conclusions

- The Structural Stress and DNV hotspot determination methods are in good agreement, regularly differing by only 1-4%. The former is a linear resolution of through thickness stresses, and the latter is a linear extrapolation of surface stresses approaching the weld.
- Increasing either the shaft diameter or wall thickness of a mast always results in a reduced hotspot stress. This hotspot reduction can potentially result in improved fatigue performance; however, this observation assumes that the load remains constant as the section is modified. This assumption may not be true for some loading types.
- For a constant base plate size, increasing a mast's diameter actually increases the stress concentration factor (SCF). This occurs because the reduction in nominal stress exceeds the reduction in hotspot stress. This observation is confirmed by all similar studies in the literature.
- For increases in wall thickness, the reduction in hotspot stress is roughly proportional to the reduction in nominal stress, thus the SCF does not change appreciably. This observation is confirmed by a majority of similar studies in the literature.

- Adding anchor rods to a high mast connection only results in an SCF reduction when the base plate connection is already relatively flexible. The SCF is shown to be insensitive to the number of anchor rods, provided the base plate is 3-in or thicker for socket details and 2-in or thicker for full penetration details.
- In full penetration groove-welded details, the SCF can be significantly reduced by decreasing the size of the base plate hole. The greatest benefit comes as the hole diameter is reduced from 22-in to 16-in. The benefit tapers as the hole diameter is then reduced further to 10-in.
- The presence of a backing ring in full penetration details can reduce the SCF by up to 20% where the backing ring is fillet welded to the inside of the pole shaft.
- Adding a collar to a socket detail with a 3-in base plate reduces the SCF by 40%. This SCF does not appear to be sensitive to the length of the collar.
- For sixteen-sided masts, the SCF shows a very small dependence on shaft bend radius when considering radii of 4-in, 2-in, and 0.5-in. Other studies have shown a greater sensitivity to bend radius for shafts eight or twelve sides (Ocel, 2006).
- The high mast fatigue data from both phases collapse well into a linear cluster, or X-curve, when plotted against geometric hotspot stress rather than nominal stress. The regression slope of this linear cluster is reasonably close to the expected value for steel.

### 7.3 Recommendations

- The use of external collars, or “ground sleeves,” is strongly recommended in high mast connection designs, both for socket and full penetration details. These stiffening attachments are at least as beneficial as stool attachments and are easier to fabricate.

- The continued use of unequal leg fillet welds is recommended where fatigue cracking is possible. Previous research has shown the importance of these welds (Miki, 1984), and they are also specified by AASHTO.
- Reduced base plate inner diameters are recommended for full penetration details. These should be as small as possible while still allowing adequate welder access to the inside of the mast.
- Use of eight or twelve anchor rods is recommended for 24-in masts; sixteen is unnecessary. This is valid only for base plates 3-in or thicker, which was recommended following Phase I (Rios, 2007).
- Continued experimental testing of thick-walled high masts is recommended to further characterize the role this variable plays in affecting fatigue performance.

## Appendix A Recommended Installation Procedure

1. With the loading box supported by scrap wide-flange sections (see Fig A1) and the roller-end (north) support lowered to the ground, remove the entire pinned-end (south) support from the strong floor using the overhead gantry crane. Set aside.
2. Install the anchor rods on the loading box in either the 8-bolt or 12-bolt configuration. Tighten top and bottom nuts with approximately 500 ft-lbs torque. Loosely hand-tighten remaining nuts to ease eventual mating of the high mast base plate. See Figure A1.
3. Install leveling nuts and washers to a stand-off length (distance from load box face to base plate underside) of 4.5". See Figure A1.

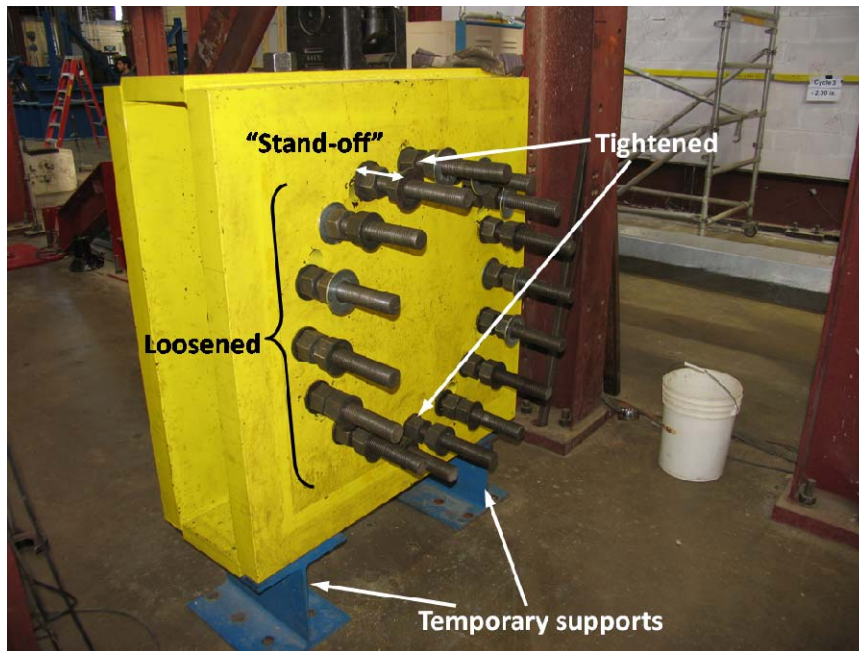


Figure A1 Supported Load Box

4. Using the gantry crane in a trial-and-error process, position load lifting straps on the incoming high mast specimen such that specimen is near horizontal when lifted. See Figure A2.



Figure A2 Lifting High Mast Specimen

5. Beginning with the pinned-end of the setup, mate the first specimen with the anchor rods. It may be necessary to alternately raise and lower the gantry crane to “walk” the specimen onto the top and bottom rods. If necessary due to misalignment, manually insert remaining rods into base plate by loosening them from loading box and drawing them towards specimen. See Figure A3.

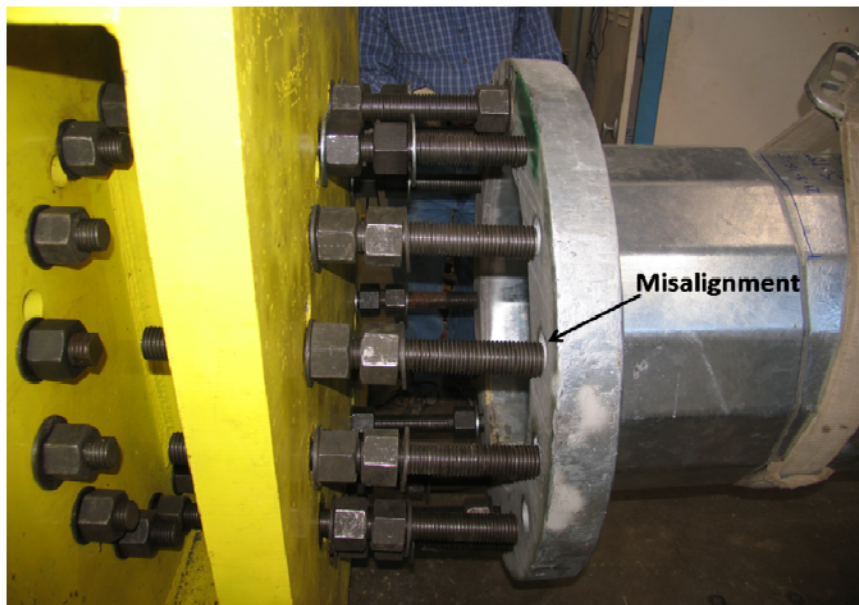


Figure A3 Mating of Specimen Base Plate

6. Once specimen is fully mated with all leveling nuts, secure to load box by tightening all remaining nuts (i.e. load box nuts, leveling nuts, and base plate nuts) on top, bottom, and side anchor rods (i.e. 3, 6, 9, and 12 o'clock positions). Use approximately 200-300 ft-lbs of torque.
7. Using overhead gantry crane in conjunction with hydraulic ram, lift specimen in a level manner until end plate bottom is 2 feet above floor. Support this end with a temporary saw-horse positioned beneath the pole. This may require wooden shims to ensure the 2 foot distance. See Figure A4. At this point, gantry crane can be lowered and straps removed.



Figure A4 Temporary Saw Horse Support

8. Once again using gantry crane, replace pinned-end support by mating its base plate with strong floor anchor rods. Hand-tighten anchor rod nuts. See Figure A5.





Figure A5 Replacing Pinned-End Support

9. Reaction plate bolt holes should nearly align with specimen end plate bolt holes. If not, it may be necessary to replace lifting straps on specimen and raise (or lower) until reaching mutual alignment. If helpful, a spud wrench end may alternately be used to draw the two holes into alignment. Once holes are aligned, install and hand-tighten nuts and bolts.
10. Repeat steps 4 through 6 with north end specimen and its supports.
11. Using hydraulic ram, lift loading box and specimens until north specimen end plate aligns with roller-end reaction plate. Install nuts and bolts hand-tight.
12. Tighten all end plate nuts using pneumatic impact wrench. See Figure A6.





Figure A6 Tightening with Pneumatic Impact Wrench

13. Tighten pinned-end base plate nuts to strong floor using slugger wrench and sledge hammer.
  
14. Secure load box connection by:
  - a. Clamping all load box nuts to box with approximately 500 ft-lbs torque.
  - b. Drawing leveling nuts out to base plate with approximately 200-300 ft-lbs torque.
  - c. Working in a star pattern, tightening all base plate nuts using pneumatic torque wrench at approximately 1000 ft-lbs torque. See Figure A7.

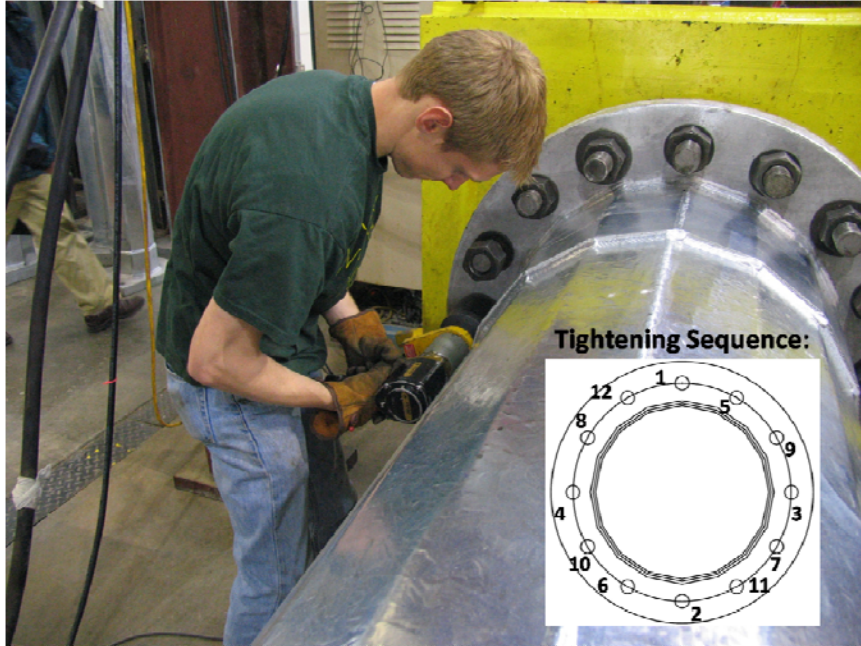


Figure A7 Tightening Base Plate Nuts

Setup is now ready to be tested.

# Appendix B Test Specimen Dimensions

## Table B1 All Measured Dimensions

Specimen	Length, in	Wall thickness at base, in				Base outer diam to flats, in			Base outer diam to corners, in			Outer diam at 12" to flats, in			Taper, in/ft
		1	2	3	Avg	1	2	Avg	1	2	Avg	1	2	Avg	
24-3-12-TXEC-VG-A	174.25	0.319	0.312	0.317	0.316	24.75	24.6875	24.71875	25	24.875	24.9375	23.882	23.882	23.882	0.83675
24-3-12-TXEC-VG-B	174	0.325	0.321	0.334	0.326667	24.875	24.5	24.6875	25.125	25.0625	25.09375	23.90333	23.90333	23.90333	0.784167
24-3-12-SEC-VG-A	174.125	0.308	0.315	0.308	0.310333	23.87067	23.87067	23.87067	24.05817	24.12067	24.08942				
24-3-12-SEC-VG-B	174.1875	0.31	0.309	0.312	0.310333	23.87067	23.87067	23.87067	24.24567	24.05817	24.15192				
24-3-12-WEC-VG-A	174.25	0.324	0.317	0.317	0.319333	24.0625	23.3125	23.6875	24.375		24.375				
24-3-12-WEC-VG-B	174.25	0.31	0.324		0.317	24.25	24.25	24.25	24.5	24.5	24.5				
24-3-12-WTh-VG-A	174.25	0.505	0.507	0.509	0.507	23.75	23.75	23.75	24	24	24	23.5		23.5	0.25
24-3-12-WTh-VG-B	174.25	0.496	0.5	0.503	0.499667	23.25	24	23.625	24.25	24	24.125	23.5		23.5	0.125
24-2-12-STL-VG-A	174.125	0.3	0.304	0.3	0.301333	23.80133	23.55133	23.67633	23.92633	23.80133	23.86383				
24-2-12-STL-VG-B	174	0.297	0.296	0.3	0.297667	23.84533	23.84533	23.84533	24.09533	24.09533	24.09533				
24-2-12-STL30-VG-A	174.125	0.3	0.306	0.302	0.302667	23.85533	23.85533	23.85533	24.10533	24.10533	24.10533				
24-2-12-STL30-VG-B	174	0.304	0.34	0.36	0.334667	23.91933	24.04433	23.98183	24.16933	24.16933	24.16933				
24-2-8-STL-VG-A	173.75					23.875		23.875	24.125		24.125				
24-2-8-STL-VG-B	173.75					23.875		23.875	24.125		24.125				
24-3-16-WY-PG	174.125	0.316	0.314	0.312	0.314	23.25	23.25	23.25	24	24	24	23	22.9375	22.96875	0.28125
24-3-16-TX-PG	174	0.317	0.316	0.342	0.325	23.25	23.125	23.1875	24	24	24	22.75	22.875	22.8125	0.375
24-3-16-SEC-PG-A	173.75	0.341	0.343	0.317	0.333667	23.91733	23.79233	23.85483	23.66733	23.54233	23.60483				
24-3-16-SEC-PG-B	173.875	0.317	0.336	0.338	0.330333	23.41067	23.41067	23.41067	23.66067	23.78567	23.72317				

110

Specimen	Base plate thickness, in				Base plate weld, long leg, in				Base plate weld, short leg, in				Base plate inner diameter, in			
	1	2	3	Avg	1	2	3	Avg	1	2	3	Avg	1	2	3	Avg
24-3-12-TXEC-VG-A	2.978	2.969	2.973	2.973333	0.84375	0.78125	0.875	0.833333	0.53125	0.46875	0.5	0.5	20.5	20.5		20.5
24-3-12-TXEC-VG-B	2.978	2.968	3.003	2.983	0.96875	1	0.9375	0.96875	0.34375	0.46875	0.3125	0.375	20.5	20.5		20.5
24-3-12-SEC-VG-A	3.009	3.005	3.004	3.006	1.125	1.125	1.09375	1.114583	0.5625	0.5625	0.59375	0.572917				n/a
24-3-12-SEC-VG-B	3.012	3.01	3.016	3.012667	1.0625	1.09375	1.0625	1.072917	0.5	0.5625	0.6875	0.583333				n/a
24-3-12-WEC-VG-A	3	3	3.03125	3.010417	1	1	1	1	0.5	0.5	0.5	0.5	12.4375	12.4375		12.4375
24-3-12-WEC-VG-B	3	3	3.0625	3.020833	1	1		1	0.5	0.5		0.5	12.5	12.5		12.5
24-3-12-WTh-VG-A	3	3	3	3	0.8125	0.875	0.875	0.854167	0.375	0.3125	0.375	0.354167	12.4375	12.375		12.40625
24-3-12-WTh-VG-B	3	3	3	3	0.8125	0.875	0.75	0.8125	0.375	0.5	0.4375	0.4375	12.4375	12.4375		12.4375
24-2-12-STL-VG-A	2	2	2	2	0.75	0.75	0.75	0.75	0.4375	0.5	0.4375	0.458333				n/a
24-2-12-STL-VG-B	2.03	2.035	2.03	2.031667	0.8125	0.8125	0.6875	0.770833	0.4375	0.4375	0.5	0.458333				n/a
24-2-12-STL30-VG-A	2.04	2.03	2.03	2.033333	0.6875	0.6875	0.625	0.666667	0.4375	0.4375	0.4375	0.4375				n/a
24-2-12-STL30-VG-B	2.05	2.04	2.04	2.043333	0.625	0.625	0.625	0.625	0.4375	0.5	0.5625	0.5				n/a
24-2-8-STL-VG-A	2.04	2.035	2.03	2.035	0.375	0.4375	0.375	0.395833	0.4375	0.375	0.375	0.395833				n/a
24-2-8-STL-VG-B	2.025	2.025	2.03	2.026667	0.5625	0.4375	0.5625	0.520833	0.4375	0.375	0.3125	0.375				n/a
24-3-16-WY-PG	3	3	3	3	0.8125	0.8125	0.8125	0.8125	0.4375	0.375	0.3125	0.375	12.5 nom			
24-3-16-TX-PG	3	3	3	3	0.75	0.75	0.75	0.75	0.4375	0.4375	0.4375	0.4375	12.5 nom			
24-3-16-SEC-PG-A	3	3	3	3	0.6875	0.75	0.6875	0.708333	0.5	0.5	0.4375	0.479167				n/a
24-3-16-SEC-PG-B	3	3	3	3	0.6875	0.75	0.8125	0.75	0.5	0.5625	0.5	0.520833				n/a

Specimen	Backing bar height, in			Collar weld, long leg, in				Collar weld, short leg, in				Collar height, in			Collar thickness, in			
	1	2	Avg	1	2	3	Avg	1	2	3	Avg	1	2	Avg	1	2	3	Avg
24-3-12-TXEC-VG-A			n/a	1.125	1	1.03125	1.052083	0.3125	0.40625	0.375	0.364583	12.375	12.3125	12.34375	0.369	0.362	0.364	0.365
24-3-12-TXEC-VG-B			n/a	0.9375	0.9375	0.875	0.916667	0.4375	0.46875	0.46875	0.458333	12.25	12.5	12.375	0.366	0.367	0.366	0.366333
24-3-12-SEC-VG-A			n/a	1	1	0.96875	0.989583	0.34375	0.375	0.375	0.364583	12.5	12.375	12.4375	0.366	0.364	0.364	0.364667
24-3-12-SEC-VG-B			n/a	0.75	0.90625	0.9375	0.864583	0.40625	0.40625	0.4375	0.416667	12.125	12.5	12.3125	0.362	0.366	0.369	0.365667
24-3-12-WEC-VG-A				0.875	0.8125	0.875	0.854167	0.375	0.3125	0.375	0.354167	12.5	12.5625	12.53125				
24-3-12-WEC-VG-B				0.875	0.8125		0.84375	0.375	0.375		0.375	12.625	12.625	12.625				
24-3-12-WTh-VG-A	3.25	3.5	3.375				n/a				n/a			n/a				n/a
24-3-12-WTh-VG-B							n/a				n/a			n/a				n/a
24-2-12-STL-VG-A			n/a				n/a				n/a			n/a				n/a
24-2-12-STL-VG-B			n/a				n/a				n/a			n/a				n/a
24-2-12-STL30-VG-A			n/a				n/a				n/a			n/a				n/a
24-2-12-STL30-VG-B			n/a				n/a				n/a			n/a				n/a
24-2-8-STL-VG-A			n/a				n/a				n/a			n/a				n/a
24-2-8-STL-VG-B			n/a				n/a				n/a			n/a				n/a
24-3-16-WY-PG							n/a				n/a			n/a				n/a
24-3-16-TX-PG			n/a				n/a				n/a			n/a				n/a
24-3-16-SEC-PG-A			n/a	0.5625	0.75	0.5	0.604167	0.5	0.625	0.5	0.541667	12	12	12	0.364	0.372	0.375	0.370333
24-3-16-SEC-PG-B			n/a	0.375	0.375	0.375	0.375	0.375	0.5	0.5	0.458333	12	12	12	0.3745	0.3745	0.3745	0.3745

Specimen	Stool rib height, in				Stool rib thickness, in				Stool rib separation, in				Stool cap plate thickness, in			
	1	2	3	Avg	1	2	3	Avg	1	2	3	Avg	1	2	3	Avg
24-3-12-TXEC-VG-A				n/a				n/a				n/a				n/a
24-3-12-TXEC-VG-B				n/a				n/a				n/a				n/a
24-3-12-SEC-VG-A				n/a				n/a				n/a				n/a
24-3-12-SEC-VG-B				n/a				n/a				n/a				n/a
24-3-12-WEC-VG-A				n/a				n/a				n/a				n/a
24-3-12-WEC-VG-B				n/a				n/a				n/a				n/a
24-3-12-WTh-VG-A				n/a				n/a				n/a				n/a
24-3-12-WTh-VG-B				n/a				n/a				n/a				n/a
24-2-12-STL-VG-A	10.875	10.9375	10.875	10.89583	0.507	0.515	0.508	0.51	3.0625	3.125	3.125	3.104167	1.26	1.27	1.26	1.263333
24-2-12-STL-VG-B	10.9375	11	10.9375	10.95833	0.511	0.504	0.51	0.508333	2.9375	3	3	2.979167	1.27	1.275	1.266	1.270333
24-2-12-STL30-VG-A	10.875	10.875	10.875	10.875	0.505	0.514	0.505	0.508	2.9375	3.1875	3.0625	3.0625	1.2669	1.265	1.265	1.265633
24-2-12-STL30-VG-B	10.9375	10.875	10.9375	10.91667	0.505	0.507	0.512	0.508	3.0625	3.0625	3.0625	3.0625	1.26	1.27	1.26	1.263333
24-2-8-STL-VG-A	10.875			10.875	0.5			0.5	3.125			3.125	1.25			1.25
24-2-8-STL-VG-B	10.75	10.875		10.8125	0.5			0.5	3			3	1.25			1.25
24-3-16-WY-PG				n/a				n/a				n/a				n/a
24-3-16-TX-PG				n/a				n/a				n/a				n/a
24-3-16-SEC-PG-A				n/a				n/a				n/a				n/a
24-3-16-SEC-PG-B				n/a				n/a				n/a				n/a

## Appendix C Testing Stresses and Loads

Table C1 Testing Stresses and Loads

Specimen	S <sub>nom</sub> , ksi	S <sub>min</sub> , ksi	S <sub>max</sub> , ksi	P <sub>min</sub> , ksi	P <sub>max</sub> , ksi
24-3-12-TXEC-VG-A	12	10	22	15.5	34.2
24-3-12-TXEC-VG-B	12	10	22	15.5	34.2
24-3-12-SEC-VG-A	18	13	31	19.8	47.3
24-3-12-SEC-VG-B	18	13	31	19.8	47.3
24-3-12-WEC-VG-A	18	7	25	10.7	38.1
24-3-12-WEC-VG-B	18	7	25	10.7	38.1
24-3-12-WTh-VG-A	11.4	4.5	15.9	10.7	38.1
24-3-12-WTh-VG-B	11.4	4.5	15.9	10.7	38.1
24-2-12-STL-VG-A	12	10	22	15.3	33.6
24-2-12-STL-VG-B	12	10	22	15.3	33.6
24-2-12-STL30-VG-A	12	10	22	15.3	33.6
24-2-12-STL30-VG-B	12	10	22	15.3	33.6
24-2-8-STL-VG-A	12	10	22	15.3	33.6
24-2-8-STL-VG-B	12	10	22	15.3	33.6
24-3-16-WY-PG	18	7	25	10.8	38.7
24-3-16-TX-PG	18	7	25	10.8	38.7
24-3-16-SEC-PG-A	18	7	25	10.8	38.7
24-3-16-SEC-PG-B	18	7	25	10.8	38.7

## Appendix D Analytical Hotspot Stresses

Table D1: All Hotspot Stresses

Parametric Study	Model	DNV Hotspot	SS Hotspot	Avg Hotspot	Nom Stress	SCF
1. Shaft Diameter and Wall Thickness Study	24-1-12-S 5/16 wall	11.06	11.35	11.20	1.25	9.0
	24-2-12-S 5/16 wall	6.14	6.45	6.29	1.25	5.0
	24-3-12-S 5/16 wall	4.39	4.52	4.46	1.25	3.6
	24-4-12-S 5/16 wall	3.75	3.88	3.82	1.25	3.1
	24-1-12-S 1/2 wall	6.89	7.05	6.97	0.78	8.9
	24-2-12-S 1/2 wall	4.10	4.19	4.14	0.78	5.3
	24-3-12-S 1/2 wall	2.86	2.93	2.90	0.78	3.7
	24-4-12-S 1/2 wall	2.33	2.41	2.37	0.78	3.0
	36-1-12-S 5/16 wall	9.25	9.52	9.38	0.55	17.1
	36-2-12-S 5/16 wall	4.81	4.93	4.87	0.55	8.9
	36-3-12-S 5/16 wall	3.02	3.11	3.07	0.55	5.6
	36-4-12-S 5/16 wall	2.27	2.34	2.30	0.55	4.2
	36-1-12-S 1/2 wall	5.61	5.79	5.70	0.34	16.8
	36-2-12-S 1/2 wall	3.24	3.33	3.29	0.34	9.7
	36-3-12-S 1/2 wall	2.05	2.10	2.08	0.34	6.1
	36-4-12-S 1/2 wall	1.50	1.54	1.52	0.34	4.5
2. Anchor Rod Study	24-2-6-S	7.21	7.52	7.37	1.25	5.9
	24-3-6-S	4.77	4.90	4.83	1.25	3.9
	24-4-6-S	3.91	4.05	3.98	1.25	3.2
	24-2-12-S	6.14	6.45	6.29	1.25	5.0
	24-3-12-S	4.39	4.52	4.46	1.25	3.6
	24-4-12-S	3.75	3.88	3.82	1.25	3.1
	24-2-16-S	5.76	6.06	5.91	1.25	4.7
	24-3-16-S	4.25	4.39	4.32	1.25	3.5
	24-4-16-S	3.71	3.84	3.77	1.25	3.0
	24-2-8-TX	4.33	4.39	4.36	1.27	3.4
	24-3-8-TX	3.02	3.06	3.04	1.27	2.4
	24-4-8-TX	2.56	2.61	2.58	1.27	2.0
	24-2-12-TX	4.08	4.15	4.12	1.27	3.2
	24-3-12-TX	2.94	2.99	2.97	1.27	2.3
	24-4-12-TX	2.53	2.58	2.55	1.27	2.0
	24-2-16-TX	3.93	4.01	3.97	1.27	3.1
24-3-16-TX	2.93	2.96	2.94	1.27	2.3	
24-4-16-TX	2.48	2.54	2.51	1.27	2.0	
3. Base Plate Inner Diameter Study	24-3-12-TX 22" hole	3.84	3.91	3.87	1.27	3.0
	24-3-12-TX 16" hole	2.94	2.99	2.97	1.27	2.3
	24-3-12-TX 10" hole	2.58	2.63	2.61	1.27	2.1
	24-3-12-WY 22" hole	3.30	3.34	3.32	1.26	2.6
	24-3-12-WY 16" hole	2.41	2.44	2.42	1.26	1.9
	24-3-12-WY 10" hole	2.03	2.06	2.05	1.26	1.6
4. Collar Length Study	24-3-12-SEC 3" collar	2.77	2.78	2.78	1.24	2.2
	24-3-12-SEC 6" collar	2.63	2.66	2.65	1.24	2.1
	24-3-12-SEC 12" collar	2.56	2.60	2.58	1.24	2.1
	24-3-12-SEC 18" collar	2.66	2.70	2.68	1.24	2.2
5. Bend Radius Study	24-3-12-S 0.5-in rad	4.78	4.76	4.77	1.24	3.8
	24-3-12-S 2-in rad	4.62	4.67	4.65	1.24	3.7
	24-3-12-S 4-in rad	4.39	4.50	4.45	1.25	3.6

Experimental Details	24-1.5-8-S	8.74	8.93	8.83	1.25	7.1
	24 -1.5-12-S	7.56	7.76	7.66	1.25	6.1
	24-2-8-S	6.62	6.78	6.70	1.25	5.4
	24-2-12-S	6.14	6.45	6.29	1.25	5.0
	24-3-8-S	4.59	4.72	4.66	1.25	3.7
	24-2-8-WY (22" hole)	5.68	5.74	5.71	1.25	4.6
	24-3-12-TX (22" hole)	3.84	3.91	3.87	1.25	3.1
	24-3-12-TXEC	2.07	2.12	2.09	1.25	1.7
	24-3-12-SEC	2.56	2.60	2.58	1.25	2.1
	24-3-12-WEC	2.23	2.28	2.26	1.25	1.8
	24-3-12-WTh	1.51	1.54	1.53	0.8	1.9

## References

1. American Association of State Highway and Transportation Officials, AASHTO Standard Specifications for Structural Supports for Highway Signs, Luminaries and Traffic Signals. Fourth Edition, AASHTO, Washington, D.C., 2001.
2. Anderson, T.H., Fatigue Life Investigation of Traffic Mast-Arm Connection Details. M.S. Thesis, Department of Civil Engineering, The University of Texas at Austin, August 2007.
3. Det Norske Veritas (DNV), Fatigue Design of Offshore Steel Structures. Recommended Practice, DNV-RP-C203, April 2008.
4. Dong, P., A structural stress definition and numerical implementation for fatigue analysis of welded joints. International Journal of Fatigue 23 (2001), pp. 865-876, June 2001.
5. Duraisamy, R., Finite Element Study of Mast Arm Socket Welded Connections. M.S. Thesis, Department of Civil Engineering, The University of Texas at Austin, December 2005.
6. Getting Started with ABAQUS. Version 6.6, Rising Sun Mills, Providence, RI, 2006.
7. High Mast Illumination Poles. Standard Plans, Texas Department of Transportation (TXDOT), August 1995.
8. Koenigs, et al., Fatigue Resistance of Traffic Signal Mast-Arm Connections. Texas Department of Transportation, Research Report 4178-2, Center for Transportation Research, August 2003.
9. Miki, Chitoshi, Fisher, J.W., Slutter, R.G., Fatigue Behavior of Steel Light Poles. Report No. 200.81.714.1. Fritz Engineering Laboratory, Lehigh University, 1984.
10. Ocel, J.M., The Behavior of Thin Hollow Structural Section (HSS) to Plate Connections. Dissertation, The Department of Civil Engineering, The University of Minnesota, October, 2006.
11. Rios, C.A., Fatigue Performance of Multi-Sided High-Mast Lighting Towers. M.S. Thesis, Department of Civil Engineering, The University of Texas at Austin, May 2007.
12. Warpinski, M.K., The Effect of Base Connection Geometry on the Fatigue Performance of Welded Socket Connections in Multi-sided High-mast Lighting Towers. M.S. Thesis, Department of Civil Engineering, Lehigh University, May 2006.



## Vita

Andrew Philip Stam was born on April 1, 1985, to John and Mary Stam in Iowa City, IA. He grew up in Enid, Oklahoma, attending Emmanuel Christian School and Oklahoma Bible Academy there. After completing an undergraduate education at Oklahoma State University in May of 2007, he enrolled in the University of Texas at Austin to pursue a Master's degree.

He enjoyed immensely the graduate program in Structural Engineering at the University of Texas and hopes to someday pursue a PhD in the same area.

**Permanent Address:** *1902 Old Post Road*  
*Enid, OK 73703*  
*andrew.stam@gmail.com*

This thesis was typed by the author.